UC San Diego

UC San Diego Electronic Theses and Dissertations

Title

Functional and Structural Connectivity, and the Effects of Neurofeedback Training, in Imitation-Related Brain Networks in Autism

Permalink

https://escholarship.org/uc/item/5rw1x2ss

Author

Datko, Michael Carl

Publication Date

2015

Peer reviewed|Thesis/dissertation

eScholarship.org Powered by the California Digital Library
University of California

UNIVERSITY OF CALIFORNIA, SAN DIEGO

Functional and Structural Connectivity, and the Effects of Neurofeedback Training, in Imitation-Related Brain Networks in Autism

A dissertation submitted in partial satisfaction of the requirements for the degree Doctor of Philosophy

in

Cognitive Science

by

Michael Carl Datko

Committee in Charge:

Professor Jaime A. Pineda, Chair
Professor Lisa Eyler
Professor Terry Jernigan
Professor Ralph-Axel Müller
Professor Ayşe Saygin

2015

The Dissertation of Michael Carl Datko is approved, and it is acceptable in quality and form for publication on microfilm and electronically:

_____

_____

_____

_____

_____

Chair

University of California, San Diego

2015

DEDICATION

To my parents, Joanie and Mike, and to MP

EPIGRAPH

"The important thing is not to stop questioning. Curiosity has its own reason for existing. One cannot help but be in awe when he contemplates the mysteries of eternity, of life, of the marvelous structure of reality. It is enough if one tries merely to comprehend a little of this mystery every day."

-Albert Einstein

TABLE OF CONTENTS

LIST OF FIGURES

LIST OF TABLES

ACKNOWLEDGEMENTS

I would like to thank Professor Jaime A. Pineda for being a wise, knowledgeable, generous, and compassionate mentor. His willingness to discuss new ideas, his insight, and critiques at a moment's notice were all invaluable in helping me cultivate and refine my scientific skills.

I would like to thank Professor Ralph-Axel Müller for giving me so many opportunities to participate in his lab, and for being an advisor to me even though I was not in an SDSU-affiliated program. I have learned so much from him about how to think critically about neuroimaging research, and I have gained invaluable technical skills from all the members of his lab.

My thanks go to the other members of my dissertation committee for taking an active interest in my work, and for providing insights and feedback that helped guide my projects.

Last but not least, I would like to thank all of my fellow graduate students, and particularly those in my cohort, for years of camaraderie on our journey through graduate school.

Chapter 2 is currently being prepared for submission for publication by Mike Datko, Jaime Pineda, and Ralph-Axel Müller. The dissertation author was the primary investigator and first author of this paper.

Chapter 3 is currently being prepared for submission for publication by Mike Datko, Jaime Pineda, and Ralph-Axel Müller. The dissertation author was the primary investigator and first author of this paper.

Chapter 4, in part, has been accepted for publication of the material as it will appear in Annals of Neurology, 2015, Fishman, Inna; Datko, Michael; Cabrera, Yuli; Carper, Ruth; Müller, Ralph-Axel. The dissertation author was the secondary investigator and co-author on this paper.

VITA

2008	Bachelor of Science, University of California, Santa Barbara
2010-2015	Teaching Assistant, Department of Cognitive Science University of California, San Diego
2012	Master of Science, Cognitive Science University of California, San Diego
2014	Instructor, Department of Cognitive Science University of California, San Diego
2015	Instructor, Department of Psychology University of California, San Diego
2015	Doctor of Philosophy, Cognitive Science, University of California, San Diego

PUBLICATIONS

Abbott, A.E., Nair, A., Keown, C.L., Datko, M.C., Jahedi, A., Fishman, I. & Müller, R.-A. Patterns of atypical functional connectivity and behavioral links in autism differ between default, salience, and executive networks. *Cerebral Cortex. In press.*

Nair A, Carper RA, Abbott AE, Chen CP, Solders S, Nakutin S, Datko MC, Fishman I, Müller R.-A. Regional Specificity Of Aberrant Thalamocortical Connectivity In Autism. *Human Brain Mapping. In Press.*

A. J. Khan, A. Nair, C.L. Keown, M. Datko, A.J. Lincoln, and R.-A. Mueller. Cerebro-cerebellar resting state functional connectivity in children and adolescents with autism spectrum disorder. Biological Psychiatry. 2015.

A. Nair, C.L. Keown, M. Datko, P. Shih, B. Keehn, R.A. Mueller. Impact of methodological variables on functional connectivity findings in Autism Spectrum Disorders. Human Brain Mapping. 2013.

Pineda, JA., Carrasco, K., Datko, M., Pillen, S., and Schalles, M. Behavioral and Electrophysiological Impact of Neurofeedback Training on High Functioning Autism and Typically Developing Brains. Mirror Neurons:

Fundamental Discoveries, Theoretical Perspectives and Clinical Implications, Phil. Trans. B. Editors: P. F. Ferrari and G. Rizzolatti. 2013.

JM Park, JH Hu, A Milshteyn, PW Zhang, CG. Moore, S Park, MC Datko, RD Domingo, CM Reyes, XJ Wang, FA Etzkorn, B Xiao, KK Szumlinski, D Kern, DJ Linden and PF Worley. Conditional prolyl isomerization of mGluR5 in plasticity of cocaine sensitization. Cell. 2013.

Juavinett, A; Datko, M; Pineda, JA. A Rationale for Neurofeedback Training in Children with Autism. The Comprehensive Guide to Autism. 2012.

Pineda, J.; Juavinett, A.; Datko, M. Self-regulation of brain oscillations as a treatment for aberrant brain connections in children with autism. Medical Hypotheses (79) 2012 790-798.

ABSTRACT OF THE DISSERTATION

Functional and Structural Connectivity, and the Effects of Neurofeedback Training, in Imitation-Related Brain Networks in Autism

by

Michael Carl Datko

Doctor of Philosophy in Cognitive Science

University of California, San Diego, 2015

Professor Jaime A. Pineda, Chair

Autism is characterized by marked dysfunction in social behaviors, but the neuropathology underlying these deficits is not fully understood. A

potential biomarker of social dysfunction in autism is impaired brain activation and abnormal connectivity in regions involved in imitation, including the human mirror neuron system (hMNS). This dissertation uses multimodal neuroimaging techniques to further characterize the function of imitation-related brain areas in autism. FMRI is used to examine activation in hMNS areas during a task that required participants to observe and execute motor movements. Resting state functional connectivity MRI is used to examine correlations in spontaneous BOLD-signal fluctuations within an imitation network. Diffusion-weighted imaging is used to examine structural characteristics of white matter fiber tracts connecting key nodes of the same imitation network.

An additional goal of this dissertation is to investigate the effects of mu-rhythm-based neurofeedback training in individuals with autism. Currently, there are few therapeutic interventions that are effective in ameliorating the social symptoms of autism, and those that do exist require heavy investments of time, effort, and money. Neurofeedback training is a novel approach that has already been shown to be efficacious to some degree in this domain. Specifically, mu-rhythm based NFT, which targets a biomarker of hMNS function, may be able to induce lasting neuroplastic changes in the autistic brain and may in turn lead to positive behavioral outcomes. This dissertation is in part a study of the effects of 20 or more hours of NFT on task-related activation and functional connectivity in the hMNS in autism.

Chapter 1: Introduction and Background

Autism spectrum disorders include a broad range of behavioral and neurophysiological symptoms, all of which are highly resistant to treatment. These symptoms fall into three broad categories: impairments in language, impairments in social behaviors, and the presence of restricted and repetitive behaviors. Within the social domain of symptoms, the ability to imitate the actions of others in social situations has been shown to be impaired in autism (Ozonoff et al., 1991). This impairment is particularly evident in automatic imitation as opposed to voluntary, "on command" imitation (McIntosh et al., 2006). Automatic imitation plays a fundamental role in the acquisition of social skills (Chartrand & Bargh, 1999; Lakin et al., 2003) and the establishment of social rapport (Lakin & Chartrand, 2003). Therefore, it is likely that deficits in imitation contribute to the social dysfunction seen in autism.

Evidence suggests that each domain of symptoms in autism is associated with disrupted function and connectivity within and between different brain networks from an early age (Just et al., 2004; Belmonte et al., 2004). The social impairments in particular have been linked to abnormalities in the human mirror neuron system (hMNS) (Williams et al., 2001; Dapretto et al., 2006; Iacoboni, 2006) as well as other networks involved in behaviors related to social cognition (Fishman et al., 2014). Since the hMNS is active during the observation and execution of biological motion, it has been proposed that this system is a core neurophysiological substrate for imitation

and, by extension, many kinds of social interactions (Iacoboni et al., 1999, 2005; Rizzolatti & Craighero, 2004). In addition to fMRI evidence for atypical hMNS functioning in autism, there is evidence from other domains such as EEG. The mu rhythm is an 8-13 Hz signal that is generated by and maximal over sensorimotor cortex (Kuhlman, 1978). Mu amplitude is suppressed in response to imitation and observation of biological motion (Pfurtscheller & Neuper, 1997), and this suppression has been shown to correlate with activation of hMNS areas in simultaneous EEG-fMRI experiments (Arnstein et al., 2011). In autism, the mu rhythm during the observation, but not performance, of biological motion does not desynchronize as it does in typically developing participants (Oberman et al., 2005). Evidence of hMNS abnormalities in autism from other modalities includes significantly decreased cortical thickness in areas of this network (Hadjikhani et al., 2006), differences in cortical excitability in hMNS areas (Theoret et al., 2005), abnormal imitation-related cortical activation sequences (Nishitani et al., 2004), increased compensatory connectivity from hMNS to areas of prefrontal cortex (Shih et al., 2010), and several other studies of abnormalities in the mu rhythm or related EEG measures (Bernier et al., 2007; Martineau et al., 2008, 2010).

Despite these findings of marked abnormalities in network function and connectivity, as well as in the behaviors associated with affected networks, some therapeutic interventions show promise in ameliorating the symptoms of autism. Treatments that appear to be effective for some individuals include

cognitive and behavioral therapies (Wood et al. 2009), pharmacological interventions (Broadstock et al., 2007), joint attention therapy (Kim et al., 2008), and several others. Interventions that specifically target and seek to improve imitation abilities have shown promise as well (Ingersoll et al., 2007, 2008, 2012). However, many of these treatments are prohibitively expensive and require large time commitments (Jacobson et al., 1998; Chasson et al., 2007). Therefore, it would be advantageous to develop therapies that are more cost-effective and that achieve longer-lasting behavioral benefits over a shorter period of time.

While many of the treatments for autism currently in use were developed with careful consideration towards the behavioral symptoms of autism, few if any combine behavioral approaches with emerging data from neuroimaging studies of autism as a disorder of network connectivity. Clinically, the most widely used diagnostic measures for ASD include the ADOS and ADI, which are largely based on the diagnostic criteria for ASD described in the Diagnostic and Statistical Manual of Mental Disorders (DSM) (American Psychiatric Association, 2000). In light of the current goal of the National Institutes of Health to create a diagnostic framework for mental disorders based on neurophysiological biomarkers instead of behavioral phenotypes (Insel et al., 2010), it is imperative that new treatments address the now well-established view that autism is a disorder of brain network connectivity.

One such potential treatment approach is neurofeedback training targeting the mu rhythm, the index of hMNS activity that shows atypical motion-related desynchrony in autism. In this type of training, which has already shown promise (Pineda et al., 2008, 2014), participants have their EEG monitored and receive positive feedback on a computer when mu amplitude surpasses a threshold. Over time, participants gain more volitional control over modulating mu amplitude in this way. By repeatedly engaging the neural substrates of the mu rhythm, namely the core areas of the hMNS, participants may be improving connectivity specifically within this network.

With these points in mind, this dissertation will address two trajectories in ASD research. First, it will attempt to contribute to the identification of biomarkers for ASD, by specifically examining the structure and function of the hMNS and other imitation-related brain regions in ASD compared to typical development. Second, it will investigate the effects of mu-rhythm based neurofeedback training on the functional organization of brain networks and on social behaviors in autism.

Chapter 2 presents a study of the effects of mu-rhythm based NFT on behavioral impairments as well as brain activation during a goal-oriented imitation task in children and adolescents with autism spectrum disorders as well as typically developing (TD) controls. It is demonstrated that prior to NFT, ASD activates the hMNS significantly less than the TD group. After NFT, within-group increases in activation in the ASD group are shown, and the

group differences shown prior to NFT are now absent. Covariate tests with brain activation data and measures of ASD social symptom severity show that the neurophysiological effects of NFT are correlated with positive changes in behavior in the ASD group.

Chapter 3 examines the effects of the same regimen of NFT on functional connectivity within a brain network involved in imitation (including some areas of the hMNS). It begins by establishing parallels between FC patterns in the study sample and those already observed in the literature; namely, that imitation areas seem to be overconnected, relative to typical development, to areas outside of the imitation network itself. It is then demonstrated that the particular NFT protocol trained with by the participants leads to a shift in this pattern of out-of-network connectivity, and that after the training connectivity within the imitation network is increased in the ASD group.

Chapter 4 explores whether and to what extent the underlying white-matter structure that connects areas of the imitation network is compromised in individuals with autism compared to typically developing controls. Diffusion weighted imaging is used to estimate the directionality and density of white matter fiber bundles, and then probabilistic tractography is used to find the most likely pathways between areas of an imitation network. Tracts found in this way are first verified with anatomical tracer atlases, and then white matter characteristics within the tracts are examined. Finally, correlations are made between these measures and autistic symptom severity.

Chapter 2: Neurofunctional and Behavioral Changes Following Mu Neurofeedback Training in Children with Autism

Introduction

Numerous findings support the hypothesis that social deficits in autism result from abnormal function in brain regions and networks associated with social cognition and action perception. In particular, functional abnormalities have been observed in brain regions constituting the human mirror neuron system (hMNS). The hMNS is a potential neurobiological substrate for understanding many key concepts in human social cognition, particularly those directly relevant to the behavioral and cognitive deficits observed in ASD (Williams et al., 2001), including the ability to comprehend actions, understand intentions, and learn through imitation. First described in single-unit recordings by Rizzolatti and colleagues in the macaque monkey (di Pellegrino et al., 1992), mirror neurons are involved in both self-initiated action and the representation of action performed by others. Neurons in the monkey analog to the human pars opercularis of the inferior frontal gyrus (IFG) and in the inferior parietal lobule (IPL) show increased firing while executing and observing the same action, representing a potential mechanism for mapping perceived biological motion onto the perceiver's sensorimotor systems (Rizzolatti et al., 2004; Pineda, 2005). Indeed, a homologous network with

similar functional properties has been described in humans using fMRI (Hari et al., 1998; Iacoboni et al., 1999; Buccino et al., 2001).

Although some studies have raised questions about the role of mirror neurons in human social behavior (Hickok et al., 2009; Turella et al., 2009; Dinstein et al., 2008), an increasing amount of work suggests that a dysfunction in the hMNS does contribute to social deficits in ASD (Nishitani et al., 2004; Hadjikhani et al., 2006; Bernier et al., 2007; Dapretto et al., 2006; Theoret et al., 2005; Oberman et al., 2005; Oberman et al., 2013). Individuals with ASD have marked impairment in social skills, from joint attention to theory of mind (Carpenter et al., 1998; Baron-Cohen et al., 2009). A number of recent reviews have noted that deficits in hMNS activity may explain the poor socialization skills prevalent in the disorder (Perkins et al., 2010; Iacoboni & Dapretto, 2006). Numerous studies show reduced activation in tasks involving social cognition and action imitation (Nishitani et al., 2004, Dapretto et al., 2006, Hadjikhani et al., 2006, Williams et al., 2006, Altschuler et al., 2000; Bernier et al., 2007; Oberman et al., 2005, Martineau et al, 2008), increased activation (Martineau et al., 2010) and in some instances selective abnormalities (Theoret et al., 2005; Oberman et al., 2008). A particularly relevant fMRI study (Dapretto et al., 2006) demonstrated decreased activation in the pars opercularis of the IFG in autistic individuals during imitation of facial expressions, and found that activity in this region was inversely related to symptom severity in the social domain, as measured by the Autism Diagnostic

Observation Interview-Revised (ADI-R) and the Autism Diagnostic Observation Schedule-Generic (ADOS-G). Notably, participants were still able to perform the task – perhaps due to compensatory activation of other brain areas.

EEG studies have shown that putative electrophysiological biomarkers of hMNS activity also show abnormalities in ASD (Bernier et al., 2007; Oberman et al., 2005; Oberman et al., 2008). A body of evidence links the spectral dynamics of an EEG signal known as the mu rhythm to the functioning of the hMNS (Pineda et al., 2005). Particularly relevant are scalp-recorded EEG patterns of activity in the alpha mu (8-13 Hz) range that are most evident over the central region of the scalp overlying the sensorimotor cortices and that are modulated by motor activity (Altschuler et al., 1998). Relative to baseline, mu power is suppressed, not only during actual execution, but also during the observation and imagination of body movements (Pfurtscheller et al., 2006; Muthukumaraswamy et al., 2004; McFarland et al., 2000). In a more recent study, Arnstein et al. (2011) used fMRI and EEG to show that suppression of mu power is correlated with BOLD signal activations in areas associated with the hMNS. In ASD, this mu rhythm suppression is absent during observation of body movements, supporting the role of an altered MNS in the disorder (Oberman et al., 2005; Oberman et al., 2007). However, there is evidence showing that the system is not beyond repair, since mu suppression is intact when the people being imitated or observed are familiar to the ASD participant (Oberman et al., 2008)

The existence of an EEG biomarker for ASD, as well as a substantial amount of research, support the rationale for using neurofeedback training (NFT) in the context of treatment for ASD. There is evidence from earlier studies that NFT produces positive behavioral and electrophysiological changes in children with ASD (Coben et al., 2010; Pineda et al., 2008; Pineda et al., 2014). Neurofeedback is a form of operant learning in which participants develop implicit control over the frequency-based spectral dynamics of scalp-recorded electrical cortical oscillations. Over time, users develop strategies, implicitly or explicitly, to control a visual representation of EEG power levels in specific frequency bands. NFT has shown promise in research and clinical applications including lowering seizure incidence in epilepsy (Sterman et al., 1996; Walker et al., 2008), affecting the subsequent corticomotor response to transcranial magnetic stimulation (Ros et al., 2010), and brain activation during a Stroop task in unmedicated children with ADHD (Lévesque et al., 2006).

NFT requires less time to be efficacious than other behavioral interventions and produces fewer side effects than pharmacotherapies (Fuchs et al., 2003; Fox et al., 2005). Coben et al. (2009) argue that while further research is necessary, a variety of studies support a Level 2 determination ("possibly efficacious") for the application of neurofeedback in autistic disorders. Mu-NFT studies in children with ASD show improvements in sociability and attention, and a normalization of action-observation-related mu-

rhythm suppression that is normally absent (Pineda et al., 2008; Pineda et al., 2014). Since mu suppression is presumably an index of hMNS activity, NFT that specifically targets the mu rhythm may be able to cause neuroplastic changes in this specific network. Because this system is thought to be critical for social behaviors, and functions abnormally in autism, mu-NFT could be beneficial in attenuating the social deficits associated with autism.

To test these hypotheses, we examined the effects of approximately 30 hours of mu-NFT in a group of 17 high functioning ASD children and a matched comparison group of 11 typically developing (TD) children, ages 8-17 years. We tested the prediction that NFT would produce changes in functional brain activation by adapting an imitation task first used to study hMNS activation in healthy adults by Iacoboni et al. (1999). The task used by these investigators required participants to observe or imitate simple finger-lifting actions. These conditions elicited activation in two areas associated with the hMNS: the inferior parietal lobule (IPL) and superior temporal sulcus (STS). The task has also been used to demonstrate activation differences between ASD and TD groups in those two areas (Williams et al., 2006). However, the Williams study did not show activation or significant group differences in inferior frontal gyrus (IFG). This exception is critical because IFG is considered a core component of the hMNS (Rizzolatti & Craighero, 2004). Therefore, for the present study, we used a modified version of this task by having participants imitate and observe a hand pressing buttons on a button

box in the scanner. This changed the task from requiring imitation and observation of meaningless movement to one based on object-directed movement. This type of action has been shown to elicit stronger activations in mirror areas, specifically in IFG (Muthukumaraswamy et al., 2004), making our task more appropriate for a comprehensive study of differences in mirroring-related activation between ASD and TD samples.

We hypothesized that neuroplastic changes could result from repeatedly engaging circuits involved in developing and sustaining volitional control of mu-frequency cortical oscillations via neurofeedback training. Furthermore, we speculated that changes in mu rhythm and associated brain circuits would be more pronounced in the ASD group, where mu dynamics are compromised, compared to the TD group. More specifically, we predicted that, prior to NFT, brain activation during the imitation task would be significantly lower in the ASD group compared to the TD group, and that this between-group difference would be localized primarily in areas associated with the hMNS. We also predicted that following NFT, hMNS activation differences between these groups would be reduced. Additionally, we predicted that the severity of social symptoms in autism would be reduced following training, and that this reduction would correlate with changes in BOLD fMRI measurements. Finally, we predicted that any functional neuroanatomical effects resulting from the training would be more significant for participants whose assessment profile reflected greater symptoms of autism.

Methods

Participants

Seventeen high-functioning ASD (mean age = 12.51 $\pm$ 0.76; 13 male) and 11 TD (mean age = 10.64 $\pm$ 0.75; 7 male) participants were recruited for the study. Seven of the original ASD participants and 4 of the original TD participants were excluded from the final statistical analyses. Among the excluded participants, 4 ASD and 1 TD had excessive head motion during one or both MRI scanning sessions, 3 ASD were excluded due to other difficulties encountered during scanning, and 3 TD did not complete the neurofeedback training. After these exclusions, groups were matched for age and IQ. Participants were recruited from San Diego and Los Angeles Counties via local support groups for children with ASD and other disabilities, from local schools and recruitment posters, and via Valerie's List, a San Diego internet-based autism support group. Participants and parents gave informed assent and consent, respectively, in accordance with the Helsinki Declaration. The University of California, San Diego's Institutional Review Board approved the study. All but three participants in the ASD group had their diagnoses verified by a clinician immediately prior to our study using the ADOS-G and ADI-R, and all but one met the criteria of high functioning autism with an IQ greater than 80 based on the Wechsler Abbreviated Scale of Intelligence (WASI) (Wechsler, 1999). For those whose diagnoses were not based on ADOS-G or ADI-R, we used their psychoeducational evaluations, which are a component

of the triennial evaluation required of all special education students in the San Diego school district. One participant received intelligence testing using the Kauffman Assessment Battery for Children (KABC) (Cahan et al., 2001) instead of the WASI. Participants' demographic information is summarized in Table 2.1A,B.

Table 2.1 Participant demographic, diagnostic, and behavioral information. **A:** only subjects with usable fMRI data. * indicates significance at p<0.05. † indicates that a one-tailed hypothesis-driven t-test was used. **B**: Same as A but for all recruited subjects, including those that did not complete post-NFT fMRI scanning sessions.

A: Demographic and Diagnostic information for participants with usable fMRI data			
	ASD (n = 10, 3 female, 1 LH) Mean (SEM) Range	TD (n = 7, 2 female, 1 LH) Mean (SEM) Range	*p<*
Age	13.3 (0.98) 9.26-18.3	11.3 (0.92) 8.64-16.7	0.20
WASI: Full-scale IQ	101.1 (7.65) 56-134	115.6 (2.95) 104-130	0.16
WASI: Verbal IQ	99.1 (7.06) 55-130	111.6 (2.91) 97-127	0.19
WASI: Non-verbal IQ	98.6 (7.93) 62-137	113.0 (3.81) 103-137	0.18
SRS Total (pre-NFT)	75.6 (3.82) 58-90	38.6 (1.20) 35-46	5.26E-07
SRS Total (post-NFT)	68.7 (3.36) 56-90	38.8 (0.76) 35-42	1.49E-06
SRS Post- vs. pre-NFT	p=.095†	p=0.692	N/A
ADOS: Com + Soc	11.55 (1.70) 3-22	N/A	N/A
ADI-R: Soc	15.33 (2.44) 6-28	N/A	N/A
ADI-R: Com	14.11 (2.18) 4-23	N/A	N/A
ATEC Total (pre-NFT)	38.7 (4.40) 15-65	N/A	N/A
ATEC Total (post-NFT)	27.2 (3.95) 7-51	N/A	N/A
ATEC Post- vs. pre-NFT (p<)	p=0.034*†	N/A	N/A
B: Demographic and Diagnostic information including participants without usable fMRI data			
	ASD (n = 17, 4 female, 2 LH) Mean (SEM) Range	TD (n = 11, 4 female, 1 LH) Mean (SEM) Range	*p<*
Age	12.5 (0.76) 9.07-18.3	10.64 (0.75) 8.39-16.69	0.109
SRS Total (pre-NFT)	79.5 (2.70) 58-90	38.6 (1.1) 35-46	5.26E-07
SRS Total (post-NFT)	70.6 (2.65) 56-90	38.8 (0.74) 35-42	1.49E-06
SRS Post- vs. pre-NFT	p=0.013*†	p= 0.87	N/A
ATEC Total (pre-NFT)	42.06 (3.43) 15-67	N/A	N/A
ATEC Total (post-NFT)	30.8 (3.67) 7-54	N/A	N/A
ATEC Post- vs. pre-NFT (p<)	p=0.016*†	N/A	N/A

Neurofeedback Training

The training process involved recording EEG activity from the C4 electrode site over right sensorimotor cortex and using power in the mu frequency band (8-13 Hz) at this site to control aspects of a video game or a movie. Both the gaming and movie activities required keeping mu power above a threshold. The threshold was determined prior to each session based on each participant's baseline amplitude at the start of the session. The training activities also required inhibiting amplitude in other specified EEG frequencies (theta: 4-8 Hz and beta: 13-30 Hz) and keeping them below a pre-defined threshold as per standard protocols (Othmer et al., 2012). During training, participants saw a display of three threshold bars alongside the game/movie window. One corresponded to the rewarded mu frequency and the other two corresponded to the inhibited frequencies. Rewards (e.g., if the video game is a racing car, the car will move; if a movie is playing, the size of the video playback will get larger to fill the screen) were given based on satisfying two conditions: 1) power in the specified frequency (8-13 Hz mu band) exceeds each participant's individually-set threshold, and 2) power from the theta (related to blinks) and beta (related to muscle movement) activity is below threshold. Theta and beta inhibition feedback was included in the design for two reasons. First, it ensured that individuals could not advance in the game or expand the DVD viewing window by producing movement-induced power increases across the entire EEG spectrum. Second, it allowed

for distinguishing between improvement effects as a function of EEG modulation as opposed to modulation of autonomic nervous system and muscle activity.

All participants began the study with the target of completing 30 hours of training, on a regimen of two 45-minute training sessions per week for 20 weeks. Due to scheduling issues, the actual amount of training was variable (20-30 hours), as detailed in Table 2.2C.

Table 2.2 Group behavioral data. **A**: Imitation Task Accuracy and Reaction Time. **B**: Head Motion and Timepoint Censoring. **C**: Training and sessions completed.

	ASD (n = 10) Mean (SEM) range	TD (n = 7) Mean (SEM) range	p
A: Imitation Task Accuracy and Reaction Time			
Pre-training % correct Trials	83.8 % (3.93) 64-97	86.6 % (3.66) 63-97	0.32
Pre-training reaction time (correct trials)	1.153 s (0.019) 0.067-3.25	1.137 s (0.023) 0.07-2.89	0.58
Post-training % correct trials	86.0 % (6.41) 47-100	87.5 % (6.87) 40-100	0.45
Post-training reaction time (correct trials)	1.234 s (0.024) 0.126-2.91	1.103 s (0.021) 0.354-2.90	<0.0001
Post- vs. pre-NFT % correct trials	p= 0.39	p= 0.46	
Post- vs. pre-NFT reaction time (correct trials)	p= 0.01	p= 0.28	
B: Head Motion and Timepoint Censoring			
Pre-training total motion RMSD (pre-censoring)	0.173 (0.034) 0.04-0.35	0.169 (0.034) 0.03-0.34	0.47
Pre-training percent censored	8.6 % (4.0) 0-41	14.0 % (4.2) 1-38	0.21
Pre-training total motion RMSD (post-censoring)	0.13 (0.02) 0.04-0.27	0.11 (0.018) 0.03-0.21	0.29
Post-training total motion RMSD (pre-censoring)	0.125 (0.026) 0.04-0.29	0.101 (0.014) 0.06-0.17	0.25
Post-training percent censored	1.4 % (0.78) 0-8	0.85 % (0.47) 0-4	0.31
Post-training total motion RMSD (post-censoring)	0.11 (0.021) 0.035-0.24	0.09 (0.01) 0.06-0.15	0.20
Post- vs. Pre-NFT RMSD (pre-censoring)	p< 0.14	p< 0.08	
Post- vs. Pre-NFT percent censored	p< 0.047	p< 0.01	
Post- vs. Pre-NFT RMSD (post-censoring)	p< 0.28	p< 0.18	
C: Training and Sessions Completed			
Total hours training	26.4 (1.72) 14.75-33.75	17.2 (1.69) 9-21.5	0.003
Total training sessions	36.4 (3.15) 20-50	18.4 (1.77) 10-24	0.0006
Days between first to last training session	211.6 (26.7) 78-335	328.0 (51.8) 179-563	0.073
Training Density (hours per month)	4.25 (0.39) 2.69-5.76	1.79 (0.26) 1.09-3.18	0.0004

Behavioral Assessments

Two pen-and-paper questionnaires were given to parents of each participant before and after training. Specifically, the Autism Treatment Evaluation Checklist (ATEC) (Magiati et al., 2011) and the Social Responsiveness Scale (SRS) (Constantino et al., 2003) were used. Scores for

these tests are summarized in Table 2.1A. The ATEC is a parental checklist to evaluate ASD treatment paradigms based on four subscale scores (speech/language/ communication, sociability, sensory/cognitive awareness, and health/physical/behavior) and a total score, which are weighted according to the response and the corresponding subscale. Each category contains multiple symptoms that are each rated on a scale of 1-5. Participant's score on each dimension of the ATEC will be calculated as a percentage of the highest possible score for that dimension. The SRS provides a quantitative metric of the type and severity of impairments in social functioning that are characteristic of ASD children with five subscales (receptive, cognitive, expressive, and motivational aspects of social behavior, plus autistic preoccupations), administered by research staff with the child.

Imitation Task

The task included six conditions plus a rest baseline. In condition one (Figure 2.1A), participants were instructed to imitate finger movements shown in 2.5-second videos of a hand pressing one or both buttons on a button box. The button box in the videos was identical to that used by participants to respond in the scanner. In condition two (Figure 2.1B), the stimuli were still images, instead of movies, of the same hand and button box, with a black dot in front of either or both of the fingers as an indicator of which button to press. This condition also required participants to respond by pressing buttons. In

condition three (Figure 2.1C), a blurred background with the same luminance as the hand picture was shown, with black dots within a rectangle as the indicators of which button the participant should press. In the remaining three conditions, participants were shown stimuli identical to those in the first three conditions, but were instructed to observe and pay attention rather than making any responses.

The task was divided into three 5-minute runs, with each run containing one block of each of the six conditions and six rest periods. The conditions were presented in a blocked design, alternating between 27-second blocks of one task condition and 20-second blocks of rest. During each of the task blocks, a total of 9 stimuli were shown in pseudo-random order for 2.5 seconds each, with 0.5 second intervals between stimuli. Regardless of condition (video hand, static hand, or spatial cue), 3 stimuli each were presented in each block to indicate button press with the middle finger, the index finger, and both fingers simultaneously. During intervals between stimuli, a white fixation cross was displayed in the middle of a black background. The same fixation cross was displayed during the 20-second rest blocks that occurred between task blocks. A schematic of this task design is shown in Figure 2.1E.

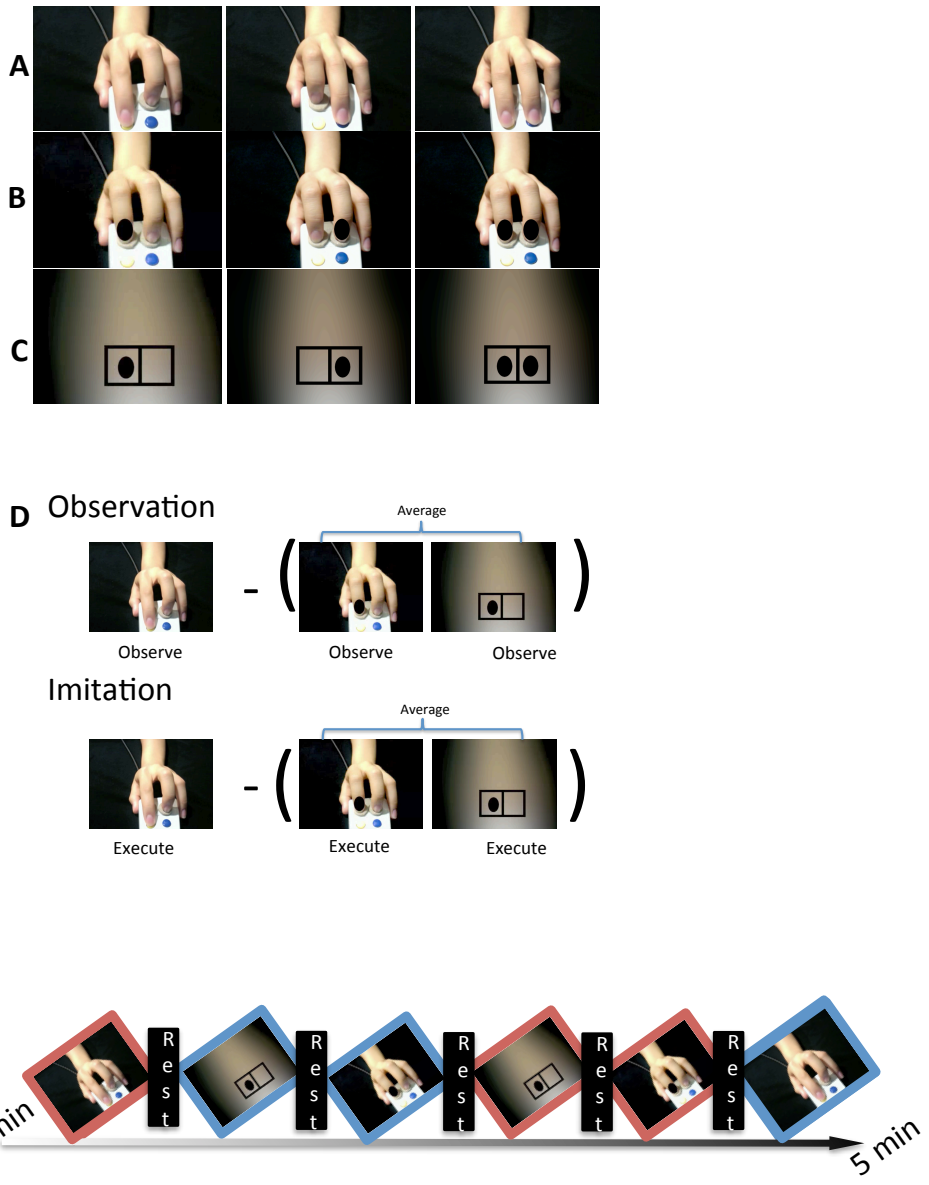

Figure 2.1 Stimuli, analysis contrasts, and task design for imitation task. A-C: Examples of the motion video (A), static image (B), and spatial cue (C) stimuli used in both the observation and execution conditions. D: Activation contrasts. Observation and Imitation contrasts were combined for most analyses. E: Blocked task design for one run of imitation task. Red borders represent imitation conditions and blue borders represent observation conditions. Stimulus blocks were 30 seconds and rest blocks were 20 seconds.

MRI Data Collection

All MRI data were acquired on a GE 3T MR750 scanner with an 8-channel head coil. High-resolution structural images were acquired with a standard FSPGR T1-weighted sequence (TR: 11.08ms; TE: 4.3ms; flip angle: 45°; FOV: 256mm; 256 x 256 matrix; 180 slices; $1mm^3$ resolution). Data for the imitation task were acquired in three functional scans, each consisting of 150 whole-brain volumes acquired in 42 interleaved slices, with the Array Spatial Sensitivity Encoding Technique (ASSET), using a single-shot, gradient-recalled, echo-planar pulse sequence (TR: 2000ms; TE: 30ms; flip angle: 90°; 64 x 64 matrix; 3.2mm slice thickness; in-plane resolution $3.4mm^2$). Cardiac and respiratory data were collected for each participant during each functional scan. These data were used to create regressors for removing physiological noise from the functional data.

Preprocessing and analysis of fMRI data

All neuroimaging data were preprocessed and analyzed using the Analysis of Functional Neuroimages suite (Cox, 1996). The first four time points for each of the three task scans were discarded to remove effects of signal instability, and slice-time correction was performed. Data from all functional scans and the structural scan were co-registered to Talairach space (Talairach, 1988), specifically using the “Colin Brain” that comes packaged

with AFNI. Functional scans were resampled to isotropic $3mm^3$ voxels, and spatially smoothed to a global full-width at half-maximum of 6mm.

Conventional motion correction was performed for all functional scans. Additionally, considering the known impact of head motion in fMRI analyses (Power et al., 2012; Van Dijk et al., 2012), further motion correction procedures were performed. Six rigid-body motion parameters, estimated based on realignment of functional volumes, were modeled as nuisance variables and their contribution to the overall signal was removed via linear regression. Time points with excessive motion (>1.5mm displacement from one time point to the next), along with the 10 time points following those, were censored and excluded from the final statistical analysis. 3 ASD and 4 TD participants with <80% remaining time points were excluded. In the remaining participants, an average of approximately 13 percent of the total time points were censored, and the average did not differ significantly between groups, but both groups had significantly less censored timepoints post-NFT compared to pre-NFT (Table 2.2B).

The voxelwise BOLD signal time-series from each of the three task scans for each participant were then scaled by dividing each by the mean, effectively converting them into a measure of percent signal change. The scaled data from the three task scans were then concatenated into a single time-series. The hemodynamic response function for each stimulus block type was estimated by convolving each block's time series with a 27-second

boxcar-shaped block function. Physiological noise from cardiac and respiratory signals, as well as BOLD signal in white matter and ventricular regions, were removed via linear regression.

Activation during the different conditions was combined into three different contrasts: one included only conditions where the participant was asked to perform an action based on the stimuli (referred to hereafter as "imitation"), another included only conditions wherein the participant was instructed to observe the stimuli ("observation"), and yet another was a combination of the first two contrasts ("imitation+observation"). For each of these, the activation during the condition with still images of hands and during the condition with simple geometric spatial cue images was subtracted from the activation during the condition with videos of finger movements. This eliminates activation associated with visual features of the hand, as well as activation related to simple visuospatial features such as luminosity. The remaining activity reflects the mapping of perceived biological movements onto the participant's own motor system, the process often referred to as "mirroring." A schematic of these contrasts is presented in Figure 2.1D.

The first analysis performed on the activation data consisted of a series of ANOVAs designed to test for interactions between group (ASD and TD) and training status (pre-NFT and post-NFT) in two different sets of regions of interest (ROIs). One of these sets of ROIs was derived from a meta-analysis of 87 fMRI studies of imitation that found fourteen regions to be consistently

activated across these studies (Caspers et al., 2010). That paper listed the center coordinates for each of these ROIs in standard MNI space. For the present analysis, those coordinates were first converted to Talairach space, and then new spherical ROIs where created based on those. Each sphere had a radius of 7mm and was centered around the converted Talairach coordinate. The center coordinates for each of these ROIs are listed in Table 2.3.

The other set of ROIs was based on the combined activation between both ASD and TD groups during the combined imitation+observation contrast discussed above. A total of seven cortical regions were derived from this combined-group activation contrast, and the coordinates of their centers of mass were used as the center coordinates for seven spherical seed ROIs. These coordinates are listed in Table 2.3.

Three whole-brain 2x2 ANOVAs were performed on the brain activation data, with group status (ASD, n = 10; TD, n = 7) and training status (pre-NFT or post-NFT) as the two main factors for each. One of these ANOVAs was performed for the imitation contrast, one for observation, and one for imitation+observation. All ANOVAs passed an uncorrected voxelwise threshold of p=0.02 and were then corrected for multiple comparisons at the cluster level, using Monte Carlo simulation (Forman et al., 1995), to $p < 0.05$.

After results were obtained for the ANOVAs, we sought to determine the activation patterns that drove any observed interaction effects. For each

ANOVA, two separate t-tests were performed to compare activation between ASD vs. TD groups for both pre-NFT and post-NFT. In addition to that, two more t-tests were performed for pre- vs. post-NFT activation within each group (i.e. ASD pre- vs. ASD post-training). Each of these t-tests was performed with a whole brain field of view. All t-tests were corrected for multiple comparisons at the cluster level using Monte Carlo simulation.

Covariance of ASD symptom severity and NFT-related changes in imitation-related brain activation

We also investigated whether ASD symptom severity covaried with the changes in fMRI activation after NFT. Specifically, we performed separate t-tests comparing the pre-NFT to post-NFT activation in the ASD group, with ADOS, ADI, ATEC, and SRS scores as covariates. ATEC and SRS from before and after NFT were converted into a difference score for each participant (post-NFT score minus pre-NFT score). The ADOS and ADI were only administered prior to NFT, so these measures had only one score per participant for this covariate analysis. Thus, all of these ANOVAs had one value per participant for each covariate. The results reported here are based on data from the imitation+observation contrast only, All covariate t-tests passed an uncorrected voxelwise threshold of $p=0.02$ and were then cluster corrected for multiple comparisons to $p < 0.0001$.

Results

Behavioral, Head Motion, and Pen-Paper/Parental Assessment Data

Groupwise accuracy and reaction time data during the imitation task are summarized in Table 2.2A. Correct trials were trials in which the participant pressed the same button or buttons being pressed in the stimuli. Accuracy on the imitation task did not significantly differ between groups either pre-NFT (ASD M = 83.8%, TD M = 86.6%, $p = 0.32$) or post-NFT (ASD M = 86.0%, TD M = 87.5%, $p = 0.45$). Accuracy also did not differ within-groups pre- vs. post-NFT (ASD $p = 0.39$, TD $p = 0.46$). Reaction time on correct trials did not differ between groups pre-NFT (ASD M = 1.153 s, TD M = 1.137 s, $p = 0.58$), but did differ significantly post-NFT (ASD M = 1.234 s, TD M = 1.103 s, $p < 0.0001$). This difference was primarily the result of an increased reaction time in ASD pre- vs. post-NFT ($p = 0.01$) because there was no pre- vs. post-NFT difference in the TD group ($p = 0.28$).

Group averages for root mean squared deviation (RMSD) of head motion during the task scans are summarized in Table 2.2B. There were no significant group differences in head motion either between-groups or within-groups before versus after the training.

Between-group t-tests were performed on the data from each pen-paper and parental assessment collected. Group averages, as well as the results of these statistical tests are summarized in Table 2.1A (for subjects with usable fMRI data) and Table 2.1B (for all subjects who completed NFT,

with or without usable fMRI data). For the usable-fMRI subset, groups did not significantly differ on age (ASD M = 13.3; TD M = 11.3) or WASI scores for either the full-scale (ASD M =101.1; TD M =115.6), verbal only (ASD M =99.1; TD M =111.6), or non-verbal only WASI (ASD M =98.6; TD M =113.0). After NFT, the ASD group showed significant improvements in the SRS for the full sample (pre-NFT M = 79.5; post-NFT M =70.6; $p = 0.013$), but not for the subset with usable fMRI data (pre-NFT M =75.6; post-NFT M = 68.7; $p = 0.095$). Also after NFT, the ASD group showed significant improvements on the ATEC for both the full sample (pre-NFT M = 42.06; post-NFT M = 30.8; $p = 0.016$) as well as the usable-MRI subset (pre-NFT M = 38.7; post-NFT M =27.2; $p = 0.034$).

In a follow-up analysis, Pearson correlations were obtained between clinical assessment scores and changes in pre- versus post-NFT parental assessment scores (ATEC and SRS). This was intended to be a measure of whether NFT was behaviorally effective for individuals on different parts of the autism spectrum. There were significant correlations between ATEC changes and ADOS-Sociocommunicative scores ($r = 0.75$, $p < 0.05$), as well as SRS changes with both the ADI-communication and ADI-Social subscores ($r = 0.82$ and $r = 0.83$, respectively, *p*s < 0.05).

Imitation-related Brain Activation

The results presented here represent the imitation+observation contrast. ROI-based ANOVAs for the fourteen ROIs in the Caspers imitation network and the seven ROIs from the combined group activation during the present study's imitation task showed several interaction effects and main effects (mostly for the training factor, not the group factor). There were significant interaction effects between group and training status in the right medial premotor cortex ($F(2,15) = 6.38$, $p = 0.017$) and right lateral dorsal premotor cortex ($F(2,15) = 4.48$, $p = 0.0427$) from the Caspers imitation ROIs. There was also a main effect of training in the more ventral of the two right inferior parietal lobule ROIs from the Caspers network (referred to as Right SII/IPL in their paper) ($F(2,15) = 4.76$, $p = 0.037$). From the set of seven seeds based on the present study's imitation task, there were significant interactions between group and training status in the right inferior frontal gyrus ($F(2,15) = 6.95$, $p = 0.013$) and right precentral gyrus ROIs ($F(2,15) = 4.5$, $p = 0.042$). Also from that set, there was a main effect of training status in the left postcentral gyrus ROI ($F(2,15) = 6.62$, $p = 0.015$). These interactions and main effects are summarized in Table 2.3. Signficant interactions for the Caspers ROIs are shown in Figure 2.2 and for the Task-Based ROIs in Figure 2.3.

Table 2.3 Main effects and interactions for ANOVA between group (ASD and TD) and training status (pre-NFT and post-NFT). Yellow highlights indicate significant main effects or interactions.

ROI	R/L	Talairach Coordinates			Main effect: Group		Main effect: Training		Interaction	
		x	y	z	F-score	*p*	F-score	*p*	F-score	*p*
Caspers ROIs										
Inferior Frontal Gyrus	L	52	-15	11	0.05	0.82	0.66	0.42	1.08	.31
Inferior Frontal Gyrus	R	-52	-19	8	0.22	0.64	0.27	0.60	1.55	0.22
Lat. Dorsal Premotor	L	31	10	55	0.12	0.73	0.08	0.78	2.76	0.11
Lat. Dorsal Premotor	R	-38	-7	49	0.98	0.33	0.56	0.46	4.48	0.0427
Med. Premotor	L	0	-15	45	0.10	0.75	0.27	0.61	1.54	0.22
Med. Premotor	R	-13	-9	57	0.50	0.49	1.59	0.22	6.38	0.017
Intraparietal Sulcus	L	33	35	46	2.22	0.15	3.54	0.07	3.19	0.08
Sup.Temporal Sulcus	L	-47	32	47	4.04	0.05	4.28	0.047	1.89	0.18
Inferior Parietal Lobule	R	47	45	11	1.04	0.32	0.01	0.91	1.05	0.31
Inferior Parietal Lob. 2	R	-54	22	18	0.02	0.88	4.76	0.037	0.07	0.80
Lat. Occipital	L	45	65	8	0.01	0.94	0.01	0.91	0.68	0.41
Anterior Insula	R	-48	59	6	0.25	0.62	0.58	0.45	1.98	0.17
Lat. Occipital	R	-38	-7	0	0.68	0.41	1.96	0.17	0.8	0.38
Fusiform Face Area	R	40	49	-17	3.34	0.08	0.01	0.9112	2.31	0.14
Seeds Derived from Imitation Task										
Post. Mid. Temporal	L	-49	54	4	2.55	0.12	3.13	0.087	2.48	0.12
Post. Mid. Temporal	R	47	57	4	0.66	0.42	2.42	0.13	1.4	0.25
Superior Parietal Lob.	L	27	52	47	1.03	0.32	3.13	0.087	3.67	0.06
Inferior Parietal Lob.	R	-33	46	47	0.02	0.89	0.43	0.52	1.39	0.25
Postcentral gyrus	L	52	22	28	0.55	0.47	6.62	0.015	3.08	0.09
Precentral gyrus	R	-40	9	47	0	0.95	0.83	0.37	4.5	0.042
Inferior Frontal Gyrus	R	-46	-16	16	0.17	0.68	4.09	0.052	6.95	0.013

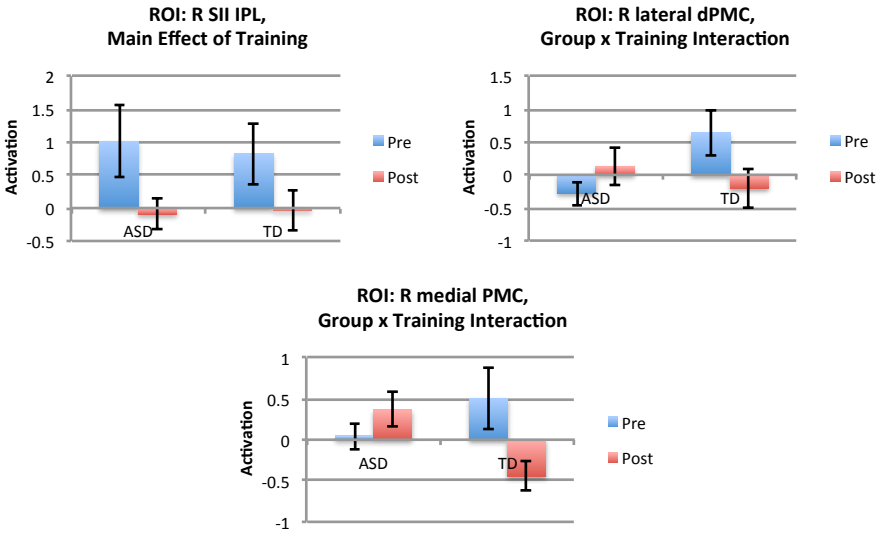

Figure 2.2 Significant main effects and interactions for activation within Caspers ROIs.

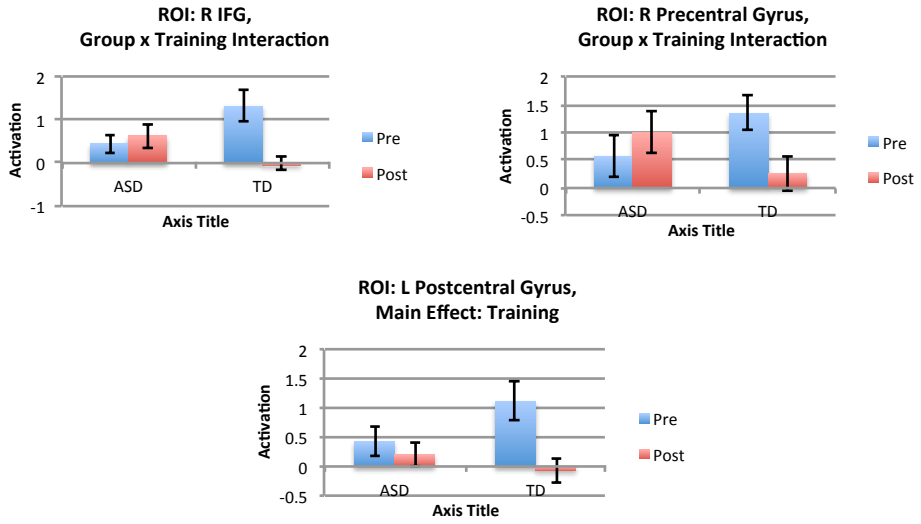

Figure 2.3 Significant main effects and interactions for activation within Task-based ROIs.

In whole brain t-tests of the pre-NFT fMRI data, ASD participants had significantly lower activation compared to the TD group in precuneus, cingulate cortex, bilateral inferior temporal cortex, and left premotor cortex, and right inferior frontal gyrus. After NFT, the ASD participants had significantly higher activation compared to before NFT in the right parietal lobe, while TD participants had widespread lower activation after NFT. In between-group t-tests, the significant differences between the ASD and TD groups seen prior to NFT were absent after NFT. The locations and t-scores for clusters of activation for each group, as well as clusters showing significant group differences are listed in Table 2.4 (pre-NFT) and Table 2.5 (post-NFT), and shown in Figure 2.4A and 2.4B.

Four significant clusters of interaction between group status and training status were observed, located in right inferior parietal lobule, left inferior parietal lobule, right precentral gyrus, and left cuneus (Table 2.4 and

Figure 2.4C). Follow-up t-tests revealed that all of these interactions were driven both by post-NFT increases in activation in the ASD group. As an example, the cluster in right IPL showed this trend (pre-NFT ß mean = -0.25, SEM = 0.13; post-NFT M = 0.71, SEM = 0.23; p = 0.002) and by post-NFT decreases in activation in the TD group (pre-NFT M = 1.24, SEM = 0.45; post-NFT M = -0.20, SEM = 0.24; p = 0.015)

Table 2.4 ANOVA results (group x training status) for Imitation+Observation Contrast. Uncorrected voxelwise threshold p = 0.02. All clusters p < .05 corrected. Coordinates are in standard Talairach space.

Peak Location	Hemisphere	x	y	z	Volume (voxels)	Peak F-score
Inferior Parietal Lobule (BA 40)	R	-44	54	42	224	13.85
Inferior Parietal Lobule (BA 40)	L	37	41	22	79	7.91
Precentral Gyrus (BA 6)	R	-31	7	49	43	14.70
Cuneus (BA 17)	L	20	68	15	40	3.76

Table 2.5 Pre-NFT BOLD activation for Imitation+Observation Contrast. † = subcortical clusters not listed. Uncorrected voxelwise threshold p = 0.0102. All clusters p < .05 corrected. Coordinates are in standard Talairach space.

Group	Peak Location	Hemi	x	y	z	Voxels	Peak t-score
TD†	Mid Occ, pMTS, pSTS	R	-51	68	-5	279	7.45
	Mid Occ, pMTS, pSTS	L	48	61	-2	156	7.80
	Inferior Parietal Lobule (BA 40)	L	31	51	39	40	1.73
	Superior Parietal Lobule (BA 7)	L	31	58	53	35	2.80
	Inferior Frontal Gyrus (BA 45,46)	R	-44	-24	19	34	2.31
	Precuneus	R	-17	75	39	28	3.23
	Inferior Frontal Gyrus (BA 44)	L	41	-4	25	25	1.87
	Precentral (BA 4,6)	R	-44	10	53	20	2.61
	Precentral (BA 4)	L	27	20	66	20	3.25
	Inferior Parietal Lobule (BA 40)	L	34	37	39	16	1.95
ASD	Lateral Occipital	R	-54	64	-2	53	5.52
	Lateral Occipital	L	51	68	5	44	6.91
	Superior Temporal Gyrus	R	-65	37	15	33	3.46
ASD > TD	Precuneus	R	-10	78	43	81	-4.95
	Cingulate Gyrus	L	10	-11	32	68	-1.81
	Inferior Temporal/Lat. Occipital	L	48	58	-16	61	-4.88
	Posterior Cingulate	R	-20	58	-2	35	-2.92
	Cuneus/Calcarine Gyrus	L	10	75	8	33	-2.42
	Fusiform Gyrus	R	-54	58	-9	30	-2.92
	Middle Temporal (BA 21, 22)	R	-54	41	5	28	-2.97
	Precentral Gyrus (BA 4,6)	L	14	27	59	27	-0.94
	Inferior Frontal Gyrus (BA 45, 13)	R	-44	-24	19	25	-2.58

Table 2.6 Post-NFT BOLD activation for Imitation+Observation Contrast. Uncorrected voxelwise threshold p = 0.0102. All clusters p < .05 corrected. † = subcortical clusters not listed. Coordinates are in standard Talairach space.

Group	Peak Location	Hemisphere	x	y	z	Voxels	Peak t-score
TD	Posterior Inferior Temporal	R	-48	68	-5	35	6.79
	Posterior Inferior Temporal	L	51	64	-5	25	12.0
ASD	Posterior Inferior/Middle Temporal	R	-51	68	-5	66	4.86
	Posterior Inferior/Middle Temporal	L	51	68	5	47	7.48
	Inferior Occipital (BA 17)	R	-31	88	-9	22	2.97
	Inferior Occipital (BA 17)	L	24	88	2	18	3.78
	Precentral Gyrus (BA 6)	L	44	7	53	16	2.62
ASD > TD	No significant clusters	-	-	-	-	-	-
ASD only: Post > Pre	Inferior Parietal Lobule (BA 40)	R	-44	51	46	55	1.81
TD only†: Post > Pre	Precentral Gyrus (BA 4,6)	L	27	20	66	221	-3.84
	Precentral Gyrus (BA 6)	R	-34	0	29	86	-2.24
	Inferior Temporal/Lateral Occipital	L	51	61	-2	85	-4.35
	Cuneus	L	7	71	8	68	-2.67
	Middle Temporal	R	-61	41	5	67	-2.82
	Precuneus	R	-14	75	42	66	-4.13
	Supramarginal Gyrus (BA 40)	L	31	47	36	54	-2.05
	Inferior Frontal Gyrus (BA 44)	R	-51	-14	15	41	-2.11
	Inferior Parietal Lobule (BA 40)	L	31	44	42	37	-1.42
	Precentral Gyrus (BA 3)	L	48	20	39	25	-2.27

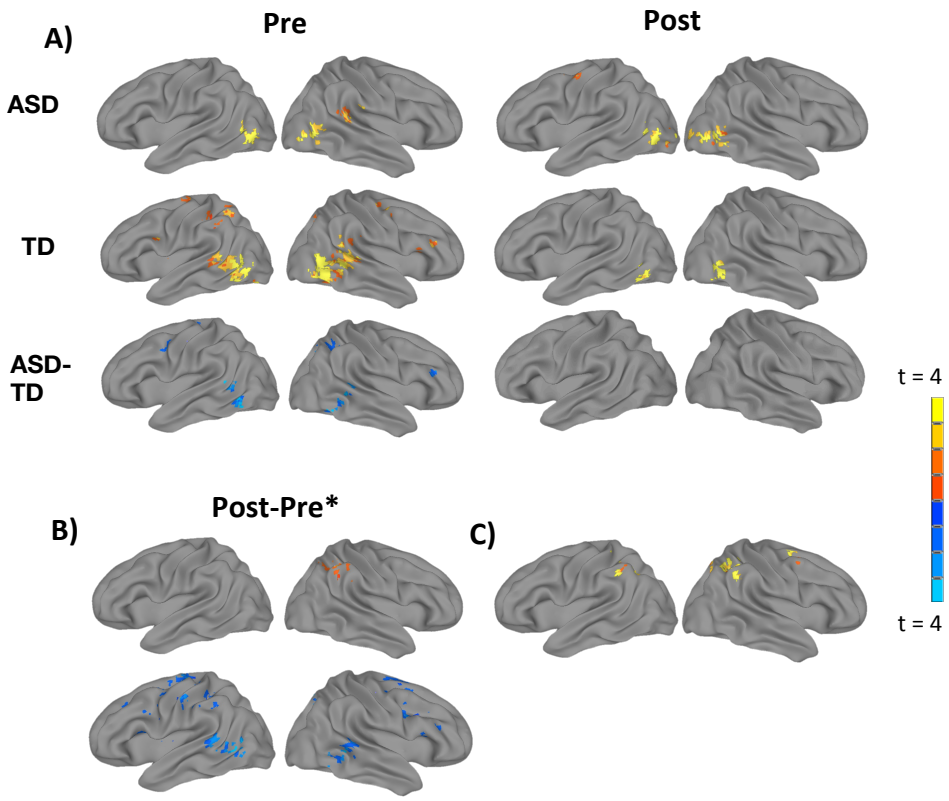

Figure 2.4 Task activation results. A: Pre- and post-NFT brain activation for imitation+observation for ASD, TD, and group differences (TD-ASD). $p<0.05$ corrected. B: Pre- versus post-NFT activation for each group (Top = ASD, Bottom = TD). $P<0.05$ corrected. C: ANOVA interaction between group (TD, ASD) and time (pre-NFT, post-NFT). $p<0.05$ corrected.

Covariance of ASD symptom severity and NFT-related changes in imitation-related brain activation

In a whole-brain t-test in the ASD group, there were two clusters of significant negative correlation between post-NFT vs. pre-NFT task activation and changes in SRS scores. The negative correlation was driven by increases in activation in these clusters and decreases in SRS scores (symptom severity). These clusters were located in left inferior/middle frontal gyrus and left pSTS. These clusters, as well as those for the subsequent clinical and

parental assessments, are shown in Figure 2.5. In a similar test that used the change in ATEC scores as a covariate, seven clusters of significant negative correlation were found. Like with the SRS scores, these correlations were driven by increases in activation and decreases in symptom severity as measured by the ATEC. There were three clusters of negative correlation between post- versus pre-NFT task activation and scores on the ADOS-Sociocommunicative subscale, located in left IPL, right cuneus, and left precentral gyrus. There was one cluster of negative correlation between post- vs pre-NFT activation and scores on the ADI-Social subscale, located in right precentral gyrus (BA 4). For both of these clinical measures, greater NFT-related changes in task activation were related to lower ASD symptom severity. Anatomical labels and spatial coordinates for all clusters in these tests are listed in Table 2.6.

Table 2.7 Areas of activation significantly covarying with diagnostic assessment scores (ASD Only). Uncorrected voxelwise threshold of $p = 0.02$, cluster corrected to $p < .0001$. Coordinates are in standard Talairach space.

Group	Peak Location	Hemi	x	y	z	Volume (voxels)	Peak t-score
SRS	IFG/Precentral Gyrus (BA 9)	L	51	-17	32	104	-0.49
	Middle Temporal Gyrus (BA 37)	L	48	61	2	99	-0.26
ATEC	Superior Parietal Lobule (BA 7)	L	24	68	56	253	-0.69
	IFG (BA 46)	L	51	-17	32	211	-0.40
	IFG (BA 6)	R	-48	-24	29	175	-0.15
	Cerebellum	R/L	3	81	-29	141	-0.74
	Precentral Gyrus (BA 4)	L	41	10	56	101	-0.17
	Superior Parietal Lobule (BA 7)	R	-37	58	56	90	-0.68
	Middle Temporal Gyrus (BA 21)	L	54	17	-12	86	-0.40
ADOS-SC	Inferior Parietal Lobule (BA 40)	L	24	58	56	181	-1.38
	Cuneus (BA 18)	R	-3	75	36	119	-0.60
	Precentral Gyrus (BA 4)	L	41	10	56	100	-0.52
ADI-Soc	Precentral Gyrus (BA 4)	R	-51	10	39	84	-0.38

Table 2.8 Pearson correlations for clinical assessment scores vs. post-pre NFT changes in parental assessment scores. * indicates significance at p<0.05, ** indicates significance at p<0.01.

	Change in ATEC	Change in SRS
ADOS Socio-Comm.	0.75*	0.52
ADI-Social	0.36	0.83**
ADI-Communication	0.55	0.82**

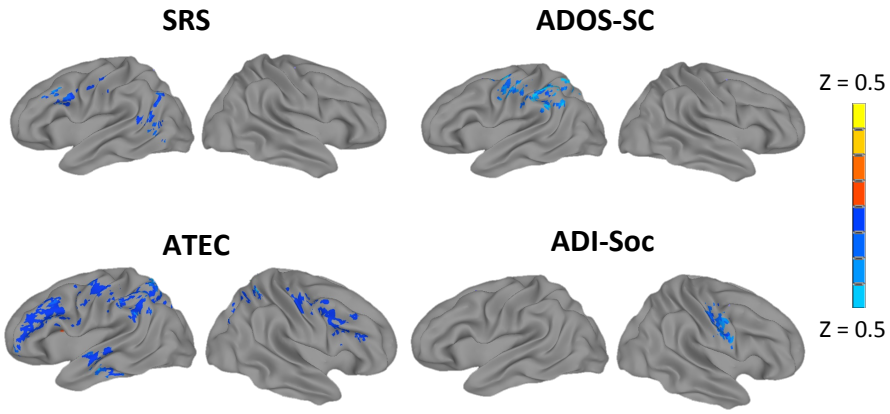

Figure 2.5 ASD group only, correlations of NFT-related activation changes with scores on SRS, ATEC, ADOS Sociocommunicative subscale, and ADI Social subscale. p<0.0001 corrected.

Discussion

This study investigated the effects of 20-30 hours of mu-based neurofeedback training (mu-NFT) on imitation-related brain activation and social behaviors in a group of children and adolescents with high functioning autism spectrum disorders (ASD), compared to a matched group of typically developing (TD) children. As hypothesized, mu-NFT had positive behavioral effects (reduced symptom severity on the ATEC and SRS) in children with ASD, and these benefits were accompanied by – and in fact correlated with – neurophysiological changes following the training.

An initial series of ROI-based ANOVAs between group status and training status revealed some marginally significant main effects of training as well as some significant interaction effects. Both seeds that showed interaction effects in the Caspers set were located in right premotor cortex, medially and laterally. Similarly, in the combined-group activation-based seed set, interaction effects were found in the seeds in right precentral gyrus and right inferior frontal gyrus. All of the p-values for these four interactions ranged between 0.0427 and .013, so they were significant independently but did not survive correction for multiple comparisons. Still, the fact that all observed significant interactions were located in right premotor regions suggests that there could be real effect of NFT in those areas. The strength of this effect might vary within premotor cortex, and the particular ROIs used in this analyses might have missed the true loci of this effect.

Using the imitation+observation contrast activation data, a whole-brain ANOVA revealed significant interaction effects between group status (ASD and TD) and training status (pre-NFT and post-NFT) in areas of the hMNS including bilateral inferior parietal lobule (IPL). Follow-up t-tests revealed that this effect in IPL was driven both by post-NFT increases in activation in the ASD group and by post-NFT decreases in activation in the TD group.

Inferior parietal lobule plays a significant role in sensorimotor integration and is considered a core area of the hMNS (Andersen, 2011; Rizzolatti & Craighero, 2004). It has also been shown to specifically play a role in the

perception and performance of goal-directed action (Bonda et al., 1996). IPL receives input from the visual system via the superior temporal sulcus, and sends outputs to the premotor cortex (BA 6) and inferior frontal gyrus (BA 45) (Andersen et al., 1990). Therefore, the increased activation shown in IPL following NFT suggests that this treatment enhanced visuomotor integration between the core areas of the hMNS during imitation in the ASD group.

Comparing the locations of clusters of significant interaction in the whole-brain ANOVA to the locations of the ROIs from the ROI-based ANOVAs, it is apparent that there was very little direct overlap. None of the Caspers-based ROIs directly overlapped with the whole-brain ANOVA clusters, and only two voxels in the combined-group activation ROIs overlapped. However, three out of the four significant interaction clusters in the whole-brain ANOVA were in the same functional area as some of the regions used for the ROI-based ANOVAs, including those found in bilateral inferior parietal lobule and in right precentral gyrus. Thus, the lack of highly significant group interactions in the ROI-based ANOVAs may have resulted from this slight discrepancy between the exact locations of NFT-related effects and the exact locations chosen for the 7mm spherical seeds.

Not only did these findings include increased imitation-related brain activation in the ASD group following NFT, they also showed co-occurring positive changes in social and adaptive behaviors. In the ASD group, but not the TD group, there were significant improvements on SRS scores following

NFT, indicating that the benefits conferred by mu-NFT may specifically benefit the neurophysiological substrates of high-functioning ASD. The ASD group also showed significant improvements on the ATEC, a commonly used measure of the effectiveness of cognitive and behavioral interventions in ASD. Taken together, these neurophysiological and behavioral findings indicate that NFT improved the functionality of the hMNS, resulting in greater recruitment of previously underutilized areas, and that these neurofunctional changes were linked to improvements in core ASD symptomatology.

The finding of a significant interaction between training status, hMNS activation, and NFT-related changes in ATEC scores suggests that the behavioral improvements previously observed with NFT (Pineda et al. 2008; Pineda et al., 2014) have a neurophysiological basis in hMNS areas. In follow-up t-tests, this interaction was driven primarily by increases in hMNS activation, as well as improvements in ATEC scores, in the ASD group after training. Together with the finding of changes in SRS, this suggests that increases in hMNS activation resulting from mu-NFT are accompanied by positive changes in parental assessments of social and personal behavior.

There was an interaction between pre-training ADOS and ADI scores and the magnitude of functional activation changes following the training. However, contrary to expectations, greater NFT-related changes were negatively correlated with these two measures of ASD symptom severity. A Pearson test revealed no correlation between ASD symptom severity on the

ADOS and hours of training completed ($r = 0.02$), meaning it was unlikely that the ADOS/ADI correlations with task activation changes were simply the result of early attrition in lower-functioning participants. Taken together, these findings suggest that the particular regimen of NFT used in this study is specifically beneficial to individuals on the highest end of the functional spectrum of ASD.

Interestingly, in the TD group, NFT was associated with activation changes opposite to those seen in the ASD group (i.e., reduced activation in clusters across frontal, parietal, and temporal lobes). Although there were no significant changes in behavioral measures in the TD group, this finding may reflect increased efficiency of hMNS functioning during performance on the imitation task.

One limitation of the present study was the lack of a sham treatment condition. Parents were aware that their children received an active treatment, and expectation of behavioral improvements may have affected their ratings on SRS and ATEC questionnaires. However, the finding of correlations between improvements in caretaker assessments of behavior and changes in brain activation suggests that the behavioral changes do in fact have an underlying neurophysiological basis. The study also had a relatively small final sample size due to time-consuming nature of the NFT procedure (across many sessions and weeks) and associated attrition, as well as excessive head motion in some participants. However, detection of significant group and post-

training differences even in this relatively small sample size suggests that NFT effects may be very robust. A final limitation was the discrepancy in total hours and frequency of training completed by each group. The TD group completed significantly fewer total hours of training and had lower training density (hours of training per month) than the ASD group. The finding of increased activations exclusively in the ASD group could result from the greater amount and frequency of training received by that group. If true, this would also mean that the benefits of NFT are not necessarily exclusive to ASD, but are simply time-dependent and not group-dependent. A series of follow-up Pearson correlations between changes in activation in areas of group by timepoint interaction effects and hours of training completed did not yield significant groupwise correlations (ASD average $r = 0.50$, ASD average $p = 0.14$; TD average $r = -0.43$, TD average $p = 0.33$). Therefore, it is not likely that the groupwise difference in hours of training was a major factor in the brain activation differences.

Our findings suggest that mu-NFT has significant positive effects on social behaviors, as well as on neurofunctional substrates underlying those behaviors, in children and adolescents with ASD. Future studies involving larger sample sizes and sham-training control groups may provide more evidence supporting the use of mu-NFT in clinical settings.

Chapter 2 is currently being prepared for submission for publication by Mike Datko, Jaime Pineda, and Ralph-Axel Müller. The dissertation author was the primary investigator and first author of this paper.

Chapter 3: Changes in Functional Connectivity and Behavior Following Mu Neurofeedback Training in Children with Autism

Introduction

A great deal of evidence links the symptomatology of autism with aberrant function and connectivity of brain networks (Belmonte et al., 2004; Kana et al., 2011; Schipul et al., 2011). Functional connectivity MRI (fcMRI) is one useful method for studying brain networks in vivo in humans. FcMRI uses correlations between the BOLD signal in distinct anatomical regions as a measure of the extent to which those areas function together as a network. In 1995, Biswal and colleagues were the first to observe that low-frequency fluctuations of the BOLD signal were correlated between areas involved in finger movement, even during a resting state when no actual movement was being performed (Biswal et al., 1995). It has since been demonstrated that this finding extends beyond the motor system, and a general principle has emerged that brain areas and networks that typically co-activate during cognitive and behavioral tasks also tend to show correlated low-frequency BOLD fluctuations in a resting state (Fox & Raichle, 2007).

Functional connectivity has since become a vital subfield of neuroimaging research, and in particular it has led to important advances in the study of the neurophysiology of autism. ASD is characterized by impairments or abnormalities in specific types of behaviors, and those

behavioral impairments have been linked to underlying patterns of atypical network connectivity. Several meta-analyses of studies of functional connectivity in ASD describe a field with mixed and sometimes inconsistent results (Belmonte et al., 2004; Müller, 2007, 2011; Anagnostou & Taylor, 2011; Vissers et al., 2012; Wass, 2011). Initial studies of functional connectivity in ASD reported underconnectivity between various networks in ASD (Just et al., 2004, Welchew et al., 2005), and these studies were the first to suggest that ASD is fundamentally a disorder of disrupted network connectivity. Underconnectivity in ASD has been shown between areas of the dorsal attention network including the human mirror neuron system during tasks involving visuomotor coordination (Villalobos et al., 2005), as well as between areas involved in inhibitory control during a response inhibition task (Kana et al., 2007). Other studies have shown intrinsic underconnectivity in a resting state in ASD, including between the insula and areas involved in emotion processing (Ebisch et al. 2011)

A number of studies have since appeared challenging the view that autism is only associated with network underconnectivity. One view is that long-range synchrony (between cortical areas located far apart from each other) is reduced in ASD, while short-range synchrony (between cortical areas located next to each other) are increased (Belmonte et al., 2004; Courchesne & Pierce, 2005; Barttfeld et al., 2011). In addition to initial studies of long-range underconnectivity discussed earlier, a more recent study shows local

overconnectivity specifically in posterior regions (Keown et al., 2013). However, support for this hypothesis of long-range hypoconnectivity and local hyperconnectivity is not unanimous; indeed, a study focusing on long-range connections with visual cortex showed overconnectivity in ASD (Keehn et al., 2012). Studies of the default mode network in autism have alternatively found both overconnectivity (Lynch et al., 2013; Redcay et al., 2013) and underconnectivity (Assaf et al., 2010; von dem Hagen et al., 2013). A consistent pattern found across several studies of DMN connectivity in ASD is underconnectivity between medial prefrontal and posterior cingulate cortices, accompanied by overconnectivity with regions outside the DMN (Monk et al., 2009; Abbott et al., 2015). In networks related to social cognition, one study found overconnectivity between the hMNS and the theory of mind network (which overlaps with parts of the DMN), accompanied by underconnectivity within those networks (Fishman et al., 2014). One view that has emerged from this consistent pattern of findings is that several networks not only display reduced within-network integration in ASD, but are also less functionally distinct from other networks (Rudie et al., 2012). Another perspective is based on findings of developmental differences in the balance of over- and underconnectivity in ASD; more specifically, this view holds that early ASD development is characterized more by overconnectivity, whereas in adolescence there is predominantly underconnectivity (Uddin et al., 2013).

Although some of the variability across these studies of FC in ASD can

be attributed to phenotypic heterogeneity in the ASD population, other possible sources include a lack of standard protocols for data collection, preprocessing, and analysis in the ASD neuroimaging field. In one meta-analysis, Müller et al. (2011) showed that findings of underconnectivity were significantly more common in studies that failed to perform particular preprocessing steps, including task-regression in studies of task-related scans, applying a lowpass or bandpass filter to the voxelwise timeseries, and using a whole-brain field-of-view for statistical comparisons. The same paper reported that other analysis variables were not statistically associated with over- or underconnectivity results; namely, global signal regression, and whether connectivity regions of interest (or seeds) were based on areas active during a task in the TD group specifically. A related, more recent paper applied various FC preprocessing and analyses pipelines to three datasets, and found that bandpass filtering, method of seed selection, and field of view were factors that significantly affected results (Nair et al., 2014). It appears that the heterogeneity of FC findings in ASD is the result of many factors ranging from study design, preprocessing, and analysis, to developmental differences, to the particular networks being examined in a given study.

In Chapter 2 it was shown that 20 or more hours of mu-NFT can lead to increases in activation of brain areas involved in social cognition and action imitation in children with autism. Since areas that co-activate together during a task have consistently been found to have correlated fluctuations during a

resting state, the results from Chapter 2 lead directly into the question of whether the functional connectivity of the networks underlying imitation is also changed or normalized after NFT.

Since there is a dynamic, mutually causal link between neuronal oscillations and behavior, and since NFT can induce lasting changes in neuronal oscillations (Pineda et al., 2008, 2014; Friedrich et al., 2014, 2015), it is possible that the positive behavioral changes that result from NFT are linked to increased correlation of neuronal oscillations in key brain networks.

It was hypothesized that NFT would lead to greater resting state functional connectivity between areas of the human mirror neuron system, as well as other areas related to action observation, imitation, and social cognition. It was further hypothesized that increases in FC following NFT would be positively correlated with behavioral improvements in ASD individuals.

Methods

Participants

17 ASD and 11 TD participants were initially recruited for the study, and this sample was identical to the sample reported on in Chapter 2. There were however different exclusion criteria for this study, based on head motion during the resting state scans as opposed to the imitation task scans. Of those initial

participants, 8 ASD and 7 TD participants remained for the final resting state analysis after excluding those who had excessive head motion (defined as having any head movements exceeding 1.5 mm) and those that did not complete post-NFT scans. These remaining subjects were matched for age, handedness, sex, and head motion, and their demographic information and clinical assessment scores are summarized in Table 3.1.

Clinical diagnoses were confirmed with the Autism Diagnostic Interview–Revised (ADI-R) (Rutter et al., 2003), the Autism Diagnostic Observation Schedule (ADOS) (Lord et al., 2001), and clinical assessment based on the DSM-IV criteria for ASD. Participants in the TD group had neither reported personal or family history of ASD nor any reported history of other neurological or psychiatric conditions. Informed assent and consent was obtained from all participants and their caregivers in accordance with the University of California, San Diego and San Diego State University Institutional Review Boards.

Table 3.1 Participant demographic and diagnostic information

	ASD (n=8) *M* ± SEM [range]	**TD (n=7)** *M* ± SEM [range]	**TD vs. ASD** *p*
Gender (M/F)	5/3	5/2	0.71
Handedness (R/L)	7/1	6/1	0.92
Age (years)	13.40 ± 1.2 [9.3-18.3]	11.3 ± 1.1 [8.6-16.7]	0.23
Verbal IQ	93 ± 7.4 [55-121]	112 ± 3.5 [97-127]	0.051
Non-verbal IQ	88.7 ± 6.8 [62-116]	113 ± 4.6 [103-137]	0.013*
Full-scale IQ	93.75 ± 7.5 [56-118]	116 ± 3.5 [104-130]	0.03*
ADOS Social+Comm.	12.1 ± 2.2 [3-22]		
ADI-R Social	14.3 ± 3.06 [6-28]		
ADI-R Comm.	14.6 ± 2.5 [4-23]		
SRS Total, Pre-NFT	76.1 ± 3.8 [58-90]	38.2 ± 1.4 [35-46]	< 0.0001
SRS Total, Post-NFT	66 ± 3 [56-78]	38.9 ± 0.91 [35-42]	< 0.0001
SRS Total post- vs. pre-NFT	p = 0.028*	p = 0.69	
ATEC Pre-NFT	36.6 ± 5.3 [15-65]		
ATEC Post-NFT	24.3 ± 3.7 [7-45]		
ATEC post- vs. pre-NFT	p = 0.038*		
RMSD, FC Head-motion, Pre-NFT	0.09 ± 0.02 [0.03-0.20]	0.11 ± 0.03 [.03-.21]	0.58
RMSD, FC Head-motion, Post-NFT	0.10 ± 0.03 [0.04-0.25]	0.07 ± 0.01 [0.04-0.11]	0.28
Hours of NFT completed	25.1±1.8 [14.75-30]	17.2 ± 2 [9-21.5]	0.012*

Data collection

Data for this study were collected concurrently with the data from the study in Chapter 2, with exactly the same group of participants during the same fMRI sessions, both before and after NFT. All participants completed the same neurofeedback training protocol.

All MRI data were acquired on a GE 3T MR750 scanner with an 8-channel head coil. High-resolution structural images were acquired with a standard FSPGR T1-weighted sequence (TR: 11.08ms; TE: 4.3ms; flip angle: 45°; FOV: 256mm; 256 x 256 matrix; 180 slices; $1mm^3$ resolution).

Resting state scans were acquired for each participant both before and after NFT. Each scan lasted 6 minutes, and consisted of 180 whole-brain volumes acquired in 42 interleaved slices using a single-shot, gradient-recalled, echo-planar pulse sequence (TR: 2000ms; TE: 30ms; flip angle: 90°;

64 × 64 matrix; 3.2mm slice thickness; in-plane resolution 3.4mm^2).

Cardiac and respiratory data were collected for each participant during each resting state scan using GE's proprietary physiological monitoring system. These data were used as regressors for removing physiological noise from the functional data.

Data preprocessing

Preprocessing and analysis of the data was performed primarily with the Analysis of Functional Neuroimages software suite [AFNI; Cox, 1996]. After initial reconstruction and slice-time correction of whole-brain volumes from slices, data were reregistered from native space to Talairach space and functional data were resampled to isotropic 3.4mm^3 voxels. Data were then spatially smoothed to a global full-width at half-maximum (FWHM) of 6 mm, using AFNI's 3dBlurToFWHM.

White matter and ventricular signal regression was performed for all FC data on the individual subject level. For each individual scan, the BOLD timeseries (180 timepoints) was extracted from a mask containing 6 clusters located only in major white matter pathways (with a total volume of 96 voxels) located in major white-matter pathways in each participant's brain. A similar procedure was performed for ventricular regression, but the signal was extracted from seeds located in the lateral ventricles with a total volume of 8 voxels.

Conventional motion correction was performed for all functional scans using AFNI's 3dvolreg command. Additionally, considering the known impact of head motion on BOLD signal correlations in functional connectivity analyses (Power et al., 2012; Van Dijk et al., 2012), further steps beyond conventional motion correction were taken. Six rigid-body motion parameters, estimated based on realignment of functional volumes, were modeled as nuisance variables and their contribution to the overall signal was removed via linear regression. Time points with excessive motion (defined as motion exceeding 1.5mm displacement from one time point to the next), along with the 10 time points immediately before and after, were censored so as to exclude them from the final statistical analysis. Though it has been shown (Power et al., 2012) that setting this motion threshold as low as possible is optimal for avoiding motion-related artifact, setting the threshold for the current dataset below 1.5mm would have resulted in an unacceptable loss of data and reduction in statistical power.

The final preprocessing step before the functional connectivity analysis began was the application of a bandpass filter (from .008 Hz to .08 Hz) to each participant's resting state time series. This step reduces the contribution of individual cognitive events and isolates the "intrinsic" fluctuations of blood flow (Cordes et al., 2001; Fox & Raichle, 2007). An identical bandpass filter was applied to the head-motion and physiological (cardiac and respiratory) data associated with each of these scans.

Seed-based functional connectivity analysis

Seed-based functional connectivity (FC) analysis was performed on each participant's resting state scan, both before and after NFT. Two sets of regions-of-interest, or seeds, were created for these analyses: one was based on a meta-analysis review of areas that activate most often across studies of imitation and action observation (Caspers et al., 2010) (these are shown in Figure 3.1), and another was based on areas activated specifically in the imitation task used for the study in Chapter 2 of this dissertation. For reference, the meta-analysis-based seeds will be referred to hereafter as the "Caspers" seeds and the task-activation-based seeds will be referred to as "task" seeds. This dual-analysis approach was performed in the interest of providing results that were both dataset-specific, in the case of the activation-based seeds, as well as generalizable to the literature, in the case of the meta-analysis-based seeds.

For both sets of seeds, each seed was a sphere with a radius of 7mm, which equaled approximately 38 voxels at the resampled resolution of the functional scans ($3.4mm^3$). The Caspers set consisted of fourteen seeds with center coordinates identical to those listed in Table 3 of the meta-analysis of imitation studies (Caspers et al., 2010). While that paper listed coordinates in MNI space, the center coordinates for the present study were converted to Talairach space using the following transformation (based on a formula posted

to an SPM mailing list in 1998 by Andreas Meyer-Lindenberg, of NIMH): $X_{TLRC} = (0.88*X_{MNI}) - 0.8$; $Y_{TLRC} = (0.97*Y_{MNI})-3.32$; $Z_{TLRC} = (0.05*Y_{MNI})+(0.88*Z_{MNI})-0.44$. The locations of these seeds, and the original MNI coordinates from the Caspers review are listed in Table 3.2.

For the second set of seeds, center coordinates were identical to the centers of clusters of activation during the imitation task from Chapter 2. To avoid possibly biasing the connectivity values towards either group, the seeds were based on the task-activation data from both ASD and TD groups combined. The seeds were derived from activation clusters that passed an initial uncorrected threshold of $p = 0.002$ and were cluster corrected to $p<0.00001$. This threshold yielded a total of 11 clusters, 7 of which were in cerebral cortex and 4 of which were subcortical or cerebellar. The centers of mass for each of the 7 cerebral cortex clusters were used as the center coordinates for the seed spheres, which were created using AFNI's 3dcalc command. The center coordinates of the task seeds are also listed in Table 3.2.

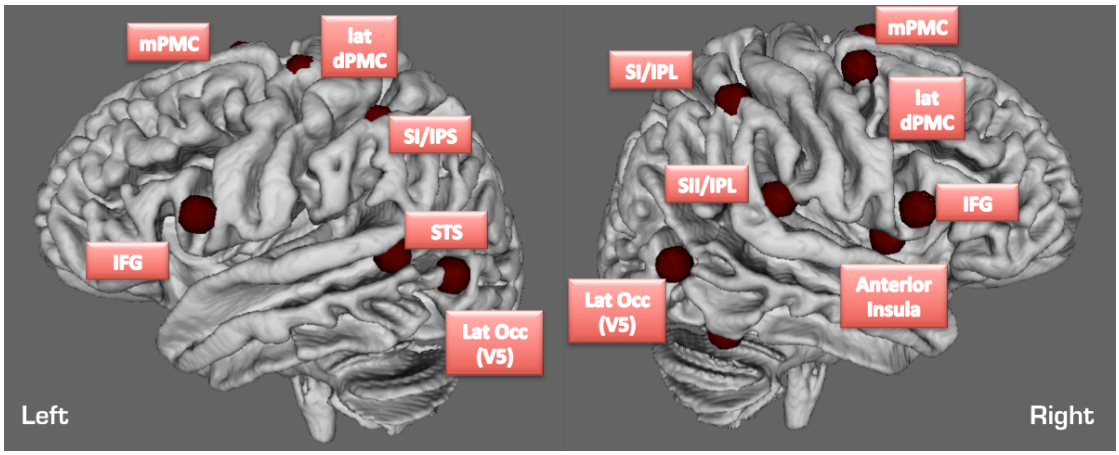

Figure 3.1 Seeds derived from the Caspers ALE meta-analysis.

Table 3.2 Center coordinates for seeds used in FC analyses

		Talairach coordinates			MNI coordinates		
Region	**Hemi**	**x**	**y**	**z**	**x**	**y**	**z**
Seeds Derived from Imitation Meta-Analysis							
Inferior Frontal Gyrus	L	52	-15	11	60	-12	14
Inferior Frontal Gyrus	R	-52	-19	8	-58	-16	10
Lat. Dorsal Premotor	L	31	10	55	36	14	62
Lat. Dorsal Premotor	R	-38	-7	49	-42	-4	56
Med. Premotor	L	0	-15	45	1	-12	52
Med. Premotor	R	-13	-9	57	-14	-6	66
Intraparietal Sulcus	L	33	35	46	38	40	50
Inferior Parietal Lob.	R	-47	32	47	-52	36	52
Sup.Temporal Sulcus	L	47	45	11	54	50	10
Inferior Parietal Lob.	R	-54	22	18	-60	26	20
Lat. Occipital	L	45	65	8	52	70	6
Lat. Occipital	R	-48	59	6	-54	64	4
Anterior Insula	R	-38	-7	0	-42	-4	1
Fusiform Face Area	R	40	49	-17	-44	54	-22
Seeds Derived from Imitation Task							
Post. Mid. Temporal	R	-49	54	4			
Post. Mid. Temporal	L	47	57	4			
Inferior Frontal Gyrus	R	-46	-16	16			
Precentral gyrus	R	-40	9	47			
Postcentral gyrus	L	52	22	28			
Inferior Parietal Lob.	R	-33	46	47			
Superior Parietal Lob.	L	27	52	47			

Next, the average time series for the voxels in each seed was extracted for each participant (this step, and all others that follow, were repeated for both the Caspers and Task seed sets separately). Then, the correlation between each individual's average timeseries for each seed and the timeseries for every voxel in the brain was obtained. Finally, Fisher's R-Z transformation

was performed on all resulting whole-brain correlation maps, transforming the voxelwise R correlations into their hyperbolic arctangents and simulating a more normally distributed dataset.

Finally, a series of pairwise tests was performed to assess changes in seed-based FC following NFT. All whole-brain T-test results (between groups: ASD vs TD Pre-NFT, ASD vs TD Post-NFT; within-groups: ASD post-NFT vs ASD pre-NFT, TD post-NFT vs TD pre-NFT) presented here passed an initial uncorrected threshold of $p = 0.001$ and then passed cluster-level correction for multiple comparisons at $p < 0.01$. All whole-brain ANOVA results (interaction effects and main effects of NFT status) presented here passed an initial uncorrected threshold of $p = 0.02$ and then were significant after cluster-level correction for multiple comparisons at $p < 0.05$.

Results

FC Analyses with ALE Meta-Analysis-based seeds

For the literature-based seed set (Caspers et al., 2010), in within-group t-tests between post-NFT versus pre-NFT scans in each participant group, both groups appeared to show general increases in connectivity following NFT. Many of these clusters of increased post-NFT connectivity were found either in regions that directly overlapped the seeds of the imitation network, or in regions that are commonly considered part of the hMNS or action-observation network. For example, in the right lateral occipital seed, the TD

group had significantly greater connectivity after NFT compared to before in a cluster located in left inferior parietal lobule. The ASD group showed some comparable effects: the seed in right insula had increased FC after the training compared to before in a cluster located in right inferior parietal lobule. Clusters that significantly differed pre- vs. post-NFT in the ASD group are shown in Figure 3.1, and the locations of these clusters are summarized in Table 3.2 (ASD) and Table 3.3 (TD).

In between-group tests prior to NFT, several seeds in the Caspers imitation network showed primarily overconnectivity in the ASD group compared to TD, and these clusters were located largely outside the imitation network. For example, the right medial premotor cortex (SMA) seed had a cluster of ASD-overconnectivity located in left prefrontal superior frontal gyrus, and the left lateral dPMC seed had a cluster of ASD-overconnectivity located medial frontal cortex. There were no clusters of ASD-underconnectivity for any of the Caspers seeds prior to NFT. Pre-NFT results are summarized in Table 3.4 and shown in Figure 3.3.

After NFT, several different clusters of overconnectivity in ASD were observed, but a large majority of them were located inside the imitation network instead of outside. Thus, the general outside-network overconnectivity that had been observed prior to the training had shifted to inside-network overconnectivity. For instance, the seed in right SI/IPL had an ASD-overconnected cluster in the right Fusiform gyrus, located directly within

the radius of the right FFA imitation network node. The post-NFT group differences in connectivity are summarized in Table 3.6.

Following NFT, there were several clusters based on several of the seeds that showed a main effect of training status (pre- vs post-NFT). These were regions where connectivity increased regardless of group status, which is evidence that NFT had at least some effects on functional connectivity regardless of autism symptom severity. Two of these clusters with a main effect of training status were located within the radius of seeds of the imitation network: one was located in right IPL and was based on the seed in right anterior insula, while the other was located in left motor/premotor cortex (BA 4 and 6) and based on the seed in right medial premotor cortex. These main effects are summarized in Table 3.7.

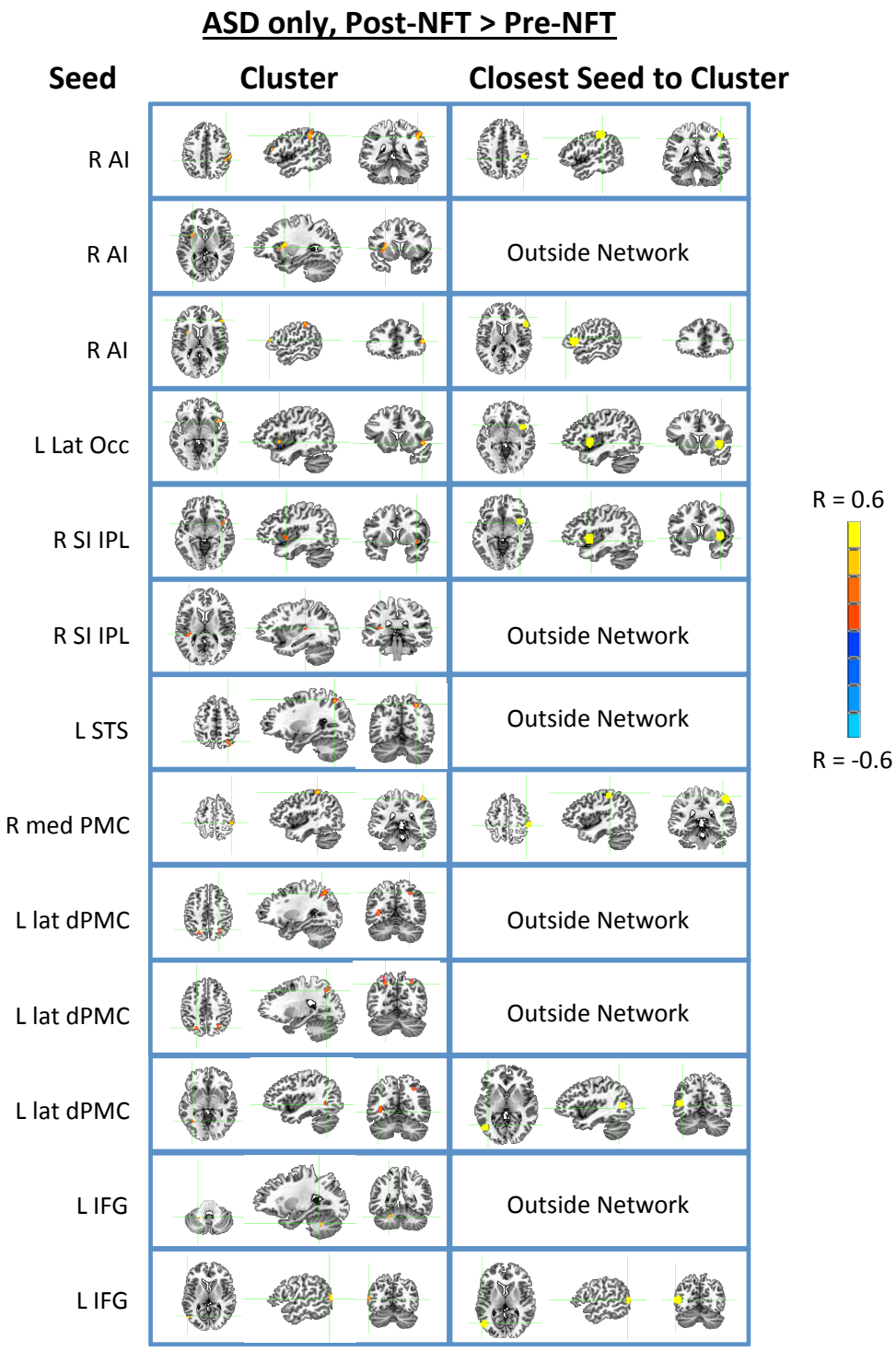

Figure 3.2 Clusters of significant differences in functional connectivity within the **ASD group only, post-NFT > pre-NFT**, for seeds of the Caspers imitation network. For clusters that fall within the regions included in the Caspers seeds, the closest seed within that network is shown adjacent to the cluster. All clusters passed an uncorrected voxelwise threshold of $p = 0.001$ and were cluster corrected for multiple comparisons at $p < 0.01$.

Table 3.3 Caspers imitation seeds showing significant differences **ASD post- > pre-NFT.** Clusters that are located within the imitation network are shown in **green**, clusters are located outside the network are shown in **red**, and clusters that are located on the same gyrus or the same functional region as a seed in the imitation network are shown in **blue**. Results reported for an uncorrected voxelwise threshold of p = 0.001, and cluster correction for multiple comparisons at p < 0.01.

Cluster (*Brodmann Areas*)	**% of**	**Vol.**		**MNI coordinates**		
Subregions	**cluster vol.**	**(μl)**	**t-score***	**x**	**y**	**z**
Seed: Right Anterior Insula						
Right Inferior Parietal Lobule (*BA 40*)		1572	3.60	-52	35	40
R IPL	81.8%					
R Supramarginal Gyrus	10.8%					
R Postcentral Gyrus	7.4%					
Left Insula (*BA 13*)		825	3.83	29	-8	9
L Insula	55.8%					
L Putamen	5.1%					
Right Inferior Frontal Gyrus (*BA 46*)		432	4.63	-21	-33	13
R IFG (p. Triangularis)	100%					
Seed: Left Lateral Occipital Cortex (V5)						
Right Insula (*BA 13*)		707	3.35	-45	-13	-3
R Insula	49.9%					
R Temporal Pole	24.5%					
R IFG (p. Orbitalis)	12.5%					
Seed: Right SI / IPL						
Right Insula (*BA 13*)		472	3.30	-42	-7	-2
R Insula	94.2%					
R Temporal Pole	1.2%					
Left Sup. Temporal Gyrus (*BA*)		472	4.97	35	32	10
L Sup. Temporal Gyrus	34.0%					
L Heschls Gyrus	17.7%					
Seed: Left Superior Temporal Sulcus						
Right Superior Parietal Lobule (*BA 7*)		472	4.57	-27	63	47
R SPL	88.4%					
R Angular Gyrus	11.6%					
Seed: Right medial PMC (SMA)						
Right Postcentral Gyrus(*BA 40*)		668	4.76	-41	34	54
R Postcentral Gyrus	99.3%					
R IPL	0.7%					
Seed: Left lateral dPMC						
Right Superior Parietal Lobule (*BA 7*)		629	4.64	-27	62	44
R SPL	49.9%					
R Angular Gyrus	41.2%					
R Sup. Occipital Gyrus	8.9%					
Left Superior Parietal Lobule (*BA 7*)		590	5.38	22	65	47
L SPL	100%					
Left Middle Occipital (*BA 18*)		511	4.64	34	56	3
L Middle Occipital Gyrus	10.8%					
L Middle Temporal Gyrus	8.3%					

Table 3.3 (continued) Caspers imitation seeds showing significant differences **ASD post- > pre-NFT**

Cluster (*Brodmann Areas*)	% of	Vol.		MNI coordinates		
Subregions	cluster vol.	(μl)	t-score*	x	y	z
Seed: Left IFG						
Left Cerebellum		472	3.63	21	49	-29
L Cerebellum	36.9%					
Left Middle Temporal (*BA 39, 37*)		432	5.08	50	66	11
L Middle Temporal Gyrus	72.8%					

Table 3.4 Caspers imitation seeds showing significant differences, **TD post- > pre-NFT.** Clusters that are located within the imitation network are shown in **green**, clusters are located outside the network are shown in **red**, and clusters that are located on the same gyrus or the same functional region as a seed in the imitation network are shown in **blue**. Results reported for an uncorrected voxelwise threshold of p = 0.001, and cluster correction for multiple comparisons at p < 0.01.

Cluster (*Brodmann Areas*)	% of	Vol.		MNI coordinates		
Subregions	cluster vol.	(μl)	t-score*	x	y	z
Seed: Right Lateral Occipital						
Left Inferior Parietal Lobule (*BA 40*)		432	3.81	44	35	46
L Postcentral Gyrus	53.4%					
L IPL	46.6%					
Seed: Left Lateral Occipital (V5)						
Left Cingulate (*BA 24*)		629	6.91	0	9	37
L Middle Cingulate Cortex	73.1%					
R Middle Cingulate Cortex	23.7%					
Seed: Right SI / IPL						
Left Middle Temporal Gyrus (*BA 21,22*)		1454	4.32	50	30	-1
L Middle Temporal Gyrus	73.5%					
L Superior Temporal Gyrus	8.7%					
Right Insula (*BA 13*)		707	3.67	-38	-11	4
R Insula	81.0%					
R IFG (p. Orbitalis)	3.1%					
R Temporal Pole	1.7%					
Left Insula (*BA 13*)		707	5.10	29	-13	11
L Insula	88.6%					
L IFG (p. Triangularis)	3.8%					
L Putamen	1.3%					
Left Medial Frontal (*BA 10,9*)		707	4.87	3	-56	16
L Sup. Medial Gyrus	95.2%					
R Sup. Medial Gyrus	4.8%					
Left Medial Frontal (*BA 10*)		668	3.98	4	-52	-6
L Rectal Gyrus	55.6%					
L Mid Orbital Gyrus	44.4%					
Left Inferior Frontal Gyrus (*BA 44,45*)		590	4.50	46	-17	18
L IFG (p. Triangularis)	83.2%					
L IFG (p. Opercularis)	16.8%					

Table 3.4 (continued) Caspers imitation seeds showing significant differences, **TD post- > pre-NFT.**

Cluster (*Brodmann Areas*)	% of	Vol.		MNI coordinates		
Subregions	cluster vol.	(*μ*l)	t-score*	x	y	z
Seed: Left Superior Temporal Sulcus						
Right Cerebellum		511	3.67	-33	45	-25
R Cerebellum	100%					
Seed: Left SI / IPS						
Left Middle Temporal Gyrus (*BA 21,22*)		1258	3.34	45	32	-1
L Middle Temporal Gyrus	48.3%					
L Superior Temporal Gyrus	3.4%					
L Inferior Temporal Gyrus	1.5%					
Right Cerebellum		865	4.06	-21	69	-41
R Cerebellum	100.0%					
Left Inferior Frontal Gyrus (*BA 45,46*)		747	3.84	50	-29	8
L IFG (p. Triangularis)	88.2%					
L IFG (p. Opercularis)	3.2%					
Left Inferior Frontal Gyrus 2 (*BA 44,45*)		550	4.77	48	-18	19
L IFG (p. Triangularis)	93.1%					
L IFG (p. Opercularis)	6.9%					
Right Middle Temporal Gyrus (*BA 21*)		432	3.63	-49	10	-11
R Middle Temporal Gyrus	70.1%					
R Sup. Temporal Gyrus	11.6%					
Seed: Left Lateral dPMC						
Left Cerebellum		550	5.66	9	81	-30
R Lingual Gyrus	86.6%					
Left Inferior Frontal Gyrus (*BA 46*)		432	4.20	47	-16	21
L IFG (p. Triangularis)	79.4%					
L IFG (p. Opercularis)	20.6%					
Seed: Right IFG						
Occipital (*BA 18*)		2201	4.10	-3	70	0
R Lingual Gyrus	45.0%					
L Lingual Gyrus	27.5%					
L Calcarine Gyrus	11.9%					
R Calcarine Gyrus	5.7%					
Seed: Left IFG						
Right Medial Frontal Gyrus (*BA 11*)		629	2.81	-12	-48	-10
R Sup. Orbital Gyrus	58.2%					
R Rectal Gyrus	39.4%					
Left Medial Frontal Gyrus (*BA 10,11*)		590	3.98	6	-51	-8
L Rectal Gyrus	64.6%					
L Sup. Orbital Gyrus	18.6%					
L Mid Orbital Gyrus	16.8%					

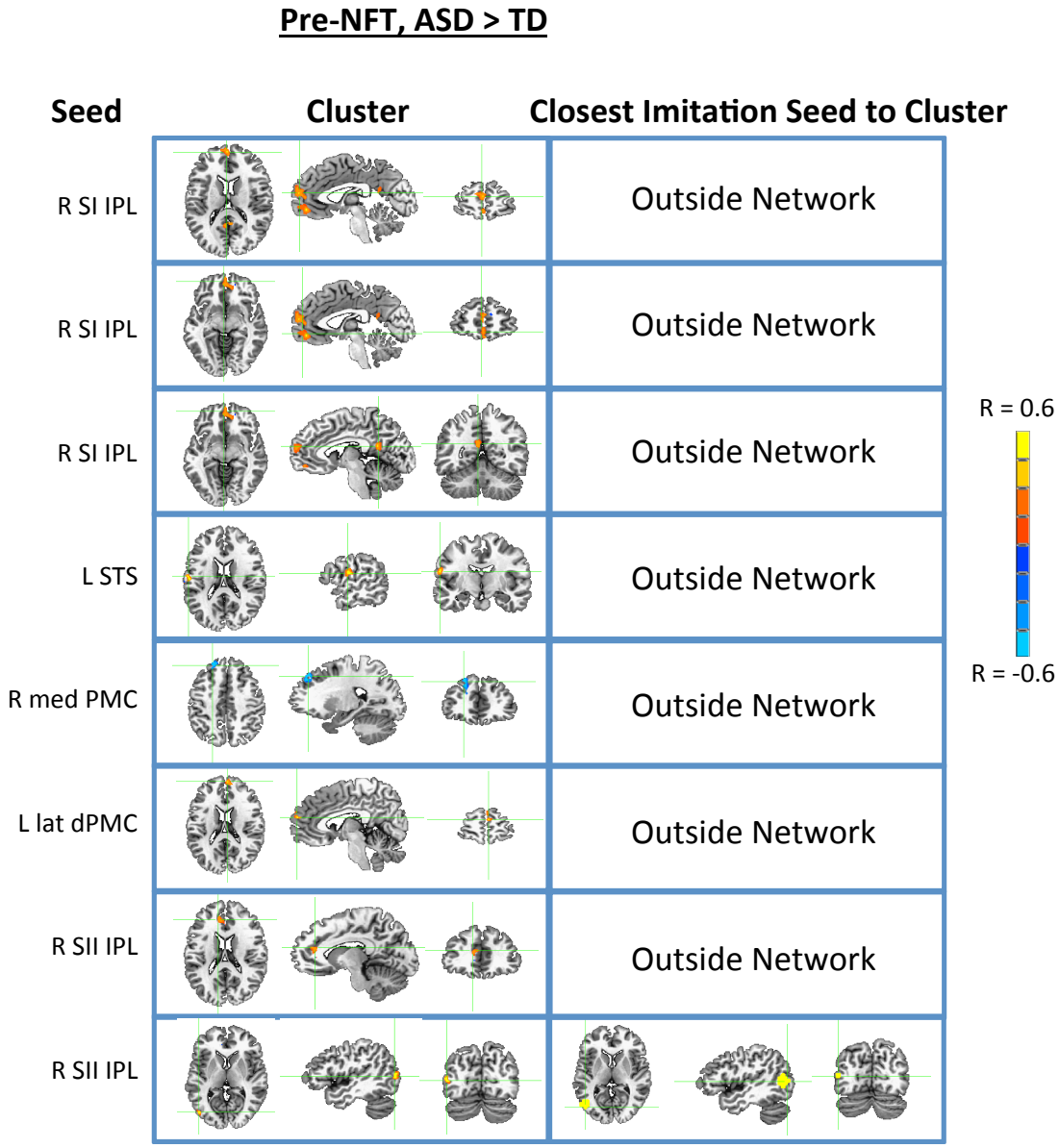

Figure 3.3 Clusters of significant differences in functional connectivity between **ASD vs. TD**, for seeds of the Caspers imitation network, **pre-NFT**. For clusters that fall within the regions included in the Caspers seeds, the closest seed within that network is shown adjacent to the cluster. All clusters passed an uncorrected voxelwise threshold of $p = 0.001$ and were cluster corrected for multiple comparisons at $p < 0.01$.

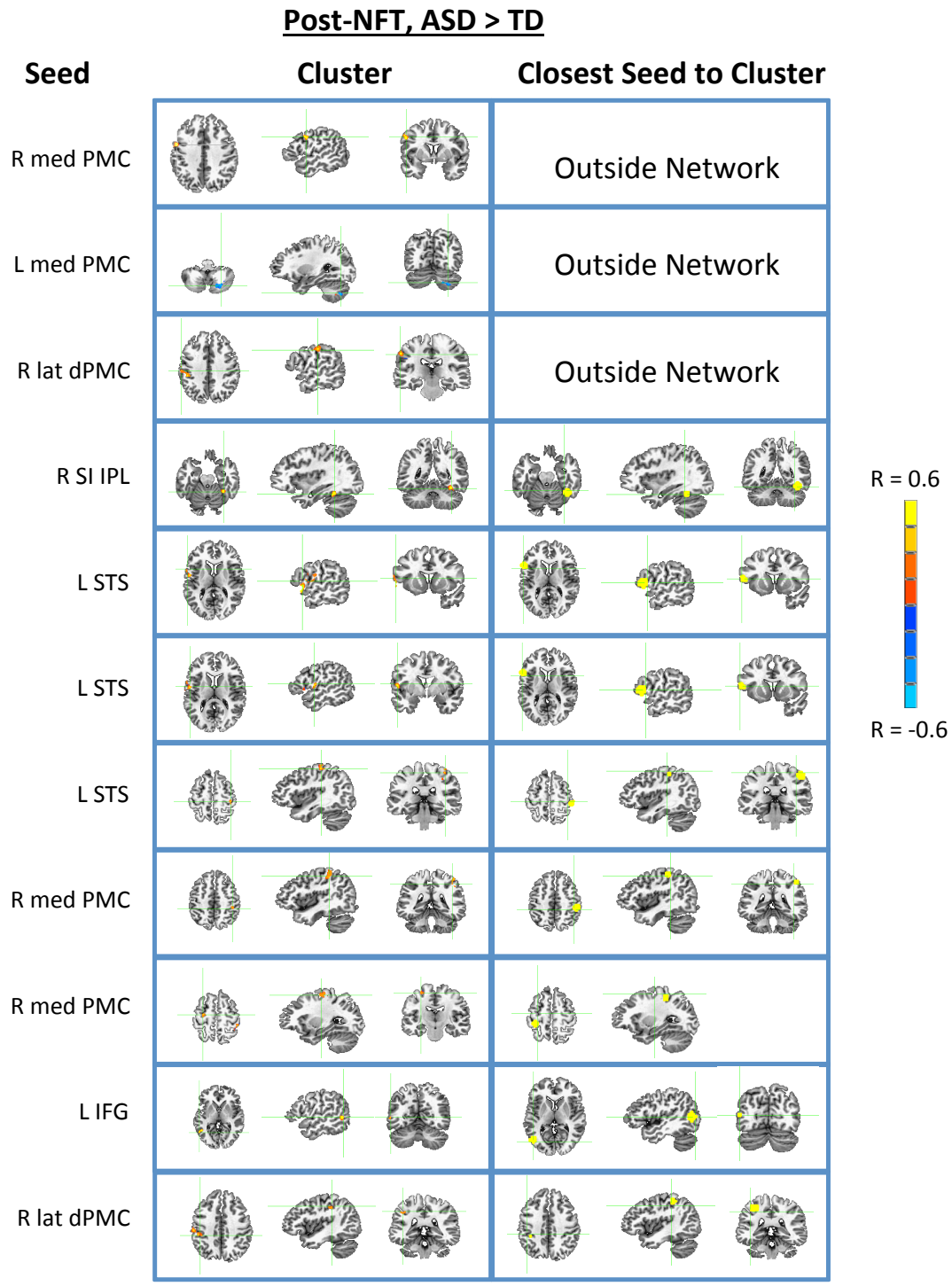

Figure 3.4 Clusters of significant differences in functional connectivity between **ASD vs. TD**, for seeds of the Caspers imitation network, **post-NFT**. For clusters that fall within the regions included in the Caspers seeds, the closest seed within that network is shown adjacent to the cluster. All clusters passed an uncorrected voxelwise threshold of $p = 0.001$ and were cluster corrected for multiple comparisons at $p < 0.01$.

Table 3.5 Caspers imitation seeds showing significant differences **pre-NFT, ASD > TD.** Clusters that are located within the imitation network are shown in **green**, clusters are located outside the network are shown in **red**. Results reported for an uncorrected voxelwise threshold of p = 0.001, and cluster correction for multiple comparisons at p < 0.01.

Cluster (*Brodmann Areas*)	**% of**	**Vol.**		**MNI coordinates**		
Subregions	**cluster vol.**	**(μl)**	**t-score***	**x**	**y**	**z**
Seed: Right SII / IPL						
Left Middle Occipital (*BA 19*)		472	1.97	43	74	7
L Middle Occipital	97.3%					
Left Anterior Cingulate (*BA 32*)		511	3.96	8	-37	17
L Anterior Cingulate	76.4%					
L Superior Medial Gyrus	2.1%					
Seed: Right SI / IPL						
Left Superior Medial Gyrus (*BA 10,9*)		1729	4.37	2	-55	17
L Superior Medial Gyrus	76.5%					
R Anterior Cingulate Cortex	8.6%					
R Sup. Medial Gyrus	8.0%					
Medial Frontal Cortex (10,11,32)		1258	4.73	-1	-48	-6
L Rectal Gyrus	42.0%					
L Mid Orbital Gyrus	26.0%					
R Mid Orbital Gyrus	20.7%					
Left Precuneus (*BA 23,30*)		668	3.52	3	50	18
L Precuneus	61.0%					
L Posterior Cingulate Cortex	22.0%					
R Precuneus	8.1%					
Seed: Left Superior Temporal Sulcus						
Left Postcentral Gyrus (*BA 43*)		472	4.54	54	12	19
L Postcentral Gyrus	93.8%					
L Rolandic Operculum	6.2%					
Seed: Right medial PMC (SMA)						
Left Superior Frontal Gyrus (*BA* 8,9)		1179	-4.18	18	-39	38
L Sup. Frontal Gyrus	77.1%					
L Mid. Frontal Gyrus	21.4%					
Seed: Left lateral dPMC						
Medial Frontal (*BA 9,10*)		511	3.07			
R Sup. Medial Gyrus	86.7%					
L Sup. Medial Gyrus	13.1%					

Table 3.6 Imitation seeds showing significant differences in **post-NFT, ASD > TD.** Clusters that are located within the imitation network are shown in **green**, clusters are located outside the network are shown in **red**, and clusters that are located on the same gyrus or the same functional region as a seed in the imitation network are shown in **blue**. Results reported for an uncorrected voxelwise threshold of p = 0.001, and cluster correction for multiple comparisons at p < 0.01.

Cluster (*Brodmann Areas*)	**% of**	**Vol.**		**MNI coordinates**		
Subregions	**cluster vol.**	**(μl)**	**t-score***	**x**	**y**	**z**
Seed: Right SI / IPL						
Right Fusiform Gyrus (*BA 37*)		590	5.69	-33	45	-18
R Fusiform Gyrus	58.2%					
R Cerebellum	41.8%					
Seed: Left Superior Temporal Sulcus						
Left Inferior Frontal Gyrus (*BA 44*)		668	4.30	56	-7	9
L IFG (p. Opercularis)	44.3%					
L Temporal Pole	12.4%					
L Rolandic Operculum	7.3%					
L Precentral Gyrus	2.8%					
Left Premotor Cortex (*BA 6,43*)		629	4.26	51	6	13
L Rolandic Operculum	69.5%					
L Postcentral Gyrus	28.3%					
Right Postcentral Gyrus (*BA 3,4*)		629	3.45	-35	27	49
R Postcentral Gyrus	40.8%					
R Precentral Gyrus	38.6%					
Seed: Right medial PMC (SMA)						
Right Inferior Parietal Lobule (*BA* 40)		904	3.33	-42	36	46
R Postcentral Gyrus	56.1%					
R IPL	26.4%					
R Supramarginal Gyrus	17.1%					
Left Premotor Cortex (*BA* 6)		590	4.11	50	0	36
L Precentral Gyrus	99.4%					
Left Premotor Cortex 2 (*BA* 6)		432	4.06	27	17	54
L Precentral Gyrus	98.1%					
L Sup. Frontal Gyrus	1.9%					
Seed: Left medial PMC (SMA)						
Right Cerebellum		472	-3.54	-23	67	-40
R Cerebellum	100%					
Seed: Right lateral dPMC						
Left Postcentral (*BA 2,3*)		472	4.96	53	22	37
L SupraMarginal Gyrus	58.7%					
L Postcentral Gyrus	22.3%					
L Inferior Parietal Lobule	19.1%					
Left Inferior Parietal Lobule (*BA 40*)		472	4.65	42	31	36
L IPL	97.6%					
L Postcentral Gyrus	2.4%					
Seed: Left IFG						
Left Post. Middle Temporal Gyrus (*BA 19*)		786	3.79	45	53	5
L Post. Mid. Temporal Gyrus	89.0%					

Table 3.7 ANOVA with Caspers imitation seeds, **main effects and interactions** between group (ASD, TD) and training status (pre-NFT, post-NFT). Clusters that are located within the imitation network are shown in **green**, clusters are located outside the network are shown in **red**, and clusters that are located on the same gyrus or the same functional region as a seed in the imitation network are shown in **blue**. Results reported for an uncorrected voxelwise threshold of p = 0.001, and cluster correction for multiple comparisons at p < 0.01.

Cluster (*Brodmann Areas*)	% of	Vol.		MNI coordinates		
Subregions	**cluster vol.**	**(μl)**	**F-score***	**x**	**y**	**z**
Main Effects of Training Status						
Seed: Right Anterior Insula						
Right Inferior Parietal Lobule (*BA 40*)		2201	16.13	-51	34	40
R Supramarginal Gyrus	64.1%					
R Inferior Parietal Lobule	33.8%					
Left Insula (*BA 13*)		1258	14.42	29	-8	8
L Insula	51.2%					
L Putamen	8.3%					
Seed: Left Superior Temporal Sulcus						
Right Sup./Inf. Parietal Lobule (*BA 7,40*)		1572	6.55	-29	53	45
R Sup. Parietal Lobule	45.8%					
R Inf. Parietal Lobule	27.5%					
R Angular Gyrus	13.7%					
Seed: Right medial PMC (SMA)						
Left Motor/Premotor Cortex (*BA 4,6*)		983	7.49	31	24	57
L Precentral Gyrus	99.1%					
L Postcentral Gyrus	0.9%					
Seed: Right lateral dPMC						
Precuneus (*BA 29,30*)		1336	10.48	-1	50	12
R Precuneus	32.7%					
L Precuneus	10.5%					
L Calcarine Gyrus	3.6%					
Group x Training Status Interaction Effects						
Seed: Right Anterior Insula						
Right Caudate		983	19.45	-15	-11	9
R Caudate Nucleus	90.3%					
R Putamen	4.1%					

Task-Activation-Based Seeds

Prior to NFT, ASD participants showed underconnectivity in two clusters for a seed in left postcentral gyrus. These clusters were located in inferior parietal lobule (within the Caspers imitation network) and right middle cingulate gyrus. After NFT, there were no significant clusters of differences in

functional connectivity between ASD and TD groups for any of the task seeds. This suggests that the modest amount of differences, and specifically within-network ASD underconnectivity, prior to the training was normalized by the NFT. For this seed set, clusters of significant group differences in FC prior to NFT are summarized in Table 3.10.

In an ANOVA with group (ASD vs. TD) and training status (Pre- vs. Post-NFT) as factors (results summarized in Table 3.11), there were two clusters showing a main effect of training status. Both were from the seed in right IPL, and were located in right IFG (BA 47) and left IPL (BA 40). There were no clusters showing a main effect of group, and no clusters showing significant interactions between group and training status. Follow up t-tests between the post- and pre-NFT scans within each group (Table 3.8 for ASD and Table 3.9 for TD) revealed that both groups showed exclusively increased FC following NFT, and these effects were the most likely drivers of the main effect of training status in the ANOVA.

Results for T-tests have an uncorrected threshold of $p = 0.001$ and are cluster corrected to $p < 0.01$. Results for F-tests (group by timepoint interactions and main effects) have an uncorrected threshold of $p = 0.01$ and are cluster corrected to $p < 0.05$.

Table 3.8 Task activation seeds showing significant differences in ASD post- vs. pre-NFT. Results reported for an uncorrected voxelwise threshold of p = 0.001, and cluster correction for multiple comparisons at p < 0.01.

Cluster (*Brodmann Areas*)	**% of**	**Vol.**	**t-**	**MNI coordinates**		
Subregions	**cluster vol.**	**(μl)**	**score**	**x**	**y**	**z**
Seed: Right IPL						
Right Inferior Frontal Gyrus (*BA 47*)		865	4.31	-51	-17	-2
R IFG	33.9%					
R Sup. Temp. Gyrus	26.1%					
R Insula	21.5%					
R Precentral Gyrus	5.2%					
L Cingulate (*BA 24, 32*)		668	5.67	0	-7	36
L Middle Cingulate	46.7%					
R Middle Cingulate	19.0%					
L Anterior Cingulate	17.7%					
L SMA	16.6%					
L Inferior Parietal Lobule (*BA 40*)		668	3.71	51	37	46
L IPL	69.7%					
L SupraMarginal Gyrus	27.5%					
Seed: Left SPL						
R Sup. Frontal Gyrus (*BA 10*)		629	4.46	-24	-55	15
R Superior Frontal Gyrus	91.8%					
R Middle Frontal Gyrus	7.4%					

Table 3.9 Task activation seeds showing significant differences in **TD post- vs. pre-NFT.** Results reported for an uncorrected voxelwise threshold of p = 0.001, and cluster correction for multiple comparisons at p < 0.01.

Cluster (*Brodmann Areas*)	**% of**	**Vol.**	**t-**	**MNI coordinates**		
Subregions	**cluster vol.**	**(μl)**	**score***	**x**	**y**	**z**
Seed: Right IFG						
Right Lingual Gyrus (*BA 18*		1140	4.83	0	68	-2
R Lingual Gyrus	49.5%					
L Lingual Gyrus	33.5%					
R Calcarine Gyrus	7.7%					
L Calcarine Gyrus	4.2%					
Seed: Left Postcentral						
Right Inferior Parietal Lobule (*BA 40*)		590	5.23	-44	34	49
R IPL	73%					
R Postcentral Gyrus	23%					
Left Superior Parietal Lobule (*BA 7*)		590	5.75	31	58	53
L SPL	82.1%					
L Precuneus	3.4%					
Right Cerebellum		511	4.06	-20	51	-22
R Cerebellum	80.9%					
Seed: Right IPL						
Left Middle Temporal Gyrus (*BA 21,22*)		707	3.83	48	27	-2
L Middle Temporal Gyrus	40.6%					
Right Inferior Frontal Gyrus (*BA 47*)		629	4.20	-51	-17	-2

Table 3.9 (continued) Task activation seeds showing significant differences in **TD post- vs. pre-NFT**

Cluster (*Brodmann Areas*)	**% of**	**Vol.**	**t-**	**MNI coordinates**		
Subregions	**cluster vol.**	**(*μ*l)**	**score***	**x**	**y**	**z**
R IFG	64.1%					
R Sup. Temporal Gyrus	12.0%					
Right Insula	4.6%					
Right Insula/IFG (*BA 13*)		511	4.34	-41	-17	8
R Insula	56%					
R IFG (p. Triangularis)	34.3%					
R IFG (p. Opercularis)	9.6%					
Left Inferior Frontal Gyrus (*BA 8*)		432	3.66	41	-24	-9
L IFG (p. Orbitalis)	86.0%					
L Temporal Pole	8.9%					
Left Middle Cingulate (*BA 24*)		432	4.01	0	7	39
L Mid. Cingulate	87.5%					
R Mid. Cingulate	10.5%					
Seed: Left SPL						
Left Middle Temporal (*BA 21,22*)		511	4.03	41	30	-2
L Middle Temporal Gyrus	28.4%					
Right Superior Temporal Gyrus (*BA 22*)		432	5.40	-65	34	12
R Sup. Temporal Gyrus	98.5%					
R Mid. Temporal gyrus	1.5%					
Seed: Left Medial Temporal						
Left Inferior Parietal Lobule (*BA 40*)		1926	3.60	34	41	49
L IPL	64.9%					
L Postcentral Gyrus	33.4%					
Left Cingulate Cortex (*BA 24*)		1140	4.76	0	7	36
L Middle Cingulate Cortex	75.2%					
R Middle Cingulate Cortex	24.4%					
Left Premotor (*BA 6*)		1022	4.13	27	10	63
L Precentral Gyrus	83.0%					
L Sup. Frontal Gyrus	16.9%					
Left Insula (*BA 13*)		472	4.42	41	7	8
L Rolandic Operculum	72.7%					
L Insula	21.7%					
L Heschls Gyrus	3.3%					

Table 3.10 Task activation seeds showing significant differences in Pre-NFT ASD > TD. Results reported for an uncorrected voxelwise threshold of p = 0.001, and cluster correction for multiple comparisons at p < 0.01.

Cluster (*Brodmann Areas*)	**% of**	**Vol.**	**t-**	**MNI coordinates**		
Subregions	**cluster vol.**	**(μl)**	**score***	**x**	**y**	**z**
Seed: Left Postcentral						
Right Inferior Parietal Lobule (*BA 40*)		432	-4.27	-31	51	29
R IPL	36.4%					
R Angular Gyrus	23.4%					
Right Cingulate (*BA 31*)		432	-4.12	-20	37	36
R Middle Cingulate	75.4%					

Table 3.11 Task activation seeds showing significant differences in Group x training status ANOVA, main effect of time. Results reported for an uncorrected voxelwise threshold of p = 0.001, and cluster correction for multiple comparisons at p < 0.01.

Cluster (*Brodmann Areas*)	**% of**	**Vol.**	**F-**	**MNI coordinates**		
Subregions	**cluster vol.**	**(μl)**	**score***	**x**	**y**	**z**
Seed: Right IPL						
Right Inferior Frontal Gyrus (*BA 47*)		1022	19.73	-48	-14	-5
R IFG	36.3%					
L Superior Temporal Gyrus	22.8%					
R Insula	21.7%					
L Precentral Gyrus	7.5%					
Left Inferior Parietal Lobule (*BA 40*)		1022	9.33	51	37	39
L IPL	68.6%					
L SupraMarginal Gyrus	29.8%					

Head Motion

There were no significant differences in head motion between groups either before (ASD mean RMSD = 0.09, TD M = 0.11, p = 0.58) or after NFT (ASD M = 0.10, TD M = 0.07, p = 0.28). Additionally, there were no head motion differences within each group when comparing pre- vs. post-NFT within either the ASD group (p = 0.84) or the TD group (p = 0.15). Average group estimates for head motion are summarized in Table 3.1.

Covariance with ASD symptom severity

The number of correlational tests with behavioral scores was kept low to reduce the need for multiple comparisons correction. Since this was a study of connectivity within an imitation network that is the putative basis for many social functions, only assessment and diagnostic scores closely related to social functioning were used for these correlation tests. Correlations were obtained between changes in functional connectivity in select nodes of the imitation network (computed by subtracting the pre-NFT from the post-NFT Z-scores for each participant) and two measures of symptom severity in the social domain in ASD, which included the change in SRS total score (obtained by subtracting the pre-NFT SRS score from post-NFT SRS score for each participant) and the changes in ATEC scores (derived analogously). The particular clusters that were selected were limited to those found within the imitation network and in which ASD was overconnected in the post-NFT t-test between ASD and TD groups (i.e., the clusters shown in green on Table 3.6). Of the six clusters that met these criteria, significant correlations were found between SRS and FC Z-scores in two clusters: one located in right FFA and based on the seed in right IPL ($r = -0.824$, $p = 0.012$), and the other located in right IPL and based on the seed in right medial PMC ($r = -0.806$, $p = 0.016$). These correlations are plotted in Figure 3.5.

In addition to symptom severity measures, correlations of FC effects with WASI were also obtained in view of the significant group differences in IQ

(ASD M = 93.75, TD M = 118, p = 0.03). All p values obtained for these correlations were non-significant (all *ps* > 0.15).

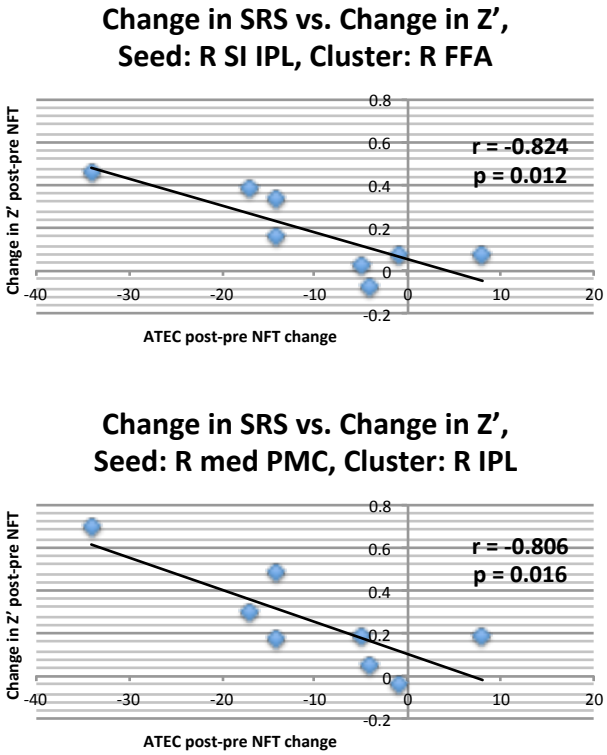

Figure 3.5 Significant correlations between changes in ASD group between improvements in SRS scores and increased functional connectivity (Z') following NFT, in two clusters within the imitation network.

Discussion

Prior to NFT, several nodes within the imitation/action-observation network defined in the Caspers ALE meta-analysis (including areas of the hMNS such as IFG) were overconnected with regions outside the imitation network, in the ASD group relative to typically developing controls. Several of the clusters of out-of-network overconnectivity were found specifically in frontal and prefrontal regions such as medial prefrontal cortex. These pre-NFT findings were consistent with previous studies showing increased, and

possibly "compensatory", connectivity with regions outside the network (Shih et al., 2010). Like the present study, Shih et al. showed that areas involved in imitation (including areas of the hMNS) are overconnected specifically with prefrontal areas that play a role in theory of mind and executive control. The present findings are also consistent with the idea that ASD is characterized by reduced segregation between networks, resulting in network cross-talk and reduced functional efficiency (Rudie et al., 2012; Fishman et al., 2014). Thus, the pre-NFT group differences in FC presented here support previous findings of reduced functional segregation in systems related to action observation and imitation in ASD.

The second and perhaps most striking pattern that emerges from these results is that the overconnectivity, predominately with regions located outside the imitation network, and with frontomedial regions specifically, in the ASD group prior to NFT was largely absent after NFT. Instead, there was overconnectivity with regions located directly within the radius of an imitation seed (clusters highlighted green in Table 3.6), or within the same functional zone or gyrus as an imitation seed (clusters highlighted blue in Table 3.6), in the ASD group. One question that is raised by these post-NFT results is whether overconnectivity relative to typical development, now found within-network instead of out-of network, may be functionally beneficial. A number of points support this positive interpretation. For one, the absence of out-of-network overconnectivity suggests an increase in functional segregation

between the imitation network and other networks. This is a reversal of the pre-NFT findings and of literature reports of reduced functional segregation between networks (Rudie et al., 2012; Fishman et al., 2014). Thus, the finding reported here suggests that imitation regions have less "cross-talk" with other networks, and are possibly relying less on frontal regions for "compensatory" reasons (Shih et al., 2010) following NFT. Secondly, the within-network overconnectivity in ASD suggests that the imitation network and parts of the hMNS, particularly the inferior parietal lobule, have stronger functional integration after the training. In the task-activation results reported in Chapter 2, one cluster of interaction between group status and training status was found in the right inferior parietal lobule. This complementary finding in the imitation task suggests that the increased FC in ASD seen after the training is both neurofunctionally and behaviorally significant.

In the ASD group, there were several clusters within imitation regions that had higher FC after NFT compared to before (highlighted green in Table 3.3). For example, there was a cluster that significantly increased in FC in right inferior parietal lobule and originating from the seed in right anterior insula. Additionally, there were other clusters of higher post-NFT vs. pre-NFT correlations in the ASD group located in either the same functional region or on the same gyrus as an imitation seed, but not falling directly within the radius of a seed (highlighted blue in Table 3.3). For instance, the seed in right anterior insula had higher post-NFT connectivity with a cluster in right

dorsolateral prefrontal cortex (BA 46). This finding of increased post-NFT FC within-network in the NFT group is corroborated by significant correlations with changes in symptom severity. In the ASD group, improvements in SRS scores were significantly correlated with post-NFT increases in FC in two clusters: one found in right FFA and for a seed in right IPL ($r = -0.824$, $p = 0.012$), and another found in right IPL and for a seed in right medial premotor cortex ($r = -0.806$, $p = 0.016$). These correlations suggest that the neurophysiological changes in functional connectivity are linked to the positive changes in behavior seen after NFT. Notably, for both of these correlations, either the seed region (for the first correlation) or the significant cluster (for the second correlation) were located in inferior parietal lobule, which is not only one of the Caspers imitation seeds but also a core region of the hMNS (Rizzolatti et al., 2004). This is strong evidence in support of the hypothesis that the mechanism underlying the behavioral changes seen after NFT involves changes specifically in the functional connections of the hMNS.

One paradoxical result obtained in the present study was the general lack of FC effects when using a set of seeds that was based on data from the same subjects, and the same scan sessions, as the resting state scan itself. Prior to NFT, whole-brain functional connectivity analyses performed with the seven task-activation-derived seeds revealed far fewer group differences than the same analyses performed with the Caspers imitation network seeds. After NFT, no significant differences were observed between groups for the task-

based seeds. Given that areas that are functionally connected at rest tend to coactivate together during tasks (Fox & Raichle, 2007), this finding contrasts with the results from Chapter 2. There it was reported that NFT led to increased activations in many of the same areas that were included in the task-based set of seeds. Therefore, we would expect areas showing increased activation during the task would show concurrent increases in within-network resting state functional connectivity. One likely explanation for this discrepancy is that the task-based seeds were based on the combined activation of only 17 subjects, whereas the Caspers meta-analysis included 87 studies, with much greater overall statistical power. However, the fact that a more significant pattern of results was obtained using the literature-based Caspers seeds suggests that these results are still generalizable, despite not being validated by the task-based seeds.

Additionally, it is worth noting that head motion, which often confounds studies of autism and of young participants in general (Power et al., 2012), likely did not significantly bias the results of the present study. There were no significant differences in motion between groups either before. Additionally, there were no differences between pre- vs. post-NFT motion in either group.

A few questions that arise from these results, as well as the results of the previous chapter, concern the duration and potency of the benefits conferred by NFT. Neuroplastic changes resulting from prolonged training in other activities are reversible (Pascual-Leone et al., 2005; Cramer et al., 2011;

May et al., 2011). It is currently unknown how long the behavioral and neurophysiological effects of NFT observed here and in previous studies last without being reinforced. This question could be addressed with follow up assessments at various intervals after the completion of training.

Another open question is how much training is required to reach the peak efficacy of NFT. In this sample, hours of training completed by each group were not correlated with changes in functional connectivity in the clusters where significant group effects were observed following NFT (ASD mean r = -0.18, mean p = 0.46; TD mean r = 0.12, mean p = 0.46). Hours of training also did not correlate with changes in SRS or ATEC scores in this group (ASD ATEC r = 0.03; ASD SRS r = -0.23). However, there might not have been an adequate number of data points for different amounts of training to detect such an effect. With a larger sample, a dose-response curve could be established for NFT, increasing the clinical usefulness of this technique. With even further study, individual differences in autism symptoms could be taken into account for modified dose-response curves.

A final question concerns the extent to which NFT is efficacious at different stages of development. A recent review proposed the developmental hypothesis that there is overconnectivity early in ASD development but underconnectivity later on (Uddin et al., 2013). In the context of Johnson's interactive specialization framework for the development of network connectivity (Johnson, 2011), in which sensory inputs interact with genetically

coded aspects of brain structure, NFT might be expected to encourage functional specialization by repeatedly engaging and strengthening connections within the same functional network. This effect might be stronger at earlier stages of development, during which connections are being actively shaped by synaptic development and pruning. If performed in very early development (during the first 24 months), it is possible that some of the behavioral regression seen in ASD could be prevented. However, since age in this sample was flatly distributed from 8 to 17 years, there was not enough power to test the present findings in this developmental context. A post-hoc correlation test revealed no significant relationship between age and NFT-related changes in functional connectivity in the ASD group (*p*s range = 0.10 - 0.92).

Much attention in the autism neuroimaging field has been centered around the directionality of connectivity abnormalities in ASD; more specifically, the question is whether ASD is primarily characterized by underconnectivity of brain networks as opposed to overconnectivity, or whether there is a more complex combination of over- and underconnectivity across different networks (Wass, 2011; Kana et al., 2011; Rudie and Dapretto, 2013). The results presented in this chapter provide support for the view that within some networks, including those responsible for social behaviors like imitation, there may be a mix of out-of-network overconnectivity and within-network underconnectivity in ASD. In the context of recent models of the

development of brain network connectivity (Johnson, 2011), the atypical patterns of connectivity between prefrontal and posterior regions observed prior to NFT in the present study may reflect an imbalance between progressive and regressive developmental mechanisms. These opposing processes can be promoted or inhibited in a variety of ways, and likely involve a combination of genetics, Hebbian learning mechanisms, and sensory inputs from the environment (Gottlieb, 2007). The effects of such an imbalance could lead to either insufficient synaptic pruning (Frith, 2004) or excessive synaptic pruning (Thomas et al., 2011, 2015), compared to typical development. Adding to the complexity, it is possible that the extent of synaptic pruning can vary across brain regions and across different stages of development (Johnson, 2011). Over time, insufficient or excessive synaptic pruning could interact with other dynamic organizational processes to influence the formation of networks, resulting in reduced within-network integration and reduced between-network segregation. However, as mentioned earlier, it is difficult to place the present dataset into this developmental framework, as there is likely insufficient statistical power to detect age-related differences in connectivity, either before or after NFT.

The present results are particularly significant because they are some of the first demonstrations that imbalanced connectivity in ASD can be normalized with a treatment approach that directly influences the oscillatory activity within brain networks. Neurofeedback training has seen much

behavioral success in certain populations, but the mechanisms behind its efficacy remain unclear. By providing evidence of neurophysiological changes in network connectivity, these results suggest that the oscillatory changes observed in EEG after NFT (Pineda et al., 2008, 2014) are also reflected on the network level.

Chapter 3 is currently being prepared for submission for publication by Mike Datko, Jaime Pineda, and Ralph-Axel Müller. The dissertation author was the primary investigator and first author of this paper.

Chapter 4: Aberrant structural connectivity in an imitation network in children with autism[*]

Introduction

Structural connectivity is, directly or indirectly, the basis for the functional connectivity discussed in Chapter 3 of this dissertation (van den Heuvel et al., 2009; Greicius et al., 2009), and the two measures are often positively correlated (Bullmore & Sporns, 2009). Structural integrity, a term often used to generally describe certain properties of white matter microstructure that can be estimated via diffusion weighted imaging (DWI), is the basis of strong connections between spatially distributed cortical regions and networks. DWI is able to quantify structural integrity and connectivity by observing the diffusion of water molecules, and quantifying the extent to which that diffusion is constrained along axonal membranes (Beaulieu, 2002). Generally speaking, denser bundles of parallel axons cause diffusion to occur more unidirectionally. Thus, DWI uses the extent to which fiber bundles are aligned within a given tract as an index of the relative strength of structural connections between cortical regions.

In autism, structural connectivity has been shown to be compromised in

[*] Work in this chapter was part of a larger study with numerous collaborators. Ruth Carper was primarily responsible for validating the tracts with tracer-based anatomical atlases, and Inna Fishman was responsible for parts of the statistical analyses.

several metrics of white matter integrity (Travers et al., 2012). Some studies have found these effects to be localized to specific tracts, particularly those connecting networks that play a role in social cognition (Koldewyn et al. 2014; Ameis et al., 2011). Studies also suggest these structural compromises are linked to differences in functional connectivity as well (Mueller et al. 2013; Nair et al., 2013). Overall patterns in these studies suggest that there is widespread reduced anisotropy and greater diffusivity of fiber tracts in ASD (Aoki et al., 2013).

This chapter will focus on differences in white matter structure in ASD in the tracts that connect areas of the same imitation network explored in Chapter 3 of this dissertation. The importance of imitation, and the brain networks that support it, for a variety of social functions has already been discussed in previous chapters. In light of that line of evidence, and considering the benefits of multimodal neuroimaging approaches have already garnered in autism research (Yerys & Herrington, 2014), addressing the structural connections that connect key nodes of imitation-related networks will provide important multimodal support for studies that have already examined related networks with fcMRI.

In the study presented in this chapter, DWI was used to examine structural connectivity within the Caspers imitation network (defined in Chapter 3, and adapted from Caspers et al., 2010) in children and adolescents with ASD and a matched group of typically developing controls. While many of

those seed regions are separated by large distances and likely do not have a single, direct, and traceable fiber tract connecting them, evidence suggests that functional connections often exist between regions that have no direct anatomical links. It has been suggested that intermediary anatomical hubs play a role in this type of long-range connectivity (Damoiseaux & Greicius, 2009).

The present study hypothesized that participants with ASD would have altered structural connectivity (SC), and specifically lower fractional anisotropy and higher mean diffusivity, in tracts connecting important nodes of the Caspers imitation network, compared to TD controls. It was further hypothesized that ASD participants with more sociocommunicative symptoms would have greater differences in these diffusion-based indexes of connectivity.

Methods

Participants

50 children and adolescents with high-functioning autism and 45 typically developing controls were initially recruited for the study. However, after excluding 23 ASD and 15 TD participants with excessive head motion, 27 ASD and 28 TD participants remained for the final analyses.

ASD and TD groups did not significantly differ on age, IQ, or head motion parameters (summarized in Table 4.1). ASD diagnoses were made

based on DSM-IV-TR criteria (American Psychiatric Association, 2000) in addition to clinical assessment with the Autism Diagnostic Interview-Revised (ADI-R) (Rutter et al., 2003) and the Autism Diagnostic Observation Schedule (ADOS) (Lord et al., 2001). Participants with a history of autism-related medical conditions (e.g., epilepsy, Fragile-X, tuberous sclerosis) were excluded. TD participants had no personal or family history of autism, or of any other neurological or psychiatric conditions. Participants with ASD with comorbid ADHD, OCD, or anxiety disorders were not excluded, because of the high comorbidity of these conditions with ASD Intelligence was assessed by the Wechsler Abbreviated Scale of Intelligence, 2nd Edition (WASI-II) (Wechsler, 2011). Social functioning was assessed in all participants with the Social Responsiveness Scale (SRS), a pen-and-paper questionnaire completed by participants' caregivers (Constantino & Gruber, 2005). Informed assent and consent were obtained from all participants and their caregivers in accordance with the University of California, San Diego and San Diego State University Institutional Review Boards.

Table 4.1 Participant Demographic and Diagnostic Information

	ASD (n=27) *M* ± SD [range]	**TD (n=28)** *M* ± SD [range]	**TD vs. ASD** *p* value
Gender (M/F)	24/3	21/7	0.12
Handedness (R/L)	25/5	25/4	0.63
Age (years)	13.7 ± 2.3 [9.6-17.7]	13.4 ± 2.4 [8.7-17.6]	0.66
Verbal IQ	105 ± 21 [70-147]	107 ± 10 [87-127]	0.60
Non-verbal IQ	108 ± 16 [53-140]	107 ± 11 [86-129]	0.78
Full-scale IQ	106 ± 19 [66-141]	108 ± 10 [88-126]	0.75
ADOS Comm.	3.7 ± 1.9 [1-8]		
ADOS Social	8.7 ± 2.7 [5-14]		
ADOS Repetitive	2.0 ± 1.4 [1-4]		
ADI-R Social	17.2 ± 6.0 [6-28]		
ADI-R Comm.	12.8 ± 6.1 [2-24]		
SRS Total	82 ± 8 [64-94]	0.058 ± 0.03 [.02-.15]	0.41
DWI Head-motion	0.92 ± 0.42 [0.0-2.35]	0.97 ± 0.29 [.59-1.74]	0.62

Diffusion Data Acquisition

All data were collected on a 3T GE 750 MRI scanner with an 8-channel headcoil. Diffusion weighted images were obtained with an echo-planar pulse sequence with full head coverage and encoded for 61 non-collinear diffusion directions at b = 1000 s/mm^2, and one at b = 0 s/mm^2, with a dual spin echo excitation to reduce eddy current artifacts (TR = 8500ms; TE = 84.9ms; flip angle = 90º; FOV = 240mm; 128x128 matrix; 1.88 x 1.88 x 2mm^3 resolution). Total diffusion weighted scan time was about 9 minutes. Field maps were collected for fMRI and DWI scans with the same spatial parameters to correct for field inhomogeneities (TR=1097ms; TE=9.5ms; flip angle=45°; 2 averages).

DWI data preprocessing, selection of tracts and tractography

Diffusion data were processed with the FSL software suite (Smith et al., 2004). During initial preprocessing, data were field-map corrected for

inhomogeneity in the magnetic field, resampled to a resolution 1.0 mm^3 isotropic voxels, and corrected for eddy current distortions. Data were visually inspected in each direction of diffusion and in all 3 planes of view to screen for motion-related artifacts, and images were rated for shifts of head placement between acquisition of individual diffusion directions, signal dropout and image noise. Scans with excessive head motion artifacts were rejected (Yendiki et al., 2013). A Diffusion Motion Index (DMI) was calculated based on eddy correction parameters (mean image translation and rotation) and the frequency of signal dropouts across all slices (adapted from Yendiki et al., 2013). ASD and TD groups were matched on head motion and signal dropout indices as well as the DMI (see Table 4.1); the DMI was also used as a covariate in all diffusion analyses (Yendiki et al., 2013). Voxelwise diffusion tensors, as well as various diffusion measures (fractional anisotropy, mean diffusivity, radial diffusivity, and axial diffusivity) were obtained with FSL's Diffusion Toolbox.

Fractional anisotropy (FA) and mean diffusivity (MD) are measures based on summation of the magnitude of diffusion in various directions within a given voxel. FA in particular quantifies water diffusion in a principal direction (the eigenvector of diffusion) on a scale of zero, indicating completely free diffusion in all directions, to one, indicating that diffusion is completely constrained along one axis. MD quantifies the average diffusion in all directions within a given voxel. FA typically increases and MD decreases

during development, and these changes are thought to correspond to greater uniformity and density of fibers within white matter tracts (Beaulieu, 2002).

FA image volumes for each subject were registered to the FMRIB58 FA template in MNI standard space, using FSL's FNIRT non-linear registration command. The resulting spatial transformation matrices were used to convert between standard (seed) and native space.

Probabilistic fiber tractography was performed in native space using FSL's ProbtrackX and BEDPOSTX commands (Smith et al., 2004, Behrens et al., 2003). Tractography seeds were based on spheres centered around the coordinates listed for imitation regions from the Caspers ALE meta-analysis of imitation-related activation (the same seeds used in the fcMRI analysis from Chapter 3) (Caspers et al., 2010). These original seeds are shown again for reference in Figure 4.1. However, given that the original seeds were centered in cortical grey matter and optimized for functional connectivity analyses, additional steps were taken to ensure that seeds encompassed white matter voxels. First, the radius of the spheres was increased from $7mm^3$ to $10mm^3$. Seeds were then manually nudged towards the local grey-white matter boundary until at least 40% of voxels within each seed had FA > 0.2 (mean = 54% of voxels; range = 40-74%). No seed was nudged more than 10 mm on any of the 3 axes, with an average Euclidean distance of 10mm (range = 6 – 15mm). Examples of seeds before and after this nudging process are shown in Figure 4.2. These steps were performed to increase the amount of viable

white-matter-containing voxels from which the tractography algorithm could initiate streamlines (Jones & Cercignani, 2010).

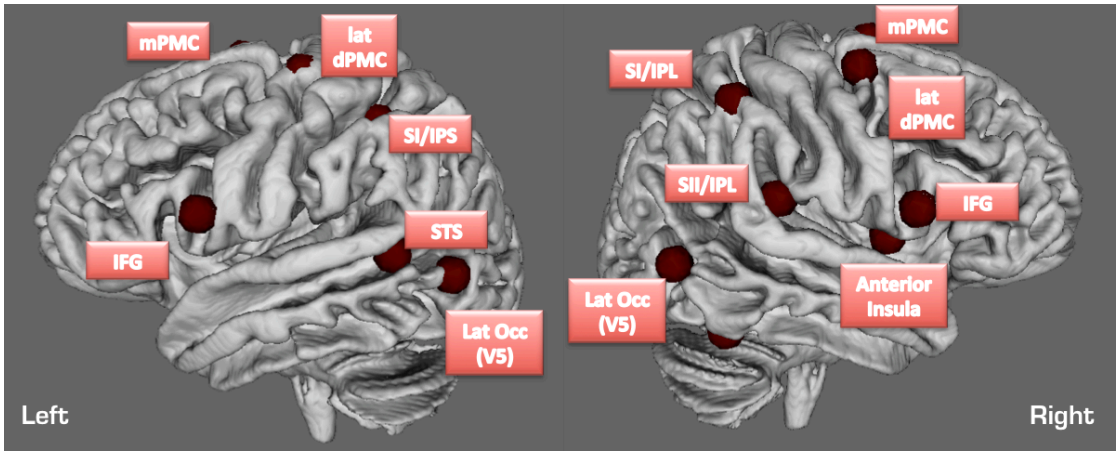

Figure 4.1 Seeds derived from the Caspers ALE meta-analysis. Modified versions of these were used as seeds for probabilistic tractography (examples of modified seeds are shown in Figure 4.2).

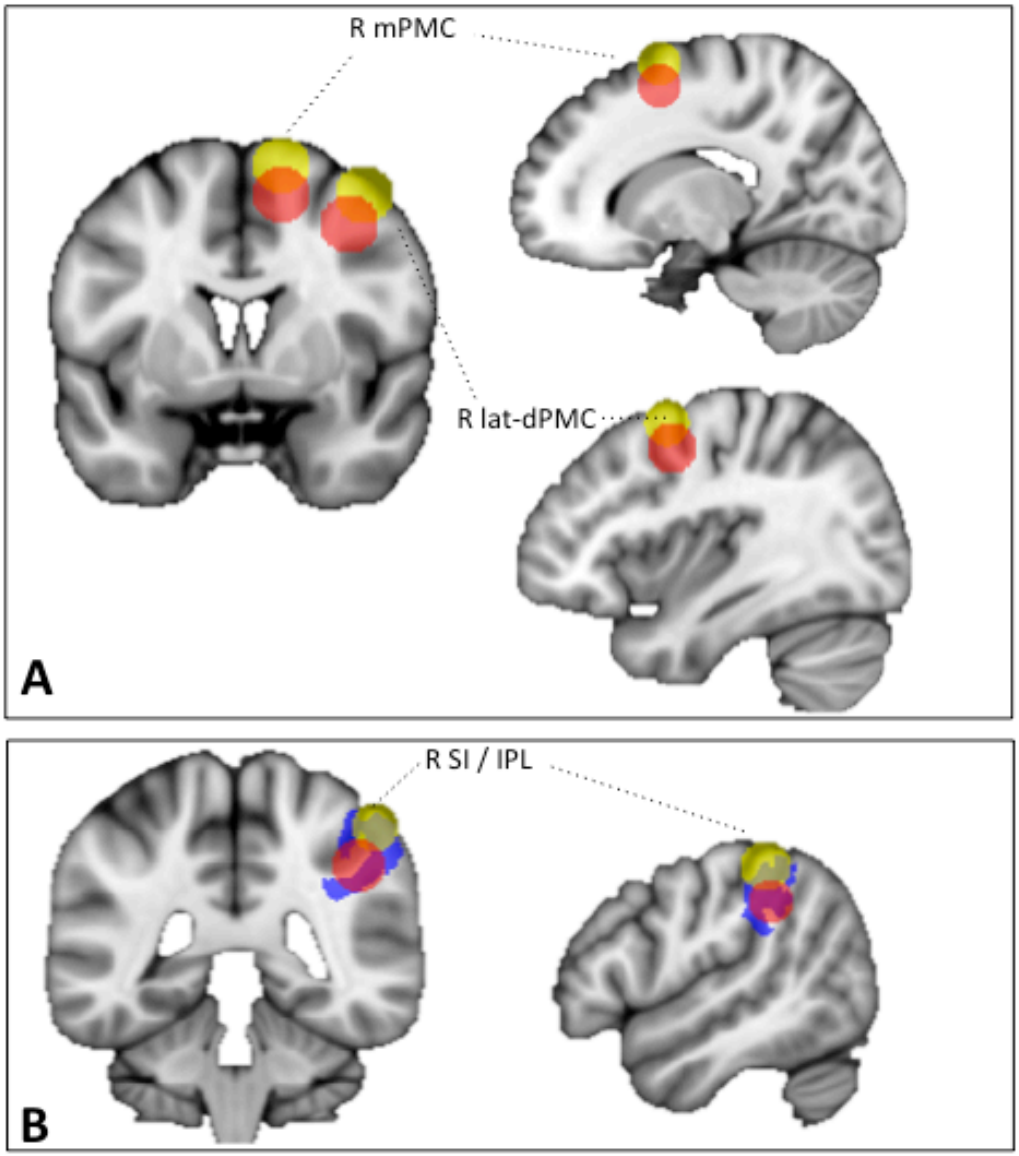

Figure 4.2 Tractography seeds before and after nudging towards grey-white matter boundary. Seeds with coordinates directly based on the Caspers ALE meta-analysis are shown in yellow, while seeds nudged to be optimal for tractography are shown in red. All nudged seeds remained in the same functional region as the originals. **A.** Coronal and sagittal views of right mPMC and right lateral dPMC, pre- and post-nudging. **B.** Coronal and sagittal views of seed in right SI / IPL, pre- and post-nudging, overlayed along with a mask of IPL from the Jülich atlas included in FSL.

Tractography success rates and anatomical validity of white matter tracts

Given the large number of possible tracts between the 14 seed regions from the Caspers meta-analysis, and given that it is highly unlikely that all of those tracts would be anatomically valid, only select tracts were investigated with diffusion tractography. The first criterion for tract selection was that only intrahemispheric connections were included to avoid major areas of crossing fibers (Wedeen et al., 2008). Furthermore, all tracts chosen for the final analysis were consistent with pre-existing anatomical white matter atlases. This process of verifying this consistency involved finding cortical regions in a primate atlas that corresponded to each imitation seed. White matter tractography atlases based on anterograde tracing with radiolabeled isotopes (Schmahmann & Pandya, 2009) were then consulted about whether tract tracing revealed direct structural connections between these primate homologues of the imitation seeds. If evidence of a real tract connecting two regions was found, a final check was performed to ensure that the tract found with FSL's tractography command passed through the same regions as reported in the literature. In the case of the tracts that did survive this criteria, many of them passed through the superior longitudinal fasciculus, a major pathway connecting frontal, parietal, and parts of occipital cortices.

Since tractography seeds were relatively small and were based on functional areas in grey matter, which is an unconventional basis for seeds in

tractography studies, steps were taken to ensure the validity of all tracts produced by FSL's probabilistic tractography software. Tracts were considered for further analyses if at least 93% of participants (which, given our sample size, equaled all but two participants per group) from each group had at least 0.01% of initiated streamlines reaching the target ROI. Since the number of voxels in each seed was approximately 4200 for a sphere of 10 mm, and since a total of 2000 streamlines were initiated per voxel in each tract, this criterion of 0.01% successful streamlines was equivalent to at least 840 streamlines reaching their target seed per tract. The tract connecting right inferior parietal lobule to the right inferior frontal gyrus is an example of a tract that passed all of these criteria. This tract fell within the superior longitudinal fasciculus, and was detected in 96% of the ASD participants and 100% of the TD participants. Thus, this tract was included in further analyses. Examples of tracts that were not included were those originating from the fusiform face area and targeting several of the superior cortical seeds. Not only were these not reflected in the anatomical literature, they also had low rates of success with the tractography algorithm. Tract identification rates for all tracts were not significantly different between ASD and TD groups ($p = 0.31$ for origin seed to target seed streamlines and $p = 0.64$ for the inverse). The groupwise (ASD and TD) percentages for identification of each tract used in the final analyses are listed in Table 4.2, and examples of these tracts are shown in Figure 4.3.

Table 4.2 Percent of subjects with identifiable tracts in each group. Criterion: Greater than 0.01% of streamlines initiated from seed ROI, adjusted for proportion of seed ROI with FA>0.2, ended at target ROI. Only TOIs for which both groups had success rates > 93% for both A to B and B to A tracts were considered for further analysis (marked in ***bold italics***).

	TOI (ROI pair)		A to B		B to A	
Hemisphere	ROI A	ROI B	ASD (%)	TD (%)	ASD (%)	TD (%)
Left	***IFG***	***lateral dPMC***	***93%***	***97%***	***93%***	***97%***
Left	***IFG***	***medial PMC***	***96%***	***97%***	***96%***	***97%***
Left	***IFG***	***SI / IPS***	***96%***	***100%***	***93%***	***100%***
Left	lateral dPMC	medial PMC	89%	97%	78%	90%
Left	lateral dPMC	SI / IPS	93%	100%	89%	100%
Left	medial PMC	SI / IPS	93%	100%	89%	100%
Right	***IFG***	***lateral dPMC***	***100%***	***97%***	***100%***	***97%***
Right	***IFG***	***medial PMC***	***100%***	***97%***	***96%***	***97%***
Right	***IFG***	***SI / IPL***	***96%***	***100%***	***96%***	***100%***
Right	IFG	FFA / FBA	93%	96%	59%	61%
Right	***lateral dPMC***	***medial PMC***	***100%***	***100%***	***100%***	***100%***
Right	lateral dPMC	SI / IPL	81%	93%	89%	96%
Right	lateral dPMC	FFA / FBA	59%	75%	48%	61%
Right	medial PMC	SI / IPL	85%	93%	85%	96%
Right	medial PMC	FFA / FBA	59%	71%	26%	32%
Right	SI / IPL	FFA / FBA	100%	93%	81%	61%

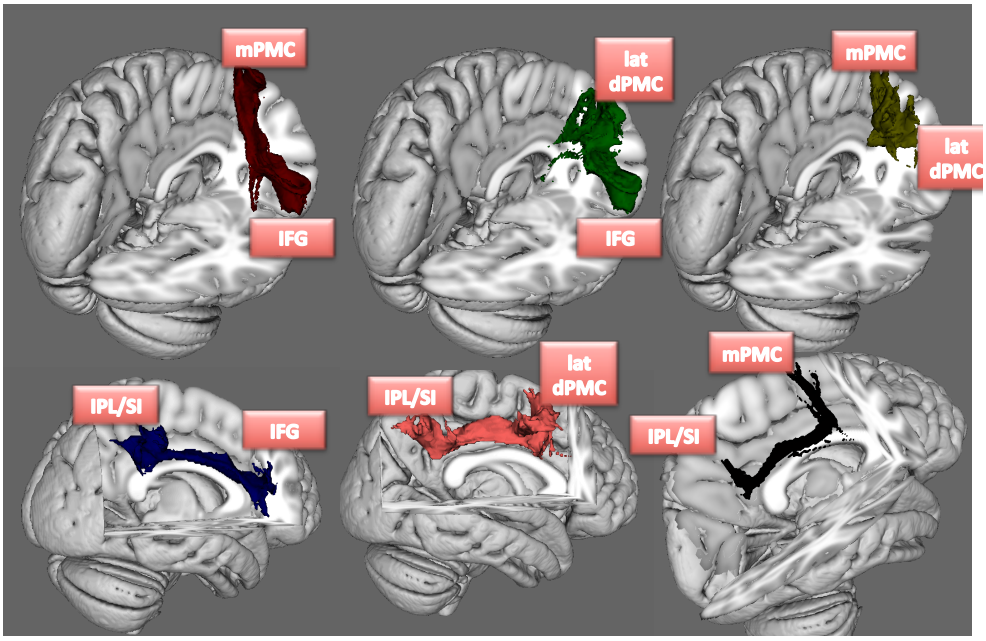

Figure 4.3 Examples of tracts found with probabilistic tractography, after original imitation seeds were nudged from primarily grey matter towards the grey-white matter boundary.

For each tract of interest (TOI), 1000 streamlines were initiated from each voxel within the origin seed towards the target seed. Streamlines were

initiated reciprocally between seed pairs for each TOI, resulting in 1000 initiated streamlines per voxel for each seed in each possible pair of seeds. Streamlines propagated with a 0.5-mm step length and a curvature threshold of 0.2. Streamlines reaching the other ROI were selected, resulting in a probability map of tract location. A minimum threshold of 150 successful streamlines per tract voxel was applied to form a binary mask of each subject-specific TOI.

Mean FA and MD values were obtained for each subject for each TOI using these thresholded TOI masks. Tract volumes were calculated as a measure of overall size (in voxels) of the thresholded TOI masks in each individual participant's brain. Total Brain Volume (TBV) excluding ventricles was derived from the eddy-corrected diffusion data using the b=0 images.

Results

Two repeated measures ANCOVAs, conducted separately for FA and MD, with TOI as a within-subjects repeated variable, group as a between-subjects variable, and DMI and age as covariates, revealed significant group effects. The ASD group had lower FA ($F(1,53) = 5.4$, $p = 0.03$; partial $\eta^2 = .11$) and higher MD values ($F(1,53) = 5.8$, $p = 0.02$; partial $\eta^2 = .11$) across all TOIs, as shown in Figure 4.4. Follow-up pairwise comparisons (univariate ANOVAs, with DMI and age as covariates) revealed that these group effects were particularly driven by the tracts connecting IFG and lateral dorsal PMC,

bilaterally (left: $p_{FA} = 0.045$ and $p_{MD} = 0.015$; right: $p_{FA} = 0.046$ and $p_{MD} = 0.045$; Figure 4.4). There were neither significant group x TOI interaction effects nor significant relationships with the DMI covariate (ps > 0.80). Age was a significant covariate for FA ($p = 0.03$), but not for MD ($p = 0.27$). A repeated measures ANCOVA performed for tract volumes, with age, DMI and TBV (to control for brain size differences) as covariates, revealed no significant effects.

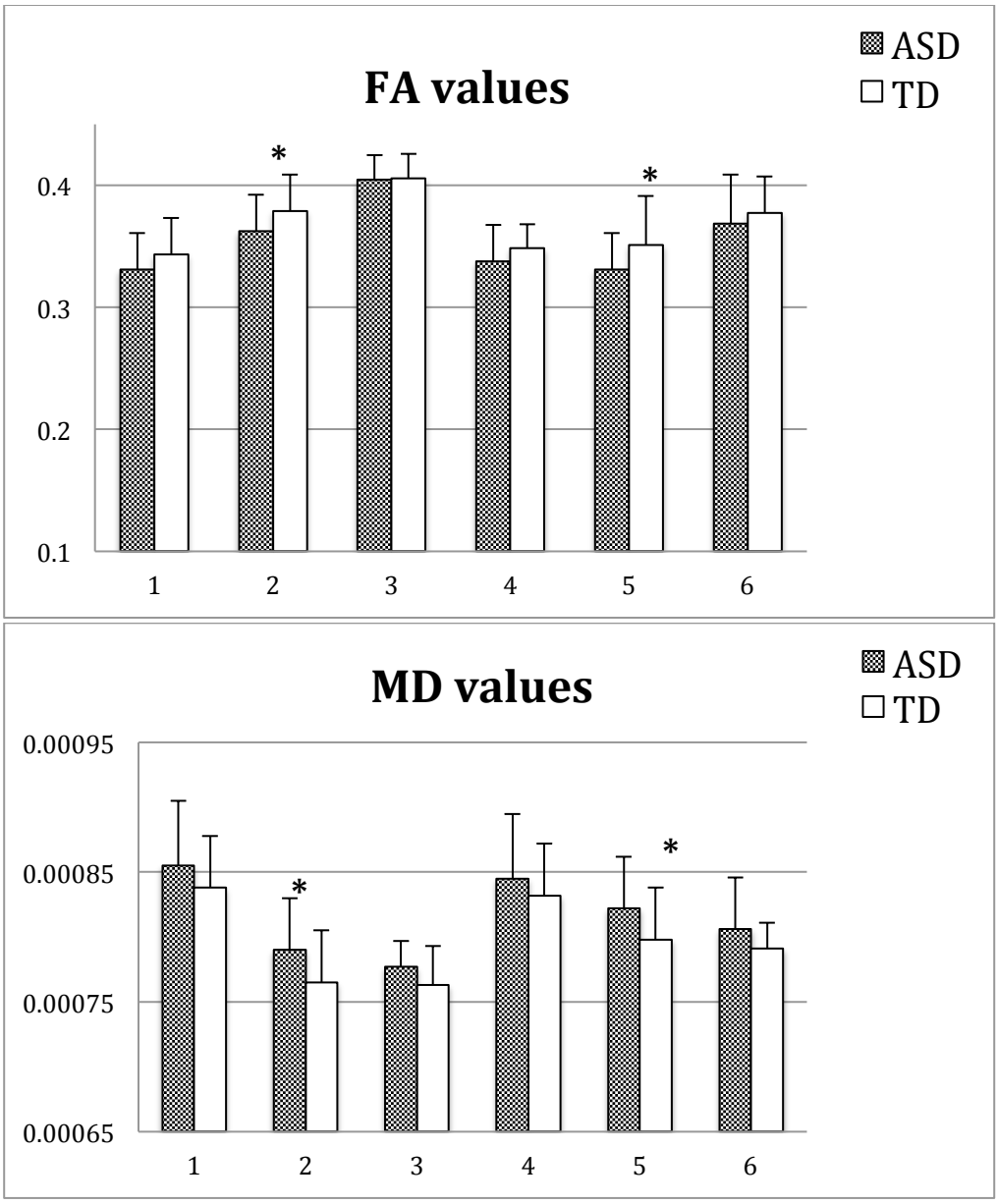

Figure 4.4 Fractional anisotropy (FA) and mean diffusivity (MD) means in white matter tracts of interest (TOIs), in ASD and TD groups. 1 = Left IFG to left medial PMC; 2 = left IFG to left lateral dorsal PMC; 3 = left IFG to left IPS; 4 = right IFG to right medial PMC; 5 = right IFG to right lateral dorsal PMC; 6 = right IFG to right IPL; * indicates significance at $p < 0.05$.

Correlation with clinical measures

The correlation between white matter microstructural properties (FA, etc.) within the imitation network and ASD symptom severity was examined. Only two diagnostic and behavioral measures, chosen for their relevance to the function of the imitation network, were used for correlational analyses. These included the total ADOS score (ASD only) and the total SRS score (both ASD and TD). This limited selection had the added benefit of reducing Type 1 error due to multiple comparisons. Also, since group differences in both FA and MD were found in the same two tracts, only the FA values were used for tests of correlations with symptom severity. As with the previous between-group tests of MD and FA, DMI values for each group were used as covariates for all correlations. While correlational findings for the SRS were not significant, there was a significant negative correlation between ADOS total score and FA such that lower FA correlated with higher symptom severity ($r = -.51$, $p = .01$). This effect was seen in the tract between the left IFG and left medial PMC tractography seeds, and a scatterplot illustrating the correlation is shown in Figure 4.5.

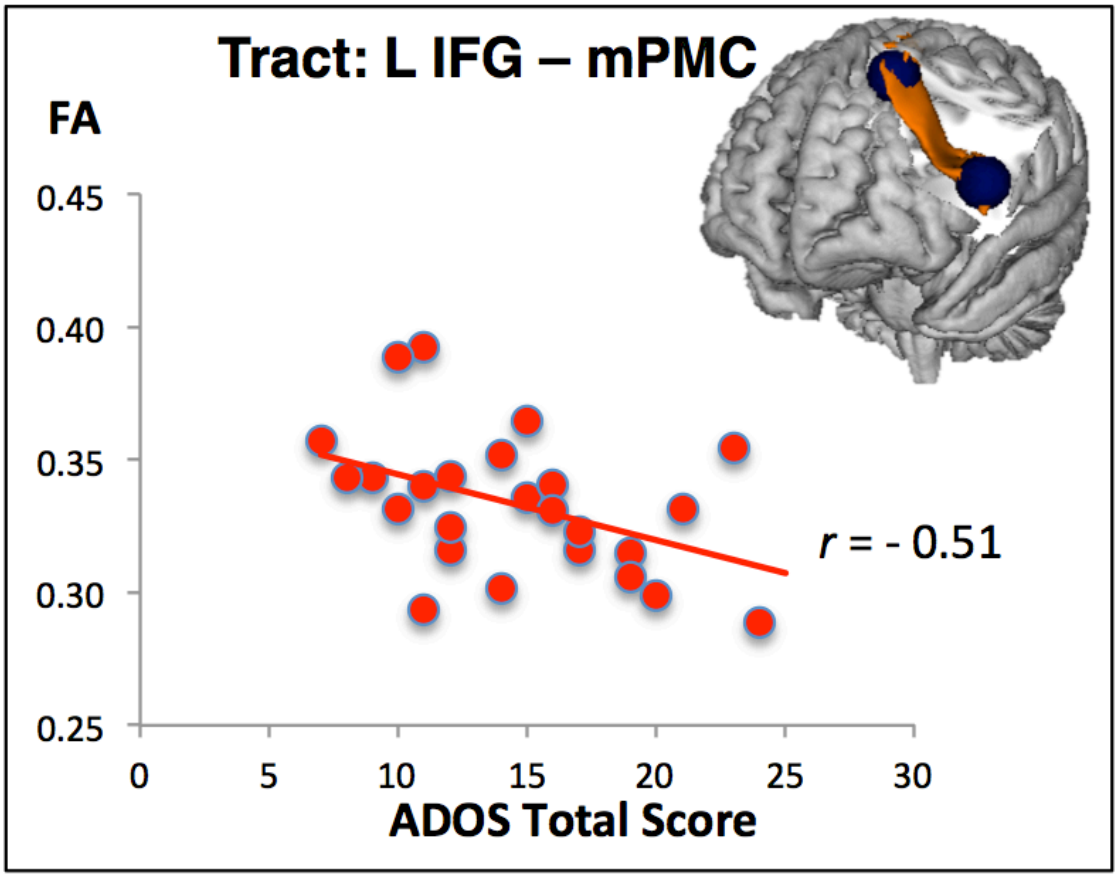

Figure 4.5 Significant correlation between ADOS total scores and average FA in the tract between Left IFG and Left medial PMC tractography seeds, in the ASD group only.

Discussion

The finding of reduced FA and increased MD in ASD in two of the intra-imitation-network tracts may indicate that impaired white matter microstructure plays a role in the aberrant functioning of that network. In a developmental context, increased mean and radial diffusivity is seen in early stages of development relative to later stages (Johnson et al., 2014), and may reflect reduced myelination or atypical patterns of synaptic pruning (Barnea-Goraly et al., 2005). Mature white matter, defined by greater FA and lower MD, is associated with normal cognitive development (Nagy et al., 2004). A similar

pattern has been observed in a longitudinal study of white matter development in ASD, in which the typically developing control group, but not the ASD group, showed decreases in radial and mean diffusivity during development (Mak-Fan et al., 2013). The present study shows this abnormal pattern of diffusion measures specifically in tracts connecting cortical areas involved in imitation.

With the exception of the tracts connecting the medial PMC to the lateral dPMC, most tracts that were included in the final analysis overlapped with superior longitudinal fasciculus (SLF) according to tracer-based tractography atlases (Schmahmann & Pandya, 2009). As mentioned in the methods section above, this is a major tract that connects larger areas of parietal, temporal and occipital cortex with frontal cortices. This area consistently shows lower FA across studies of diffusion within the ASD population (Aoki et al., 2013). In this context, reduced FA and increased MD could be indicative of white matter compromise in tracts linking key imitation regions. The correlation between diffusion measures in these tracts and ASD symptom severity suggests that the groupwise differences in white matter microstructure may be related to the behavioral etiology of autism in this sample. However, since tracts outside the imitation network were not examined as part of this study, the specificity of the link between microstructure in this network and social behavior remains undetermined.

Tracts that may exist between the Caspers imitation ROIs would pass through regions that typically contain crossing fibers. This may partially

explain why the probabilistic tractography software we used was unable to trace tracts through such regions. For instance, the only anatomically valid routes from many of the dorsal seeds (such as lateral dorsal PMC) towards the ventral seeds (such as FFA) intersect with the internal capsule, which is known to contain many crossing fibers that cannot be resolved with standard tractography methods (Wedeen et al., 2008). It is therefore possible that there are important between-group differences in white matter microstructure within these highly complex tracts that we were unable to detect.

Another issue concerns the results of the correlational analyses between white matter diffusion properties and ASD symptom severity. The tract between left IFG and left medial premotor cortex (SMA) was the only one showing a significant correlation between FA values and ADOS. That tract was not one of the two tracts that showed group differences in FA or MD, weakening the claim of a connection between differences in white matter and ASD symptom severity. However, all tracts showed similar trends with respect to groupwise differences, even though only two reached statistical significance. In the tract that showed a significant correlation with symptom severity, a potential group difference in white matter properties may not have been detected due to insufficient statistical power. However, it is equally possible that there are no real correlations between diffusion measures and symptom severity in those tracts.

We found evidence of abnormalities in white matter fiber tracts linking key regions of an imitation network. Since the functional nodes of this network play a role in imitation, and since imitation is a critical component of many social behaviors, it is possible that these structural anomalies underlie many of the social symptoms seen in autism. However, since only a select few tracts were analyzed in this study, we cannot presently make a strong claim that atypical white matter specifically in these tracts causes ASD social symptoms; it is possible that abnormalities in other tracts outside the imitation network play an equal or greater role.

Other chapters of this dissertation have demonstrated that mu neurofeedback training can alter brain activity in the functional homologues of the structural areas studied in this chapter. However, it is currently unknown whether the underlying white matter structure can be positively changed as a result of this intervention as well. In conjunction with the other chapters, this chapter helps establish microstructure between imitation-related brain regions as both a possible cause and potential target of intervention for the social symptoms of autism.

Chapter 4, in part, has been accepted for publication of the material as it will appear in Annals of Neurology, 2015, Fishman, Inna; Datko, Michael; Cabrera, Yuli; Carper, Ruth; Müller, Ralph-Axel. The dissertation author was the secondary investigator and co-author on this paper.

Chapter 5: Conclusion

This dissertation investigated two parallel threads in the study of autism as a disorder of brain network connectivity. First, it explored in detail how brain systems underlying social behaviors such as action observation and imitation show atypical structure and function in ASD. Second, it showed that mu-rhythm-based neurofeedback training can lead to significant changes in the connectivity and function of these social brain areas, along with positive increases in behaviors that are normally compromised in ASD.

Chapter 2 examined the effects of NFT on activation in the human mirror neuron system during a goal-oriented imitation task. It was found that there were interaction effects of group status and training status in parietal areas that are critical for sensorimotor integration and act as key hubs in the hMNS. Prior to NFT, imitation-related activation differences between groups were seen in other core MNS areas, including inferior frontal gyrus. Furthermore, it was found that the ASD group specifically had the greatest increases in activation after the training, and that those increases correlated with improvements on parental assessments of behavior.

Chapter 3 investigated the effects of NFT on functional connectivity in an imitation network that includes areas of the human mirror neuron system. It was found that, prior to training, the ASD group showed overconnectivity from many imitation seeds to regions outside of that network, and specifically to frontal and prefrontal regions. After training, both groups had several clusters

of significantly increased FC relative to before training. In between-group comparisons after NFT, ASD showed overconnectivity to regions that were largely within the imitation network. This shift from out-of-network to within-network overconnectivity relative to TD may be indicative of increases in network segregation and integration within the imitation network.

Chapter 4 examined white matter microstructure in fiber pathways connecting cortical areas involved in imitation, and found evidence of more diffuse white matter projections in autism compared to matched controls. Differences were found specifically in several tracts that passed through bilateral superior longitudinal fasciculus, a pathway known to connect many distributed areas of association cortex. The finding that reduced anisotropy was significantly correlated with a measure of ASD symptom severity in the social domain suggests that white matter abnormalities connecting imitation regions through the SLF are partly the basis for some of the social deficits commonly seen in children and adolescents with autism. However, since only tracts within the imitation network were examined as part of this study, it is unclear how specific those effects and behavioral correlations are to those tracts. It is entirely possible that microstructural properties of tracts connecting other regions might correlate just as well or even better with symptom severity than they do within the imitation network tracts. Furthermore, many tracts within the imitation network were not fully explored in this study due to the limitations of the diffusion data and the probabilistic tractography algorithm.

This study was only able to use 61 directions to model voxelwise diffusion, which limited the capacity to accurately model crossing fibers and to find streamlines through areas with many such fibers.

One methodological constant throughout this study was the use of regions of interest based on the Caspers meta-analysis of 87 studies of imitation-related brain activation. In Chapter 2, activation values were extracted for each participant from these ROIs before and after NFT, and ANOVAs with group status and training status were performed on these extracted values. In Chapter 3, seed-based functional connectivity analysis was performed before and after NFT using the Caspers ROIs as seeds. In Chapter 4, probabilistic tractography was used to find white matter tracts between these ROIs. Across all of these chapters, consistent group differences between ASD and TD were found using the Caspers ROIs in premotor and somatosensory integration areas. In the two chapters that examined longitudinal effects of NFT, these areas showed training-related changes. Finally, correlations between symptom severity and effects of the training were found in parietal and dorsolateral frontal areas as well. The consistency of these findings across neuroimaging modalities and analysis techniques indicates that dysfunctions in those areas are an important factor in the deficits in imitation and social behaviors in autism.

Furthermore, this is the first time that fMRI and fcMRI have been used to show NFT-induced changes in dynamics of the hMNS, which typically

displays aberrant function in autism. While previous studies of mu-NFT in ASD participants have shown evidence of positive behavioral changes, they relied exclusively on electrophysiology for findings related to neurophysiology. By expanding on those results with fMRI, which has the superior spatial resolution necessary to pinpoint changes in key hMNS structures, the studies in this dissertation have further localized both the neurophysiological substrates of autism as well as the sites that play a role in the benefits conferred by NFT.

Both chapters that examined the effects of NFT on neurophysiology and behavior relied on parental reports for measuring behavioral changes. These included the Social Responsiveness Scale (SRS) and the Autism Treatment Evaluation Checklist (ATEC). Parental reports are not ideal measures of behavior, especially in longitudinal studies with a treatment component such as those presented here. Parents can be understandably biased by an expectation that their child will show behavioral improvements after training. However, the finding that improvements in parental reports of behavior were well correlated with increases in activation and connectivity of relevant brain areas suggests that the behavioral assessments were able to detect real changes that had a neurophysiological basis.

The functional changes that were shown in chapters 2 and 3 may have a structural component as well. While DTI data was collected for many of the subjects that underwent NFT, the subsample in which diffusion data was of

high enough quality was even smaller than for the functional data. Thus, it remains unknown whether the amount of NFT completed in these studies is sufficient to cause measurable changes in white matter microstructure. A future study could test this within pathways connecting the areas in which functional effects of NFT have already been observed. Evidence from studies of other forms of training indicate that significant structural changes can take place after relatively short periods of time (May et al., 2011; Hölzel et al., 2011).

While the studies on NFT included in this dissertation have relatively small sample sizes, the robust results are evidence of the largely untapped potential of neurofeedback training and related biofeedback techniques for improving physiology and behavior in autism. The mu-NFT protocol used in these studies, while apparently somewhat effective in its current form, has the potential for improvements and optimization. Other recent EEG-based work has shown that NFT may be more effective when combined with socially-relevant dynamic feedback, instead of the relatively simple format of the games and movies used in the present studies (Friedrich et al., 2014, Friedrich et al., 2015). Additionally, in the present NFT protocol only one electrode is used to control the feedback received by the participant. The hMNS is a complex and distributed system, and it is possible that new NFT protocols that utilize multiple electrode sites can be even more effective in fine-tuning the oscillatory dynamics of this system and in causing positive behavioral

changes. Thus, the work presented in this dissertation not only adds to the body of knowledge about the neurophysiological pathology of autism, but also sets a precedent for evidence-based interventions that specifically target that underlying pathology.

Bibliography

Abbott, A.E., Nair, A., Keown, C.L., Datko, M.C., Jahedi, A., Fishman, I. & Müller, R.-A. (2015) Patterns of atypical functional connectivity and behavioral links in autism differ between default, salience, and executive networks. *Cerebral Cortex.*

Ameis, S. H., Fan, J., Rockel, C., Voineskos, A. N., Lobaugh, N. J., Soorya, L., Anagnostou, E. (2011). Impaired structural connectivity of socio-emotional circuits in autism spectrum disorders: A diffusion tensor imaging study. *PLoS ONE*, *6*(11). http://doi.org/10.1371/journal.pone.0028044

American Psychiatric Association (2000): *Diagnostic and Statistical Manual of Mental Disorders, IV-TR*. Washington, DC: American Psychiatric Press.

Anagnostou, E., & Taylor, M. J. (2011). Review of neuroimaging in autism spectrum disorders: what have we learned and where we go from here. *Molecular Autism*, *2*(1), 4.

Andersen, R. a, Asanuma, C., Essick, G., & Siegel, R. M. (1990). Corticocortical connections of anatomically defined subdivisions within the inferior parietal lobe. *Jcn*, *296*, 65–113.

Andersen, R. A. 2011. Inferior Parietal Lobule Function in Spatial Perception and Visuomotor Integration. Comprehensive Physiology. 483–518.

Aoki, Y., Abe, O., Nippashi, Y., & Yamasue, H. (2013). Comparison of white matter integrity between autism spectrum disorder subjects and typically developing individuals: a meta-analysis of diffusion tensor imaging tractography studies. *Molecular Autism*, *4*(1), 25. http://doi.org/10.1186/2040-2392-4-25

Arnstein, D., Cui, F., Keysers, C., Maurits, N. M., & Gazzola, V. (2011). μ-suppression during action observation and execution correlates with BOLD in dorsal premotor, inferior parietal, and SI cortices. *The Journal of Neuroscience : The Official Journal of the Society for Neuroscience*, *31*(40), 14243–9. http://doi.org/10.1523/JNEUROSCI.0963-11.2011

Barnea-Goraly, N., Menon, V., Eckert, M., Tamm, L., Bammer, R., Karchemskiy, A., ... & Reiss, A. L. (2005). White matter development during childhood and adolescence: a cross-sectional diffusion tensor imaging study.*Cerebral cortex*, *15*(12), 1848-1854.

Baron-Cohen, S. (2009). Autism: the empathizing-systemizing (E-S) theory. *Annals of the New York Academy of Sciences*, *1156*, 68–80. http://doi.org/10.1111/j.1749-6632.2009.04467.x

Barttfeld, P., Wicker, B., Cukier, S., Navarta, S., Lew, S., & Sigman, M. (2011). A big-world network in ASD: Dynamical connectivity analysis reflects a deficit in long-range connections and an excess of short-range connections. *Neuropsychologia*, *49*(2), 254–263. http://doi.org/10.1016/j.neuropsychologia.2010.11.024

Beaulieu, C. (2002). The basis of anisotropic water diffusion in the nervous system - A technical review. *NMR in Biomedicine*, *15*(7-8), 435–455. http://doi.org/10.1002/nbm.782

Behrens, T. E. J., Woolrich, M. W., Jenkinson, M., Johansen-Berg, H., Nunes, R. G., Clare, S., Smith, S. M. (2003). Characterization and Propagation of Uncertainty in Diffusion-Weighted MR Imaging. *Magnetic Resonance in Medicine*, *50*(5), 1077–1088. http://doi.org/10.1002/mrm.10609

Belmonte, M. K., Allen, G., Beckel-Mitchener, A., Boulanger, L. M., Carper, R. a, & Webb, S. J. (2004). Autism and abnormal development of brain connectivity. *The Journal of Neuroscience : The Official Journal of the Society for Neuroscience*, *24*(42), 9228–31. http://doi.org/10.1523/JNEUROSCI.3340-04.2004

Bernier, R., Dawson, G., Webb, S., & Murias, M. (2007). EEG mu rhythm and imitation impairments in individuals with autism spectrum disorder. *Brain and Cognition*, *64*(3), 228–37. http://doi.org/10.1016/j.bandc.2007.03.004

Biswal, B., Yetkin, F. Z., Haughton, V. M., & Hyde, J. S. (1995). Functional connectivity in the motor cortex of resting human brain using echo-planar MRI. *Magnetic Resonance in Medicine : Official Journal of the Society of Magnetic Resonance in Medicine / Society of Magnetic Resonance in Medicine*, *34*(4), 537–41. Retrieved from http://www.ncbi.nlm.nih.gov/pubmed/8524021

Bonda, E., Ostry, D., & Evans, A. (1996). Specific Involvement of Human Parietal Systems in the Perception of Biological Motion and the Amygdala. *The Journal of Neuroscience*, *16*(11), 3737–3744.

Broadstock, M., Doughty, C., & Eggleston, M. (2007). Systematic review of the effectiveness of pharmacological treatments for adolescents and adults with autism spectrum disorder. *Autism : The International Journal of*

Research and Practice, *11*(4), 335–348. http://doi.org/10.1177/1362361307078132

Buccino, G., Binkofski, F., Fink, G. R., Fadiga, L., Fogassi, L., Gallese, V., … Freund, H. J. (2001). Action observation activates premotor and parietal areas in a somatotopic manner: An fMRI study. *European Journal of Neuroscience*, *13*(2), 400–404. http://doi.org/10.1046/j.1460-9568.2001.01385.x

Bullmore, E., Bullmore, E., Sporns, O., & Sporns, O. (2009). Complex brain networks: graph theoretical analysis of structural and functional systems. *Nat Rev Neurosci*, *10*(3), 186–198. http://doi.org/10.1038/nrn2575

Cahan, S., & Noyman, a. (2001). The Kaufman Ability Battery for Children Mental Processing Scale: A Valid Measure of “Pure” Intelligence? *Educational and Psychological Measurement*, *61*(5), 827–840. http://doi.org/10.1177/00131640121971545

Carpenter, M., Nagell, K., & Tomasello, M. (1998). Social cognition, joint attention, and communicative competence from 9 to 15 months of age. *Monographs of the Society for Research in Child Development*, *63*(4).

Caspers, S., Zilles, K., Laird, A. R., & Eickhoff, S. B. (2010). ALE meta-analysis of action observation and imitation in the human brain. *NeuroImage*, *50*(3), 1148–1167. http://doi.org/10.1016/j.neuroimage.2009.12.112

Chartrand, T. L., & Bargh, J. A. (1999). The chameleon effect: the perception–behavior link and social interaction. *Journal of personality and social psychology*, *76*(6), 893.

Chasson, G. S., Harris, G. E., & Neely, W. J. (2007). Cost comparison of early intensive behavioral intervention and special education for children with autism. *Journal of Child and Family Studies*, *16*(3), 401–413. http://doi.org/10.1007/s10826-006-9094-1

Coben, R., Linden, M., & Myers, T. E. (2010a). Neurofeedback for autistic spectrum disorder: A review of the literature. *Applied Psychophysiology Biofeedback*, *35*(1), 83–105. http://doi.org/10.1007/s10484-009-9117-y

Constantino, J. N., Davis, S. a., Todd, R. D., Schindler, M. K., Gross, M. M., Brophy, S. L., … Reich, W. (3AD). Validation of a Brief Quantitative Measure of Autistic Traits: Comparison of the Social Responsiveness

Scale with the Autism Diagnostic Interview -revised. *Journal of Autism and Developmental disorders2*, *33*(4).

Cordes, D., Haughton, V. M., Arfanakis, K., Carew, J. D., Turski, P. a, Moritz, C. H., … Meyerand, M. E. (2001). Frequencies contributing to functional connectivity in the cerebral cortex in "resting-state" data. *AJNR. American Journal of Neuroradiology*, *22*(7), 1326–33. Retrieved from http://www.ncbi.nlm.nih.gov/pubmed/11498421

Courchesne, E., & Pierce, K. (2005). Why the frontal cortex in autism might be talking only to itself: local over-connectivity but long-distance disconnection. *Current Opinion in Neurobiology*, *15*(2), 225–30. http://doi.org/10.1016/j.conb.2005.03.001

Cox, R. W. (1996). AFNI: software for analysis and visualization of functional magnetic resonance neuroimages. *Computers and Biomedical Research, an International Journal*, *29*(3), 162–73. Retrieved from http://www.ncbi.nlm.nih.gov/pubmed/8812068

Cramer, S. C., Sur, M., Dobkin, B. H., O'Brien, C., Sanger, T. D., Trojanowski, J. Q., … Vinogradov, S. (2011). Harnessing neuroplasticity for clinical applications. *Brain*, *134*(6), 1591–1609. http://doi.org/10.1093/brain/awr039

Damoiseaux, J. S., & Greicius, M. D. (2009). Greater than the sum of its parts: a review of studies combining structural connectivity and resting-state functional connectivity. *Brain Structure & Function*, *213*(6), 525–33. http://doi.org/10.1007/s00429-009-0208-6

Dapretto, M., Davies, M. S., Pfeifer, J. H., Scott, A. a, Sigman, M., Bookheimer, S. Y., & Iacoboni, M. (2006). Understanding emotions in others: mirror neuron dysfunction in children with autism spectrum disorders. *Nature Neuroscience*, *9*(1), 28–30. http://doi.org/10.1038/nn1611

Dinstein, I., Thomas, C., Behrmann, M., & Heeger, D. J. (2008). A mirror up to nature. *Current Biology*, *18*(1), 13–18.

DiPelligrino, G., Fadiga, L., Fogassi, L., Gallese, V., & Rizzolatti, G. (1992). Understanding motor events: a neurophysiological study. *Experimental Brain Research*, *91*, 176–180.

Ebisch, S. J., Gallese, V., Willems, R. M., Mantini, D., Groen, W. B., Romani, G. L., ... & Bekkering, H. (2011). Altered intrinsic functional connectivity of anterior and posterior insula regions in high-functioning participants with autism spectrum disorder. *Human brain mapping*, *32*(7), 1013-1028.

Fishman, I., Keown, C. L., Lincoln, A. J., Pineda, J. a, & Müller, R.-A. (2014). Atypical cross talk between mentalizing and mirror neuron networks in autism spectrum disorder. *JAMA Psychiatry*, *71*(7), 751–60. http://doi.org/10.1001/jamapsychiatry.2014.83

Forman, S. D., Cohen, J. D., Fitzgerald, M., Eddy, W. F., Mintun, M. A. and Noll, D. C. (1995), Improved Assessment of Significant Activation in Functional Magnetic Resonance Imaging (fMRI): Use of a Cluster-Size Threshold. Magn Reson Med, 33: 636–647. doi: 10.1002/mrm.1910330508

Fox, D. J., Tharp, D. F., & Fox, L. C. (2005). Neurofeedback: an alternative and efficacious treatment for Attention Deficit Hyperactivity Disorder. *Applied Psychophysiology and Biofeedback*, *30*(4), 365–73. http://doi.org/10.1007/s10484-005-8422-3

Fox, M. D., & Raichle, M. E. (2007). Spontaneous fluctuations in brain activity observed with functional magnetic resonance imaging. *Nature Reviews. Neuroscience*, *8*(9), 700–11. http://doi.org/10.1038/nrn2201

Friedrich, E. V. C., Sivanathan, A., Lim, T., Suttie, N., Louchart, S., Pillen, S., & Pineda, J. a. (2015). An Effective Neurofeedback Intervention to Improve Social Interactions in Children with Autism Spectrum Disorder. *Journal of Autism and Developmental Disorders*, (August). http://doi.org/10.1007/s10803-015-2523-5

Friedrich, E. V. C., Suttie, N., Sivanathan, A., Lim, T., Louchart, S., & Pineda, J. a. (2014). Brain-computer interface game applications for combined neurofeedback and biofeedback treatment for children on the autism spectrum. *Frontiers in Neuroengineering*, *7*(July), 1–7. http://doi.org/10.3389/fneng.2014.00021

Frith, C. (2004). Is autism a disconnection disorder?. *The Lancet Neurology*,*3*(10), 577.

Fuchs, T., Birbaumer, N., Lutzenberger, W., Gruzelier, J. H., & Kaiser, J. (2003). Neurofeedback treatment for attention-deficit/hyperactivity disorder in children: a comparison with methylphenidate. *Applied*

Psychophysiology and Biofeedback, *28*(1), 1–12. Retrieved from http://www.ncbi.nlm.nih.gov/pubmed/12737092

Greicius, M. D., Supekar, K., Menon, V., & Dougherty, R. F. (2009). Resting-state functional connectivity reflects structural connectivity in the default mode network. *Cerebral Cortex (New York, N.Y. : 1991)*, *19*(1), 72–8. http://doi.org/10.1093/cercor/bhn059

Hadjikhani, N., Joseph, R. M., Snyder, J., & Tager-Flusberg, H. (2006). Anatomical differences in the mirror neuron system and social cognition network in autism. *Cerebral Cortex (New York, N.Y. : 1991)*, *16*(9), 1276–82. http://doi.org/10.1093/cercor/bhj069

Hari, R., Forss, N., Avikainen, S., Kirveskari, E., Salenius, S., & Rizzolatti, G. (1998). Activation of human primary motor cortex during action observation: a neuromagnetic study. *Proceedings of the National Academy of Sciences of the United States of America*, *95*(25), 15061–15065. http://doi.org/10.1073/pnas.95.25.15061

Hickok, G. (2009). Eight problems for the mirror neuron theory of action understanding in monkeys and humans. *Journal of Cognitive Neuroscience*, *21*(7), 1229–43. http://doi.org/10.1162/jocn.2009.21189

Hölzel, B. K., Carmody, J., Vangel, M., Congleton, C., Yerramsetti, S. M., Gard, T., & Lazar, S. W. (2011). Mindfulness practice leads to increases in regional brain gray matter density. *Psychiatry Research: Neuroimaging*, *191*(1), 36-43.

Iacoboni, M. (1999). Cortical Mechanisms of Human Imitation. *Science*, *286*(5449), 2526–2528. http://doi.org/10.1126/science.286.5449.2526

Iacoboni, M., & Dapretto, M. (2006). The mirror neuron system and the consequences of its dysfunction. *Nature Reviews. Neuroscience*, *7*(12), 942–51. http://doi.org/10.1038/nrn2024

Ingersoll, B., & Gergans, S. (2007). The effect of a parent-implemented imitation intervention on spontaneous imitation skills in young children with autism. *Research in developmental disabilities*, *28*(2), 163-175.

Ingersoll, B. (2008). The social role of imitation in autism: Implications for the treatment of imitation deficits. *Infants & Young Children*, *21*(2), 107-119.

Ingersoll, B. (2012). Brief report: Effect of a focused imitation intervention on social functioning in children with autism. *Journal of autism and developmental disorders*, *42*(8), 1768-1773.

Insel, T., Cuthbert, B., Garvey, M., Heinssen, R., Pine, D. S., Quinn, K., … Wang, P. (2010). Research Domain Criteria (RDoC): Toward a new classification framework for research on mental disorders. *American Journal of Psychiatry*, *167*(7), 748–751. http://doi.org/10.1176/appi.ajp.2010.09091379

Jacobson, J. W., Mulick, J. a, & Green, G. (1998). Cost-Benefit Estimates for Early Intensive Behavioral Intervention for Young Children with Autism-General Model and Single State Case. *Behavioral Interventions*, *13*, 201–226. http://doi.org/10.1002/(SICI)1099-078X(199811)13:4<201::AID-BIN17>3.0.CO;2-R

Johnson, M. H. (2011). Interactive specialization: a domain-general framework for human functional brain development?. *Developmental Cognitive Neuroscience*, *1*(1), 7-21.

Johnson, R. T., Yeatman, J. D., Wandell, B. A., Buonocore, M. H., Amaral, D. G., & Nordahl, C. W. (2014). Diffusion properties of major white matter tracts in young, typically developing children. *NeuroImage*, *88*, 143-154.

Just, M. A., Cherkassky, V. L., Keller, T. a, & Minshew, N. J. (2004). Cortical activation and synchronization during sentence comprehension in high-functioning autism: evidence of underconnectivity. *Brain : A Journal of Neurology*, *127*(Pt 8), 1811–21. http://doi.org/10.1093/brain/awh199

Kana, R. K., Keller, T. A., Minshew, N. J., & Just, M. A. (2007). Inhibitory control in high-functioning autism: decreased activation and underconnectivity in inhibition networks. *Biological psychiatry*, *62*(3), 198-206.

Kana, R. K., Libero, L. E., & Moore, M. S. (2011). Disrupted cortical connectivity theory as an explanatory model for autism spectrum disorders. *Physics of life reviews*, *8*(4), 410-437.

Keehn, B., Shih, P., Brenner, L. a., Townsend, J., & Müller, R. A. (2013). Functional connectivity for an “Island of sparing” in autism spectrum disorder: An fMRI study of visual search. *Human Brain Mapping*, *34*(10), 2524–2537. http://doi.org/10.1002/hbm.22084

Keown, C. L., Shih, P., Nair, A., Peterson, N., Mulvey, M. E., & Müller, R. A. (2013). Local functional overconnectivity in posterior brain regions is associated with symptom severity in autism spectrum disorders. *Cell reports*, *5*(3), 567-572.

Kim, J., Wigram, T., & Gold, C. (2008). The effects of improvisational music therapy on joint attention behaviors in autistic children: A randomized controlled study. *Journal of Autism and Developmental Disorders*, *38*(9), 1758–1766. http://doi.org/10.1007/s10803-008-0566-6

Koldewyn, K., Yendiki, A., Weigelt, S., Gweon, H., Julian, J., Richardson, H., … Kanwisher, N. (2014). Differences in the right inferior longitudinal fasciculus but no general disruption of white matter tracts in children with autism spectrum disorder. *Proceedings of the National Academy of Sciences of the United States of America*, *111*(5), 1981–6. http://doi.org/10.1073/pnas.1324037111

Kuhlman, W. N. (1978). Functional topography of the human mu rhythm.*Electroencephalography and clinical neurophysiology*, *44*(1), 83-93.

Lakin, J. L., & Chartrand, T. L. (2003). Using nonconscious behavioral mimicry to create affiliation and rapport. *Psychological science*, *14*(4), 334-339.

Lakin, J. L., Jefferis, V. E., Cheng, C. M., & Chartrand, T. L. (2003). The chameleon effect as social glue: Evidence for the evolutionary significance of nonconscious mimicry. *Journal of nonverbal behavior*, *27*(3), 145-162.

Lévesque, J., Beauregard, M., & Mensour, B. (2006). Effect of neurofeedback training on the neural substrates of selective attention in children with attention-deficit/hyperactivity disorder: a functional magnetic resonance imaging study. *Neuroscience Letters*, *394*(3), 216–21. http://doi.org/10.1016/j.neulet.2005.10.100

Lord C, Rutter M, DiLavore P, Risi S (2001): *Autism Diagnostic Observation Schedule*. Los Angeles: Western Psychological Services.

Magiati, I., Moss, J., Yates, R., Charman, T., & Howlin, P. (2011). Is the Autism Treatment Evaluation Checklist a useful tool for monitoring progress in children with autism spectrum disorders? *Journal of Intellectual Disability Research*, *55*(3), 302–312. http://doi.org/10.1111/j.1365-2788.2010.01359.x

Mak-Fan, K. M., Morris, D., Vidal, J., Anagnostou, E., Roberts, W., & Taylor, M. J. (2013). White matter and development in children with an autism spectrum disorder. *Autism*, *17*(5), 541-557.

May, A. (2011). Experience-dependent structural plasticity in the adult human brain. *Trends in Cognitive Sciences*, *15*(10), 475–482. http://doi.org/10.1016/j.tics.2011.08.002

McFarland, D. J., Miner, L. a, Vaughan, T. M., & Wolpaw, J. R. (2000). Mu and beta rhythm topographies during motor imagery and actual movements. *Brain Topography*, *12*(3), 177–86. Retrieved from http://www.ncbi.nlm.nih.gov/pubmed/10791681

McIntosh, D. N., Reichmann-Decker, A., Winkielman, P., & Wilbarger, J. L. (2006). When the social mirror breaks: deficits in automatic, but not voluntary, mimicry of emotional facial expressions in autism. *Developmental science*, *9*(3), 295-302.

Mueller, S., Keeser, D., Samson, A. C., Kirsch, V., Blautzik, J., Grothe, M., … Meindl, T. (2013). Convergent Findings of Altered Functional and Structural Brain Connectivity in Individuals with High Functioning Autism: A Multimodal MRI Study. *PloS One*, *8*(6), e67329. http://doi.org/10.1371/journal.pone.0067329

Müller, R. (2007). The Study of Autism as a Distributed Disorder. *Mental Retardation and Developmental Disabilities Research Reviews*, *95*(225), 85–95. http://doi.org/10.1002/mrdd

Müller, R. A., Shih, P., Keehn, B., Deyoe, J. R., Leyden, K. M., & Shukla, D. K. (2011). Underconnected, but how? A survey of functional connectivity MRI studies in autism spectrum disorders. *Cerebral Cortex*, *21*(10), 2233–2243. http://doi.org/10.1093/cercor/bhq296

Muthukumaraswamy, S. D., Johnson, B. W., & McNair, N. a. (2004). Mu rhythm modulation during observation of an object-directed grasp. *Brain Research. Cognitive Brain Research*, *19*(2), 195–201. http://doi.org/10.1016/j.cogbrainres.2003.12.001

Nagy, Z., Westerberg, H., & Klingberg, T. (2004). Maturation of white matter is associated with the development of cognitive functions during childhood.*Journal of cognitive neuroscience*, *16*(7), 1227-1233.

Nair, A., Treiber, J. M., Shukla, D. K., Shih, P., & Müller, R.-A. (2013). Impaired thalamocortical connectivity in autism spectrum disorder: a study of functional and anatomical connectivity. *Brain : A Journal of Neurology*, *136*(Pt 6), 1942–55. http://doi.org/10.1093/brain/awt079

Nair, A., Keown, C. L., Datko, M., Shih, P., Keehn, B., & Müller, R. A. (2014). Impact of methodological variables on functional connectivity findings in autism spectrum disorders. *Human brain mapping*, *35*(8), 4035-4048.

Nishitani, N., Avikainen, S., & Hari, R. (2004). Abnormal imitation-related cortical activation sequences in Asperger's syndrome. *Annals of Neurology*, *55*(4), 558–62. http://doi.org/10.1002/ana.20031

Oberman, L. M., Hubbard, E. M., McCleery, J. P., Altschuler, E. L., Ramachandran, V. S., & Pineda, J. a. (2005). EEG evidence for mirror neuron dysfunction in autism spectrum disorders. *Brain Research. Cognitive Brain Research*, *24*(2), 190–8. http://doi.org/10.1016/j.cogbrainres.2005.01.014

Oberman, L. M., McCleery, J. P., Hubbard, E. M., Bernier, R., Wiersema, J. R., Raymaekers, R., & Pineda, J. a. (2013). Developmental changes in mu suppression to observed and executed actions in autism spectrum disorders. *Social Cognitive and Affective Neuroscience*, *8*(3), 300–4. http://doi.org/10.1093/scan/nsr097

Oberman, L. M., Pineda, J. a, & Ramachandran, V. S. (2007). The human mirror neuron system: a link between action observation and social skills. *Social Cognitive and Affective Neuroscience*, *2*(1), 62–6. http://doi.org/10.1093/scan/nsl022

Oberman, L. M., Ramachandran, V. S., & Pineda, J. a. (2008). Modulation of mu suppression in children with autism spectrum disorders in response to familiar or unfamiliar stimuli: the mirror neuron hypothesis. *Neuropsychologia*, *46*(5), 1558–65. http://doi.org/10.1016/j.neuropsychologia.2008.01.010

Ozonoff, S., Pennington, B. F., & Rogers, S. J. (1991). Executive function deficits in high-functioning autistic individuals: Relationship to theory of mind. *Journal of child Psychology and Psychiatry*, *32*(7), 1081-1105.

Pascual-Leone, A., Amedi, A., Fregni, F., & Merabet, L. B. (2005). The plastic human brain cortex. *Annual Review of Neuroscience*, *28*, 377–401. http://doi.org/10.1146/annurev.neuro.27.070203.144216

Perkins, T., Stokes, M., McGillivray, J., & Bittar, R. (2010). Mirror neuron dysfunction in autism spectrum disorders. *Journal of Clinical Neuroscience : Official Journal of the Neurosurgical Society of Australasia*, *17*(10), 1239–43. http://doi.org/10.1016/j.jocn.2010.01.026

Pfurtscheller, G., & Neuper, C. (1997). Motor imagery activates primary sensorimotor area in humans. *Neuroscience letters*, *239*(2), 65-68.

Pfurtscheller, G., Brunner, C., Schlögl, a, & Lopes da Silva, F. H. (2006). Mu rhythm (de)synchronization and EEG single-trial classification of different motor imagery tasks. *NeuroImage*, *31*(1), 153–9. http://doi.org/10.1016/j.neuroimage.2005.12.003

Pineda, J. a. (2005). The functional significance of mu rhythms: translating “seeing” and “hearing” into “doing”. *Brain Research. Brain Research Reviews*, *50*(1), 57–68. http://doi.org/10.1016/j.brainresrev.2005.04.005

Pineda, J. a., Brang, D., Hecht, E., Edwards, L., Carey, S., Bacon, M., … Rork, a. (2008). Positive behavioral and electrophysiological changes following neurofeedback training in children with autism. *Research in Autism Spectrum Disorders*, *2*(3), 557–581. http://doi.org/10.1016/j.rasd.2007.12.003

Pineda, J. A., Carrasco, K., Datko, M., Pillen, S., & Schalles, M. (2014). Neurofeedback training produces normalization in behavioural and electrophysiological measures of high-functioning autism. *Philosophical Transactions of the Royal Society B*, *369*(April).

Power, J. D., Barnes, K. a, Snyder, A. Z., Schlaggar, B. L., & Petersen, S. E. (2012). Spurious but systematic correlations in functional connectivity MRI networks arise from subject motion. *NeuroImage*, *59*(3), 2142–54. http://doi.org/10.1016/j.neuroimage.2011.10.018

Rippon, G., Brock, J., Brown, C., & Boucher, J. (2007). Disordered connectivity in the autistic brain: challenges for the ‘new psychophysiology’. *International journal of psychophysiology*, *63*(2), 164-172.

Rizzolatti, G., & Craighero, L. (2004). The mirror-neuron system. *Annual Review of Neuroscience*, *27*, 169–92. http://doi.org/10.1146/annurev.neuro.27.070203.144230

Ros, T., Munneke, M. a M., Ruge, D., Gruzelier, J. H., & Rothwell, J. C. (2010). Endogenous control of waking brain rhythms induces neuroplasticity in humans. *The European Journal of Neuroscience*, *31*(4), 770–8. http://doi.org/10.1111/j.1460-9568.2010.07100.x

Rudie, J. D., Shehzad, Z., Hernandez, L. M., Colich, N. L., Bookheimer, S. Y., Iacoboni, M., & Dapretto, M. (2012). Reduced functional integration and segregation of distributed neural systems underlying social and emotional information processing in Autism spectrum disorders. *Cerebral Cortex*, *22*(5), 1025–1037. http://doi.org/10.1093/cercor/bhr171

Rudie, J. D., & Dapretto, M. (2013). Convergent evidence of brain overconnectivity in children with autism?. *Cell reports*, *5*(3), 565-566.

Rutter M, LeCouteur A, Lord C (2003): *Autism Diagnostic Interview, Revised (ADI-R)*. Los Angeles: Western Psychological Services.

Schipul, S. E., Keller, T. a, & Just, M. A. (2011). Inter-regional brain communication and its disturbance in autism. *Frontiers in Systems Neuroscience*, *5*(February), 10. http://doi.org/10.3389/fnsys.2011.00010

Schmahmann, J. D., & Pandya, D. (2009). *Fiber pathways of the brain*. OUP USA.

Shih, P., Shen, M., Öttl, B., Keehn, B., Gaffrey, M. S., & Müller, R.-A. (2010). Atypical network connectivity for imitation in autism spectrum disorder. *Neuropsychologia*, *48*(10), 2931–2939. http://doi.org/10.1016/j.neuropsychologia.2010.05.035

Smith SM, Jenkinson M, Woolrich MW, Beckmann CF, Behrens TE, Johansen-Berg H, *et al.* (2004): Advances in functional and structural MR image analysis and implementation as FSL. *NeuroImage* 23(1): S208-219.

Sterman, M. B. (1996). Physiological origins and functional correlates of EEG rhythmic activities: implications for self-regulation. *Biofeedback and Self-Regulation*, *21*(1), 3–33. Retrieved from http://www.ncbi.nlm.nih.gov/pubmed/8833314

Talairach, J., & Tournoux, P. (1988). Co-planar stereotaxic atlas of the human brain. 3-Dimensional proportional system: an approach to cerebral imaging.

Théoret, H., Halligan, E., Kobayashi, M., Fregni, F., Tager-Flusberg, H., & Pascual-Leone, a. (2005). Impaired motor facilitation during action observation in individuals with autism spectrum disorder. *Current Biology : CB*, *15*(3), R84–5. http://doi.org/10.1016/j.cub.2005.01.022

Thomas, M.S.C., Knowland, V.C.P., & Karmiloff-Smith, A. (2011). Mechanisms of developmental regression in autism and the broader phenotype: a neural network modeling approach. Psychological Review, 118 (4), 637–654.

Thomas, M. S.C., Davis, R., Karmiloff-Smith, A., Knowland, V. C.P. and Charman, T. (2015), The over-pruning hypothesis of autism. Developmental Science. doi: 10.1111/desc.12303

Travers, B. G., Adluru, N., Ennis, C., Tromp, D. P., Destiche, D., Doran, S., ... & Alexander, A. L. (2012). Diffusion tensor imaging in autism spectrum disorder: a review. *Autism Research*, *5*(5), 289-313.

Turella, L., Pierno, A. C., Tubaldi, F., & Castiello, U. (2009). Mirror neurons in humans: consisting or confounding evidence? *Brain and Language*, *108*(1), 10–21. http://doi.org/10.1016/j.bandl.2007.11.002

Uddin, L. Q., Supekar, K., & Menon, V. (2013). Reconceptualizing functional brain connectivity in autism from a developmental perspective. *Frontiers in Human Neuroscience*, *7*(August), 458. http://doi.org/10.3389/fnhum.2013.00458

Van Den Heuvel, M. P., Mandl, R. C. W., Kahn, R. S., & Hulshoff Pol, H. E. (2009). Functionally linked resting-state networks reflect the underlying structural connectivity architecture of the human brain. *Human Brain Mapping*, *30*(10), 3127–3141. http://doi.org/10.1002/hbm.20737

Van Dijk, K. R. a, Sabuncu, M. R., & Buckner, R. L. (2012). The influence of head motion on intrinsic functional connectivity MRI. *NeuroImage*, *59*(1), 431–8. http://doi.org/10.1016/j.neuroimage.2011.07.044

Villalobos, M. E., Mizuno, A., Dahl, B. C., Kemmotsu, N., & Müller, R.-A. (2005). Reduced functional connectivity between V1 and inferior frontal cortex associated with visuomotor performance in autism. *NeuroImage*, *25*(3), 916–25. http://doi.org/10.1016/j.neuroimage.2004.12.022

Vissers, M. E., Cohen, M. X., & Geurts, H. M. (2012). Brain connectivity and high functioning autism: a promising path of research that needs refined

models, methodological convergence, and stronger behavioral links.*Neuroscience & Biobehavioral Reviews*, *36*(1), 604-625.

Walker, J. E. (2008). Power Spectral Frequency and Coherence Abnormalities in Patients with Intractable Epilepsy and Their Usefulness in Long-Term Remediation of Seizures Using Neurofeedback. *Clinical EEG and Neuroscience*, *39*(4), 203–205. http://doi.org/10.1177/155005940803900410

Wass, S. (2011). Distortions and disconnections: disrupted brain connectivity in autism. *Brain and cognition*, *75*(1), 18-28.

Wedeen, V. J., Wang, R. P., Schmahmann, J. D., Benner, T., Tseng, W. Y. I., Dai, G., … de Crespigny, a. J. (2008). Diffusion spectrum magnetic resonance imaging (DSI) tractography of crossing fibers. *NeuroImage*, *41*(4), 1267–1277. http://doi.org/10.1016/j.neuroimage.2008.03.036

Welchew, D. E., Ashwin, C., Berkouk, K., Salvador, R., Suckling, J., Baron-Cohen, S., & Bullmore, E. (2005). Functional disconnectivity of the medial temporal lobe in Asperger's syndrome. *Biological psychiatry*, *57*(9), 991-998.

Williams, J. H. G., Waiter, G. D., Gilchrist, A., Perrett, D. I., Murray, A. D., & Whiten, A. (2006). Neural mechanisms of imitation and "mirror neuron" functioning in autistic spectrum disorder. *Neuropsychologia*, *44*(4), 610–21. http://doi.org/10.1016/j.neuropsychologia.2005.06.010

Williams, J. H., Whiten, a, Suddendorf, T., & Perrett, D. I. (2001). Imitation, mirror neurons and autism. *Neuroscience and Biobehavioral Reviews*, *25*(4), 287–95. Retrieved from http://www.ncbi.nlm.nih.gov/pubmed/11445135

Wood, J. J., Drahota, A., Sze, K., Har, K., Chiu, A., & Langer, D. a. (2009). Cognitive behavioral therapy for anxiety in children with autism spectrum disorders: a randomized, controlled trial. *Journal of Child Psychology and Psychiatry, and Allied Disciplines*, *50*(3), 224–34. http://doi.org/10.1111/j.1469-7610.2008.01948.x

Yendiki, A., Koldewyn, K., Kakunoori, S., Kanwisher, N., & Fischl, B. (2014). Spurious group differences due to head motion in a diffusion MRI study. *NeuroImage*, *88*, 79–90. http://doi.org/10.1016/j.neuroimage.2013.11.027

Yerys, B. E., & Herrington, J. D. (2014). Multimodal imaging in autism: an early review of comprehensive neural circuit characterization. *Current Psychiatry Reports*, *16*(11), 496. http://doi.org/10.1007/s11920-014-0496-2